Distribution Agreement

In presenting this thesis or dissertation as a partial fulfillment of the requirements for an advanced degree from Emory University, I hereby grant to Emory University and its agents the non-exclusive license to archive, make accessible, and display my thesis or dissertation in whole or in part in all forms of media, now or hereafter known, including display on the world wide web. I understand that I may select some access restrictions as part of the online submission of this thesis or dissertation. I retain all ownership rights to the copyright of the thesis or dissertation. I also retain the right to use in future works (such as articles or books) all or part of this thesis or dissertation.

Signature

_____

Arthur E. Morrissette

Date

_____

Role of Basal Ganglia Output on Thalamo-Cortical Activity and Licking Behavior in Mice

By

Arthur E. Morrissette V
Doctor of Philosophy

Graduate Division of Biological and Biomedical Sciences
Neuroscience

_____
Dr. Dieter Jaeger
Advisor

_____
Dr. Robert Hampton
Committee Member

_____
Dr. Robert Liu
Committee Member

_____
Dr. Samuel Sober
Committee Member

_____
Dr. Lena Ting
Committee Member

_____
Dr. Thomas Wichmann
Committee Member

Accepted:

_____
Lisa A. Tedesco, Ph.D.
Dean of the James T. Laney School of Graduate Studies

_____
Date

Role of Basal Ganglia Output on Thalamo-Cortical Activity and Licking Behavior in Mice

By

Arthur E. Morrissette V
B.S.

Advisor: Dieter Jaeger, Ph.D.

An abstract of
A dissertation submitted to the Faculty of the
James T. Laney School of Graduate Studies of Emory University
In partial fulfillment of the requirements for the degree of
Doctor of Philosophy
In the Graduate Division of Biological and Biomedical Sciences
Neuroscience
2018

Abstract

Role of Basal Ganglia Output on Thalamo-Cortical Activity and Licking Behavior in Mice

By Arthur Morrissette

The planning and execution of voluntary movement involves multiple brain areas including the cortex, thalamus, and basal ganglia. How these areas interact to control movement remains unknown. The basal ganglia are thought to contribute to motor control by providing tonic inhibitory output to the thalamus in order to suppress unwanted movements and facilitate desired ones. To test this prediction, we used rapid optogenetic activation and inactivation of the GABAergic output of the basal ganglia to the motor thalamus in mice that were trained in a sensory cued left/right licking task. We found that 1s of unilateral optogenetic inhibition of GABAergic output from the substantia nigra reticulata (SNr) biased decision making towards the contralateral lick spout even during ipsilaterally cued trials. In contrast, 1s of optogenetic excitation of SNr terminals in motor thalamus resulted in a bias towards the ipsilateral direction. Output from the SNr continues to the motor thalamus which then projects widely across sensorimotor cortex. Thus, in order to examine cortical activity across cortex with high spatiotemporal resolution, we utilized mice expressing the fluorescent voltage indicator in excitatory cortical neurons. While previous studies have shown that the pupil provides important insights in neural processing as a proxy for arousal, it is unknown how arousal signals as measured by pupil diameter are represented by changes in cortical activity. We found that pupil diameter is tightly coupled to global changes in cortical voltage. This coupling is dependent on both frequency and location, with lower frequency signals and medial areas of the sensory-motor cortex most strongly coupled with arousal especially during periods of orofacial movements. Finally, we measured voltage activity across cortex in behaving mice to determine the voltage changes across cortex while mice prepared, withheld, and initiated licking movements. We found that membrane voltage in the contralateral motor cortex before the onset of the response period predicts the reaction time on a trial-to-trial basis such that increased voltage activity preceding the first lick is elevated on faster reaction time trials. Together, these experiments provide new insight in to the mechanisms by which the basal ganglia-thalamocortical circuits contribute to voluntary motor behavior.

Role of Basal Ganglia Output on Thalamo-Cortical Activity and Licking Behavior in Mice

By

Arthur E. Morrissette V
B.S.

Advisor: Dieter Jaeger, Ph.D.

A dissertation submitted to the Faculty of the
James T. Laney School of Graduate Studies of Emory University
In partial fulfillment of the requirements for the degree of
Doctor of Philosophy
In the Graduate Division of Biological and Biomedical Sciences
Neuroscience
2018

Acknowledgements

I would like to thank the neuroscience program faculty and students for making me feel at home in Atlanta, and for guiding me throughout this process. A special thank you to my fellow lab members who have contributed to this project. Lastly, I would like to thank my wife, Megan Morrissette, for her endless support and encouragement as well as my family for their constant love and guidance.

Table of Contents

Chapter 1: General Introduction 1
1.1 The Basal Ganglia 2
1.1.1 Basal Ganglia Anatomy 2
1.1.2 Basal Ganglia Control of Movement: 5
1.1.3 Basal Ganglia Disorders and Movement: 9
1.2 Cognitive Control of Movement 10
1.2.1 Thalamic Control of Movement 11
1.2.2 Cortical Motor Systems 16
1.2.3 Control of Voluntary Licking Behavior 23
1.3 Thesis Organization 26
Chapter 2: Unilateral optogenetic inhibition and excitation of basal ganglia output show opposing effects on directional lick choices and movement initiation in mice 27
2.1 Abstract 27
2.2 Significance Statement 29
2.3 Introduction 30
2.4 Methods 32
2.5 Results 41
2.6 Discussion 59
Chapter 3: Wide-Field Imaging of Spatiotemporal Cortical Voltage Activity Underlying Arousal During Spontaneous Behavior 66
3.1 Abstract 66
3.2 Introduction 67
3.3 Methods: 69
3.4 Results 77
3.5 Discussion 92
Chapter 4: Cortical Voltage Dynamics Underlying Movement Preparation and Initiation in Awake, Behaving Mice 96
4.1 Introduction 96
4.2 Methods 100
4.3 Results 105
4.4 Discussion 116
Chapter 5: General Discussion 119
5.1 Establishment of Cortical Voltage Imaging Techniques in Awake, Behaving Mice 120
5.2 Cortical Voltage Dynamics in During Awake, Spontaneous Behavior 122
5.3 Cortical Voltage Imaging of Movement Preparation and Initiation 123
5.4 Future Directions 124
References 127

List of Figures

Figure 1.1 - Basal Ganglia Input and Output Anatomical Pathways
Figure 1.2 - Differences in thalamo-cortical projection pathways from the motor thalamus
Figure 1.3 - Neural circuits for preparation and initiation of directed licking in the mouse
Figure 2.1 - Mice learn to perform anticipatory and withholding versions of a forced choice licking task
Figure 2.2 - Unilateral inactivation of the SNr biases towards contralateral licking behavior
Figure 2.3 - Unilateral inhibition of the SNr increases anticipatory licks and decreases reaction time towards the contralateral direction
Figure 2.4 - Unilateral excitation of the SNr impairs both contra- and ipsilateral licking activity
Figure 2.5 - Unilateral excitation of the SNr increases reaction time towards both lick directions
Figure 2.6 - Unilateral excitation of the SNr projections to the BGMT biases licking towards the ipsilateral direction
Figure 2.7 - Unilateral excitation of nigro-thalamic terminals facilitates suppression and increases reaction time for contralateral licking
Figure 2.8 - Summary of optogenetic manipulations and main results
Figure 3.1 - Transgenic expression of a genetically encoded voltage indicator
Figure 3.2 - Cortical global signal from wide-field voltage imaging is tightly coupled to pupil diameter
Figure 3.3 - Cortical Voltage Imaging Is Correlated with Laminar LFP Activity in Awake Mice
Figure 3.4 - Global Cortical Signals Are Differentially Coupled to Pupil Diameter Across Multiple Frequencies
Figure 3.5 - Cortical Activity and Pupil Diameter Are Differentially Coupled Across Functional Cortical Areas
Figure 3.6 - Patterns of Cortical Coupling to Pupil Diameter Are Dependent on Behavioral State
Figure 4.1 - Wide-Field Cortical Imaging of Mice Performing Forced Choice Licking Task
Figure 4.2 - Spatiotemporal Cortical Voltage Activity During Sensory-Guided Licking Behavior
Figure 4.3 - Lateralized Voltage Signals in Anterior Lateral Motor Cortex Underlying Licking Preparation and Initiation
Figure 4.4 - Voltage Activity in ALM Underlying Proper Movement Suppression and Initiation
Figure 4.5 - Neural Correlates Predicting Reaction Time Emerge in Over 1s Before Onset of Movement Response

Chapter 1: General Introduction

The ability to properly initiate and suppress movements is a critical aspect of animal behavior. Several brain centers have been implicated in the control of movement including the motor cortex, the cerebellum, and the basal ganglia. The basal ganglia (BG), a collection of subcortical nuclei, are thought to influence the control of movement by inhibiting and facilitating selected motor programs to accomplish and reinforce goal-directed behavior (Albin et al., 1989, DeLong, 1990). Our long-standing understanding of the BG's role in the control of movement suggests that the output nuclei of the BG provide tonic inhibition over motor areas of the thalamus and brainstem to suppress unwanted movements, with pauses in the inhibitory output facilitating movement initiation (Deniau and Chevalier, 1985, Mink, 1996, Hikosaka, 2007). In support of this classic basal ganglia functional model, optogenetic excitation of the basal ganglia direct pathway has been found to be pro-kinetic, leading to a reduction in the inhibitory output of the substantia nigra pars reticulata (SNr), the primary basal ganglia output nucleus in the rodent, and disinhibition of downstream targets (Freeze et al., 2013, Oldenburg and Sabatini, 2015). Additionally, pauses in SNr activity preceded initiation of orienting movements in rats performing an auditory-cued Go-Stop task (Schmidt et al., 2013). It remains unclear, however, how cortical planning activity and motor initiation is affected by output from the basal ganglia.

In order to examine basal ganglia contributions to cortical processing underlying motor control, we adapted an existing behavioral task in mice previously shown to require cortical (and thalamic) processing for successful task execution. This task requires a head-fixed mouse to distinguish sensory stimuli (air-puffs) towards the left or right

whiskers and provide a lick response to either a left or right lick spout positioned in front of the mouse in order to receive a sucrose liquid reward. Similar behavioral tasks from which ours was adapted have shown increases in activity before and during voluntary licking behavior in a specific region in the pre-motor territory of the mouse cortex known as the anterior lateral motor cortex (ALM) (Li et al., 2015).

The following chapters will focus on two associated neural systems contributing to cognitive motor control. First, I will discuss the influence of basal ganglia output via the SNr and the SNr projections to the motor thalamus (MT) on control (including preparation and initiation) of directional licking behavior. In the following chapter, I will describe the voltage dynamics across the dorsal cortex underlying arousal as measured by fluctuations in pupil dilation in spontaneously behaving mice. Finally, I will examine the cortical voltage dynamics of the sensory-motor cortex (which receives input from the motor thalamus) underlying movement preparation, suppression and execution using the same licking behavioral task.

1.1 The Basal Ganglia

1.1.1 Basal Ganglia Anatomy

The basal ganglia are a set of interconnected subcortical nuclei that are critical for voluntary behavior. The BG integrates input from a large array of cortical, thalamic, and brainstem inputs, and influences downstream circuits through two major pathways. These include a direct, descending projection to brainstem targets as well as an ascending projection to several nuclei in the motor thalamus (Kultas-Ilinsky et al., 1978, Parent and Parent, 2004). The input nucleus, the striatum, receives heavy, roughly topographic

cortical input (Albin et al., 1989, Alexander and Crutcher, 1990). Cortical pyramidal neurons synapse with spines of medium spiny neurons, the projection neurons of the striatum. The medium spiny neurons are GABAergic and make up more than 90% of the striatal neurons. They fall into two major categories that can be distinguished based on their gene expression profiles and connectivity.

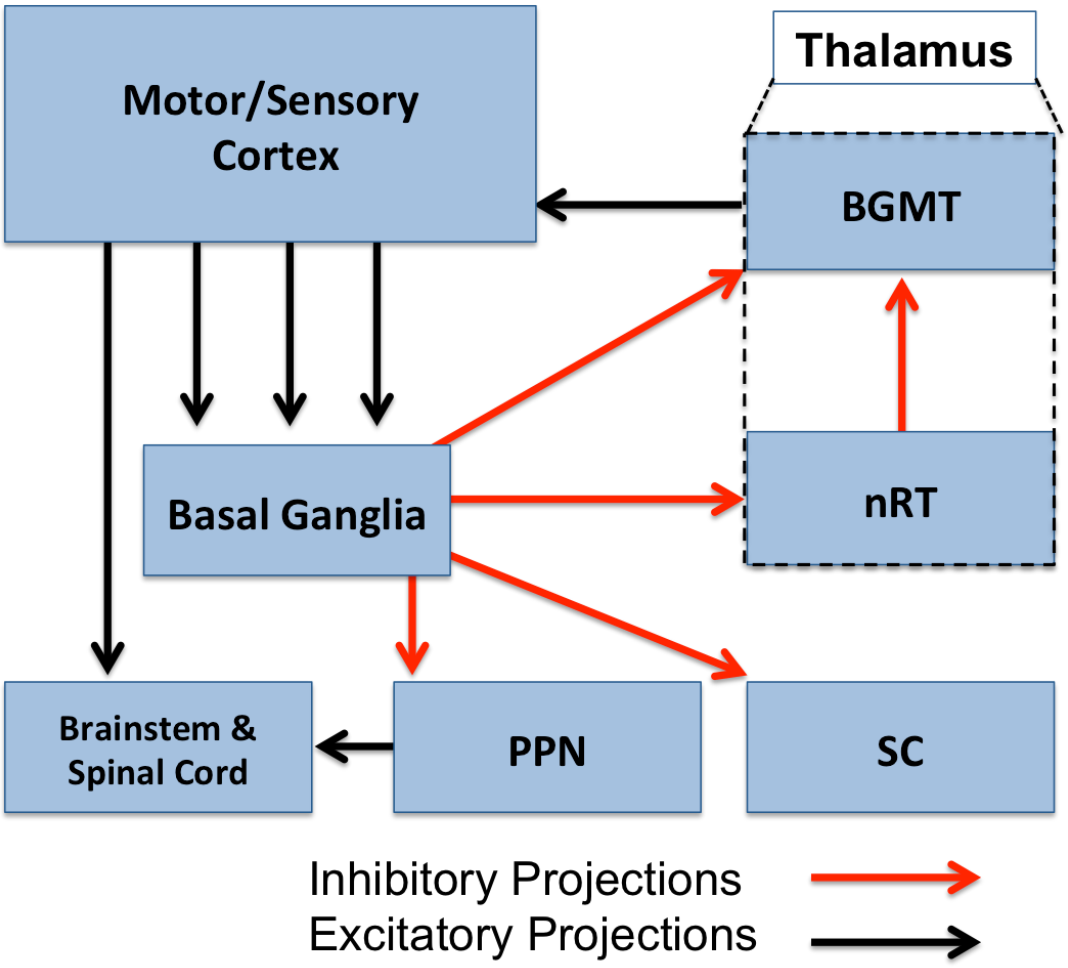

Figure 1.1 Basal Ganglia Input and Output Anatomical Pathways

The basal ganglia receive cortical input from many areas including motor and sensory regions. The basal ganglia internal circuitry is removed for simplification. The output from the basal ganglia projects to downstream circuits via an ascending pathway to the thalamus including a region of the motor thalamus referred to as the basal ganglia recipient motor thalamus (BGMT) as well as the reticular thalamic nucleus (nRT). The

basal ganglia output also projects to the brainstem via a descending pathway to targets such as the superior colliculus (SC) and the pedunculopontine nucleus (PPN). The basal ganglia are therefore able to influence motor control via cortico-basal ganglia-thalamocortical loops as well as through the brainstem motor centers that project to the spinal cord. While most projection pathways throughout this motor system are excitatory (black lines), the basal ganglia output pathways are inhibitory projections (red lines).

The striatonigral (or 'Direct') pathway is composed of medium spiny neurons that express dopamine D1-like receptors and project directly to the output nuclei of the basal ganglia. The striatopallidal (or 'Indirect') pathway is composed of medium spiny neurons that project to the external segment of the globus pallidus and express dopamine D2-like and adenosine A2A receptors (Alexander and Crutcher, 1990, Gerfen et al., 1990, Fuxe et al., 2005). Neurons from both pathways receive neuromodulatory input from dopamine neurons located in the ventral midbrain, composed of the ventral tegmental area (VTA) and substantia nigra pars compacta (SNc). The direct and indirect pathways are thought to regulate motor output in an opposing manner. It has been argued that activation of direct pathway medium spiny neurons facilitates movement, whereas activation of indirect pathway medium spiny neurons inhibits movement (Kravitz et al., 2010).

The major output nucleus of the basal ganglia in rodents is the SNr. The SNr neurons receive inhibitory afferent projections from striatal projection neurons (direct pathway) as well as from globus pallidus neurons (indirect pathway). They also receive glutamatergic input from the subthalamic nucleus and the thalamus. SNr neurons are GABAergic and project to the thalamus and brainstem and are critical for movement planning, initiation, and execution (Faull and Mehler, 1978, Parent and Hazrati, 1995). Of particular interest to the data presented in this thesis are the projections from the SNr to

the midbrain tectum, specifically, to the superior colliculus (SC). The SNr neurons that project to the SC tend to be restricted to the more deep and lateral regions. That is, neurons located more laterally in the SNr tend to project to the SC, while more superficial and medial neurons target the thalamus (Faull and Mehler, 1978). A large proportion of basal ganglia outputs are directed to several nuclei in the thalamus including the ventral lateral, ventral anterior, ventral medial, mediodorsal, parafascicular, centromedial, and thalamic reticular nuclei (Graybiel and Ragsdale, 1978, Parent, 1990). The ventral portions of the thalamus receiving input from the basal ganglia are referred to as the motor thalamus, or more specifically the basal ganglia recipient motor thalamus (BGMT). While the remaining basal ganglia receiving regions may influence motor behaviors, they are considered to primarily serve associative or executive functions (Alexander et al., 1990, Haber and McFarland, 2001, Schmitt et al., 2017, Gent et al., 2018). Finally, outputs to the thalamic reticular nucleus are also of interest as this area of the thalamus provides inhibitory control over many of the other thalamus nuclei including those not receiving direct input from the basal ganglia and is implicated in sleep/wake cycles and arousal (Halassa et al., 2014, Lewis et al., 2015).

1.1.2 Basal Ganglia Control of Movement:

The function of the basal ganglia has for decades been the subject of extensive debate (Wichmann and DeLong, 1996, Nelson and Kreitzer, 2014, Yin, 2014, Dudman and Krakauer, 2016, Wallace et al., 2017). However, there is apparent consensus that the basal ganglia are critical for control of movement. As noted above, the medium spiny neurons of the striatum receive both glutamatergic input from diffuse cortical regions as well as neuromodulatory input from dopamine cells located in the ventral midbrain.

Dopamine signaling on medium spiny neurons is thought to underlie the synaptic plasticity that accompanies changes in behavior during learning via opposing actions of D1-like and D2-like receptors (Nicola et al., 2000, Shen et al., 2008). These opposing actions are thought to lead to long term potentiation or depression of medium spiny neuron activity, which are thought to underlie learning.

However, the function of dopamine in continuous regulation of motor behavior is less clear than its role in synaptic modification. In patients with Parkinson's disease, in which nigrostriatal dopamine neurons die, voluntary movement is severely impaired: PD patients ultimately become unable to produce voluntary movements. Similarly, when striatal dopamine is depleted in primates and rodents, movement is disrupted, producing symptoms that mimic Parkinson's disease including tremors and akinesia (Bergman et al., 1990). In contrast, dopamine receptor agonists within the striatum can potentiate locomotion (Essman et al., 1993). Based on these results and because dopamine cannot directly activate neurons but instead modulates the existing signals, it is proposed that dopamine acts as a gain function on the descending cortico-striatal signals (Servan-Schreiber et al., 1990).

Given the effects of striatal dopaminergic receptor manipulations on movement, it is unsurprising that striatal projection neurons have been implicated in the control of movement. The direct and indirect pathways are thought to act in opposition to one another (Kravitz et al., 2010, Kravitz et al., 2012). It is thought that activation of the direct, striatonigral, pathway facilitates movement, whereas activation of the indirect, striatopallidal, pathway inhibits movement. While this schematic of basal ganglia function in which the direct pathway acts as an accelerator for movement and the indirect pathway

acts as a brake, provides a convenient functional characterization, the actual functions of these pathways are much less dichotomous. For example, recent studies have shown that neurons in both pathways are activated during action initiation (Cui et al., 2013, Isomura et al., 2013), and that activation of both pathways is necessary for movement (Tecuapetla et al., 2014, Tecuapetla et al., 2016). Together, these results suggest that binary activation of one pathway is insufficient to explain movement. Rather, dynamic, balanced activity between the two likely determines motor output.

The SNr is a major output nucleus of the basal ganglia that is downstream of both the direct and indirect pathways. SNr neurons have been widely thought to act as a gate, facilitating movement when they are inhibited and preventing movement when they are active (Hikosaka and Wurtz, 1983a, b). This has proven a particularly attractive hypothesis in light of the supposed antagonistic nature of the direct and indirect pathways. This 'model' was largely based on electrophysiological recordings from neurons in the SNr and downstream targets as restrained monkeys performed discrete eye movements. Because of the discrete nature of these tasks, it was difficult to understand how SNr neurons contribute to continuous limb movement. However, accumulating evidence suggests that SNr neurons do not regulate movement in such a binary manner. Selective activation of medium spiny neurons belonging to either the direct or indirect pathways has both inhibitory and excitatory effects on SNr output neurons (Freeze et al., 2013). During free movement, putative GABAergic output neurons recorded from the SNr of mice show both increased and decreased activity during movement. Additionally, during postural changes and goal-directed head movements, subsets of SNr neurons exhibit both increased and decreased activity patterns based on the specific movement of the animal

(Barter et al., 2015). In a recent paper, researchers investigated the effects of either direct or indirect pathway activation on firing rate activity in motor cortex (Oldenburg and Sabatini, 2015). In these experiments, cell-type specific optogenetic activation of either the direct or indirect pathway striatal MSNs was achieved using transgenic mice expressing cre in the direct pathway MSNs (D1-cre) or indirect pathway MSNs (A2A-cre). Optogenetic activation of the direct pathway (inhibiting SNr thereby disinhibiting thalamus) led to an increase in firing rates in the motor cortex. Conversely, activating the indirect pathway (exciting the SNr and inhibiting the thalamus) led to a decrease in firing rates in motor cortex. While these pathways exhibited opposite or antagonistic effects on cortical activity, the changes were not symmetric, such that certain cortical neurons exhibited biphasic firing rate modulation by indirect pathway activation with brief increases followed by prolonged suppression of activity. Interestingly, the effects on motor cortex by both direct and indirect pathway stimulation were diminished when the animal performed a lever pulling action. Another recent study sought to examine brain-wide changes in neural activity following basal ganglia manipulation, specifically optogenetically stimulating the direct or indirect pathways in the striatum (Lee et al., 2016). To observe and record activity throughout the entire mouse brain, they performed the optogenetic manipulations while the mouse was anesthetized in an fMRI scanner, allowing imaging of the entire extent of the brain at a temporal resolution on the level of seconds. Stimulating direct pathway MSNs led to large increases of blood volume in downstream targets like the thalamus and various regions of sensory and motor cortices, supporting the idea that inhibiting basal ganglia output will disinhibit downstream thalamic and cortical circuits.

The basal ganglia have additionally been implicated in the control of rodent orofacial behaviors specifically. Systemic injections of dopamine receptor agonists produce oral stereotypy, which includes tongue and jaw movements (Redgrave et al., 1980). The SNr is especially implicated in the control of orofacial behaviors. For example, SNr neurons fire bursts of action potentials during orofacial behavior associated with syntactic grooming sequences in rats (Meyer-Luehmann et al., 2002) as well as drinking (Joseph et al., 1985). When muscimol, a GABA receptor agonist, or GABA is injected directly into the SNr firing of SNr output neurons is effectively shut down (Westby et al., 1994) and rapid licking is observed (Taha et al., 1982). Inactivation of the SNr with lidocaine significantly reduces oral stereotypies induced by injections of amphetamine into the ventrolateral striatum (Canales and Graybiel, 2000). Finally, bilateral optogenetic excitation of SNr output to the superior colliculus disrupts voluntary licking behavior and interval timing (Rossi et al., 2016, Toda et al., 2017).

1.1.3 Basal Ganglia Disorders and Movement:

Basal ganglia disorders often result in severe motor impairment. This motor impairment falls along a spectrum ranging from hypokinesia, in which patients cannot move as much as they would like to, to hyperkinesia, in which patients are often unable to suppress unwanted movements (DeLong, 1990). The classic example of a hypokinetic disorder is Parkinson's disease (PD). In these patients, the dopaminergic neurons of the substantia nigra die, resulting in significantly reduced dopamine release in the dorsal striatum. Common behavioral consequences of the death of nigral dopamine neurons in PD are resting tremors, bradykinesia, and impaired posture.

Conversely, Huntington's disease (HD) is a hyperkinetic disorder. The chief symptom is chorea, or involuntary movements. The motor symptoms of HD are thought to be driven in part by death of striatal medium spiny neurons which is caused by buildup of Huntingtin protein and subsequent neurotoxicity. Numerous observations in humans and animal models have established that very large disturbances of the basal ganglia, such as those seen in PD and HD patients, are sufficient to generate profound impairments in movement. However, since the pathologies that result in changes in motor control tend to be very wide-spread it can be difficult to dissociate specific motivational symptoms from more motor-related symptoms.

Basal ganglia disorders can also lead to orofacial specific motor impairments. For instance, PD patients treated with chronic L-DOPA can develop tardive dyskinesia, which is characterized by uncontrolled movement of limbs as well as the tongue and jaws (Gerlach et al., 1974, Gerlach, 1977). Speech deficits also occur as the result of basal ganglia pathologies. Proper control of the muscles of the tongue and jaw is necessary for articulation during speaking. PD patients often have disrupted speech, both on and off medication, because they have limited control of the tongue and jaw (Ackermann and Ziegler, 1991). Moreover, the inability to initiate speaking or slowness of speech are common outcomes of focal basal ganglia lesions and are particularly common when lesions are restricted to the putamen and globus pallidus (Bhatia and Marsden, 1994).

1.2 Cognitive Control of Movement

While many basic motor functions can be executed by highly conserved motor programs stored in brain stem centers, it is thought that movements requiring complex preparation, sequencing, and coordination are primarily controlled by forebrain circuits

(Svoboda and Li, 2018). This “cognitive” control of movement requires complex processing between memory, sensory, and executive functions and it thought to be mediated in part by cortico-basal ganglia-thalamocortical pathways. While a central node in this BG-thalamocortical loop, it remains unclear how the thalamus acts to coordinate and influence motor control, though several past and present studies have begun to investigate thalamic function in goal-directed sensory-motor behavior.

1.2.1 Thalamic Control of Movement

While the thalamus was long considered a simple relay (Sommer, 2003, Sherman, 2007), researchers are beginning to uncover the complex interactions and importance of the thalamus in coordinating activity across cortical and sub-cortical circuits. Early studies implicating the thalamus in control of movement focused on the oculomotor system and activity of the central thalamic nuclei on targeting and fixating on visual stimuli (Schlag and Schlag-Rey, 1971). The thalamus has additionally been the target for several neurosurgical techniques that relieve motor dysfunction in diseases like Parkinson’s and dystonia (Lee and Marsden, 1994, Cury et al., 2017). The traditional motor areas of the thalamus, aptly referred to as the “motor thalamus” or “mthal” includes ventral areas such as the ventral lateral (VL), ventral anterior (VA), and ventromedial (VM) nuclei. While the delineations between these nuclei differ slightly between species, in the mouse thalamus the VL and VA portions primarily receive excitatory input from the cerebellum while parts of the VA and the VM nuclei receive GABAergic input from the basal ganglia output nuclei such as the SNr and Globus Pallidus internal segment (GPi). Throughout the rest of the thesis, the cerebellar receiving motor thalamus will be referred to as the CBMT, while the basal ganglia receiving motor thalamus will be referred to as the BGMT. Pathways from

the motor thalamus project to the entire motor-related cortex including primary, pre-motor, and supplementary motor areas (Kuramoto et al., 2009, Kuramoto et al., 2015). These two pathways from the motor thalamus differ, however, in their primary cortical targets, with the CBMT primarily targeting primary motor cortex and the BGMT projecting more diffusely across frontal cortex the same axon collaterals reaching sensory, motor, and prefrontal cortices. Lastly, an important anatomical difference between the two projection pathways that has a large impact on how these pathways influence cortical function is that the CBMT projections typically target pyramidal cell somas in L5 and L2/3 while the BGMT projections primarily contact apical dendrites of the same cells in layer 1 as well as L1 inhibitory interneurons (Garcia-Munoz and Arbuthnott, 2015). While both ascending pathways from the motor thalamus deserve thorough consideration regarding their contributions to motor control, the remaining background will focus primarily on the basal ganglia recipient region when possible and features of the motor thalamus broadly.

The primary hypothesis as to the function of the BGMT is that is facilitates generation of willful or voluntary movements (Mushiake and Strick, 1995, van Donkelaar et al., 1999, Hikosaka et al., 2000, Middleton and Strick, 2000, van Donkelaar et al., 2000). Unlike neurons in the in the CBMT, BGMT activity lacks sensory responses and typically shows purely motor related activity changes. The BGMT has also been shown to be preferentially associated with internally generated movements as opposed to visually triggered movements as inactivation studies have found that internally generated movements and not externally cued movements were impaired (van Donkelaar et al., 1999, 2000).

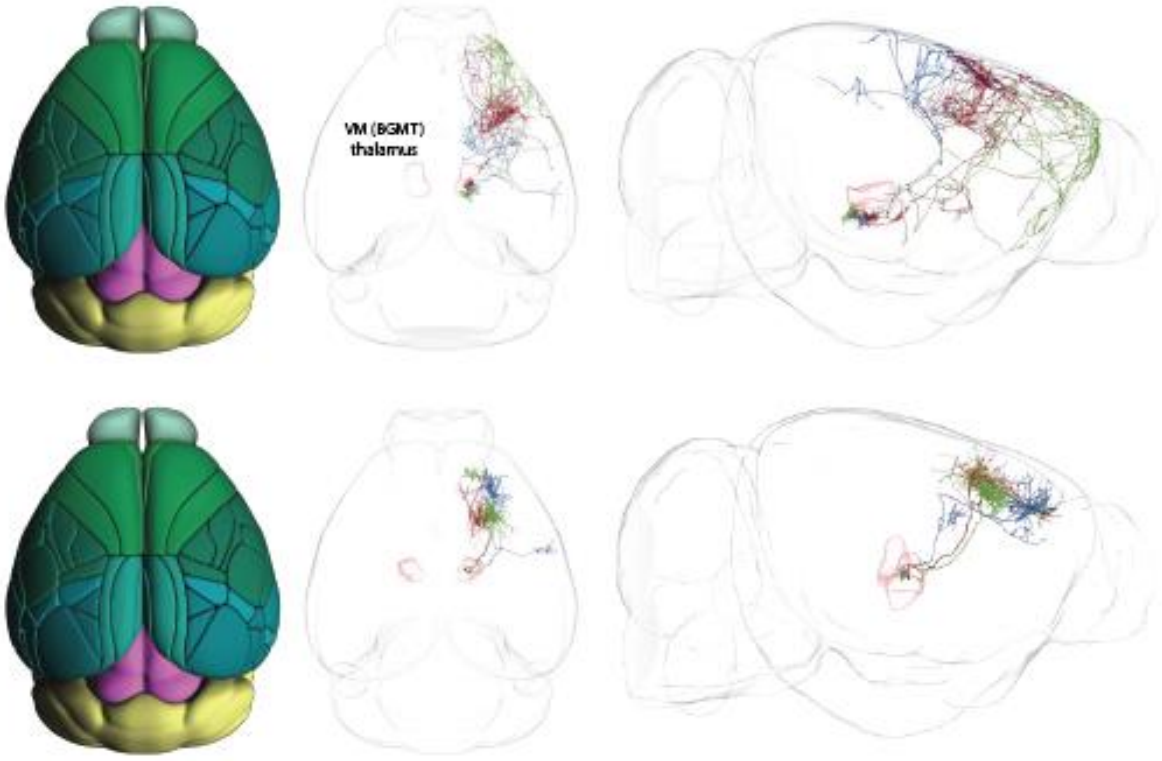

Figure 1.2 Differences in thalamocortical pathways from the motor thalamus
Single neuron reconstructions from the VM (BGMT) thalamus (top, middle, right). Three different neurons are labelled green, red, and blue. All axonal projections from the VM ascend towards superficial (layer 1) cortex across pre-frontal (green), primary motor (red), and somatosensory (blue) areas of cortex with large axon arbors. In contrast to VM neurons, reconstructed neurons from the VL (CBMT) thalamus (bottom, middle, right) project to deep cortical layers with restricted axonal arbors from each cell almost entirely within the primary motor cortex. Allen Brain Atlas Surface Maps are provided on left for reference. Data and projection renderings from Janelia MouseLight project (http://mouselight.janelia.org/).

Recent studies in rodents have continued to provide support for the role of the motor thalamus in movement. One study has utilized optogenetic strategies to try and recover motor function in a hemi-parkinsonian mouse model (Seeger-Armbruster et al., 2015). In this study, rats performing a reach-to-grasp task during a drug-induced

parkinsonian state demonstrate akinesia similar to that seen in Parkinson's disease. Using the neural activator, Channelrhodopsin (ChR2), they stimulated the motor thalamus at various frequencies and patterns of activity. Interestingly, stimulation frequencies used for deep brain stimulation were not effective at increasing reaching movements, however optically stimulating the thalamus with more complex patterns such as "theta burst stimulation" and "physiological" stimulation patterns recorded from healthy motor thalamus units was effective at partially recovering the rats reaching ability. These results point to the pattern of activity in motor thalamus as being as important or more important that simply the frequency of activity for movement initiation.

Another study optogenetically inhibited motor thalamus by stimulating inhibitory axons (from the thalamic reticular nucleus) projecting to the VAL/VM thalamus to determine the role of the thalamus in directed licking behavior (Guo et al., 2017). During normal behavior, the motor thalamus showed ramping activity preceding lick initiation during the HOLD period of a forced choice task. They found that inhibiting the motor thalamus (including both CBMT and BGMT regions) disrupted the ramping activity and reduced performance in the licking task to chance. Since the optogenetic inhibition of the thalamus was performed during the HOLD period of the task when the mice are relying on working memory to plan its upcoming movement, the authors interpret these results as the motor thalamus is required for maintenance of preparatory activity prior to movement initiation.

Finally, recent work has further examined motor thalamus activity in mice performing a two-forced choice task where mice must orient towards a right or left lick port based on an auditory cue (Gaidica et al., 2018). This study suggests that there may

be two types of neurons in the motor thalamus that encode different aspects of movement. In this study, authors recorded single-unit motor thalamus activity in male rats performing a two-alternative forced choice task. Their results found that within a large population of thalamic neurons that increased their activity briefly near movement initiation, one functional group of neurons were tightly locked to the instructional cues while another was more tightly locked to movement onset. In addition to the timing of the neural responses, the movement onset units predicted the direction of orienting movement while the cue-locked units did not predict which direction the rat would move. Activity in movement onset neurons was also anti-correlated with reaction time and movement time, together suggesting that motor thalamus activity influences choice behavior in two stages: first showing a short-latency, non-specific increase in activity followed by direction specific activity representing action selection and movement vigor. While the location of these recordings were based on histological reconstruction, their anatomical results show that these two functional groups of neurons are not segregated within the cerebellar or basal ganglia receiving zones of the motor thalamus (VAL and VM thalamus, respectively). While seemingly functionally intermixed, these two areas of the thalamus have very different projection patterns and influence on cortical activity (Kuramoto et al., 2009). Future studies may utilize juxta-cellular recordings with cell labelling or optogenetic tagging of basal ganglia or cerebellar receiving areas of the thalamus to better understand the functional heterogeneity of basal ganglia vs. cerebellar receiving thalamus, especially in the context of action selection and movement vigor (See Future Directions).

While the motor thalamus has clear links to motor control and movement initiation, there are several other nuclei that are also situated to influence cognitive control of

movements, though receive far less focus than the classic motor thalamus. One such nucleus is the mediodorsal (MD) thalamus. The MD thalamus is placed within another brainstem-thalamic-cortical motor loop; in this case receiving input from the superior colliculus (SC) and projecting to the frontal eye fields (or anterior lateral /prefrontal cortex of rodents). Studies recording from the MD thalamus during alternative choice tasks found activity relating to the more cognitive aspects of behavior such as working memory or attentional control (Schmitt et al., 2017). The MD thalamus also receives substantial input from the basal ganglia output nuclei and projects primarily to prefrontal cortical regions, providing further support for the idea that MD influences more cognitive aspects of behavior (Halassa and Kastner, 2017).

1.2.2 Cortical Motor Systems

The primary motor cortex, or M1, is one of the principal brain areas involved in motor function. The role of the primary motor cortex is to generate signals that control the execution of movement. Signals from M1 cross the body's midline to activate skeletal muscles on the opposite side of the body, meaning that the left hemisphere of the brain controls the right side of the body, and the right hemisphere controls the left side of the body. Other regions of the cortex involved in motor function are called the secondary motor cortices. These regions include the premotor cortex and the supplementary motor area (SMA), which are collectively considered part of the premotor cortex in rodents. In humans and non-human primates, the supplementary motor area lies above, or medial to, the premotor area, and also in front of the primary motor cortex. Both the premotor and SMA are involved in the planning of complex movements and both send information to the primary motor cortex as well as to brainstem motor regions and spinal cord.

Neurons in M1, SMA and the premotor cortex give rise to the fibers of the corticospinal tract. The corticospinal tract is the only direct pathway from the cortex to the spinal cord and is composed of over a million fibers in humans. These fibers descend through the brainstem where the majority of them cross over to the opposite side of the body at the level of the medulla. After crossing, the fibers continue to descend through the spinal cord, terminating at the appropriate spinal levels. The corticospinal tract is the main pathway for control of voluntary movement in humans. There are other motor pathways which originate from subcortical groups of motor neurons (nuclei). These pathways control posture and balance, coarse movements of the proximal muscles, and coordinate head, neck and eye movements in response to visual targets. Subcortical pathways can modify voluntary movement through interneuron circuits in the spine and through projections to cortical motor regions (Pivetta et al., 2014, Arber, 2017, Arber and Costa, 2018).

Movement Preparation

Recent research has shown that a particular area of the premotor cortex in rodents known as the anterior lateral motor cortex is required for proper execution and planning of directed licking movements (Guo et al., 2014c, Li et al., 2015, Allen et al., 2017, Chen et al., 2017, Guo et al., 2017, Guo et al., 2018). Additional work by the same authors has implicated the thalamus and more specifically the motor thalamus (encompassing the ventral medial and ventral lateral nuclei) as an additional piece of the circuit critical to generating preparatory activity that is necessary to perform a delayed licking task (Guo et al., 2017). This area of the thalamus is important as it is considered the primary bridge by which the basal ganglia can influence the cortex. The ventral medial nucleus of the

thalamus receives dense inhibitory input from the SNr and projects primarily to apical dendrites of neurons in the superficial layers of the cortex, including sensory, motor, and prefrontal regions (Guo et al., 2018). This is different than the ventral lateral nucleus that receives excitatory input from the cerebellum and projects to the cell bodies of layer 2/3 and layer 5 neurons located primarily in the motor cortex (Kuramoto et al., 2009).

Activity in the pre- and primary motor cortex predicts specific movements seconds before they occur and is often referred to as “preparatory” activity or “motor readiness” (Alexander and Crutcher, 1990, Cisek and Kalaska, 2005, Churchland et al., 2006b, Churchland et al., 2010, Kaufman et al., 2010, Kaufman et al., 2014, Li et al., 2015, Svoboda and Li, 2018). There is abundant evidence that voluntary movements are prepared before they are initiated (Day et al., 1989, Riehle and Requin, 1993). A large body of evidence comes from “instructed-delay tasks” where a temporal delay separates an instruction stimulus from a subsequent “go” cue. In addition to featuring a temporal delay to distinguish sensory information from the following movement, delay tasks also allow for the measurement of reaction times (RTs) following the “go” cue as well as the effects of the delay length on the RT. Previous work has shown that RT decreases and then plateaus as a function of the delay period length (occurring during the first 200ms) which suggests that some time-consuming preparation process is provided a head start by the forced delay (Riehle and Requin, 1989, Requin et al., 1990, Crammond and Kalaska, 2000). This ability to prepare movements ahead of initiation/execution is considered to be related to preparatory activity that is present throughout cortex and subcortical structures. Two areas of focus regarding preparatory neural activity are the premotor cortex (referred to as “M2” in the mouse) and primary motor cortex (referred to

as “M1”), which both show changes in activity such as ramping increases during the delay period (Tanji and Evarts, 1976, Godschalk et al., 1985, Wise et al., 1986, Kalaska et al., 1997, Crammond and Kalaska, 2000). While population averages may show what appears to be coordinated preparatory activity, examination of single cells shows wide variety in the types of temporal activity structure (Churchland et al., 2006a, Li et al., 2015).

Recent studies have begun examining preparatory activity in rodents. In a delayed response where rats must orient towards one of two reward ports, preparatory activity was measured in an area of motor cortex known as the frontal orienting fields (FOF). A substantial proportion of FOF neurons participate in rat choice behavior, though neurons selective for both movement directions are intermixed within the same hemisphere (Erlich et al., 2011). Additional studies have been performed in mice that are required to report a decision by directional licking. Using both calcium imaging and electrophysiological techniques, activity was recorded as the mice whisked to determine the location of a pole in front of the whiskers, during a 1s delay period, and finally during the response period signaled by an auditory tone. Preparatory activity that was selective for licking direction appeared earliest in the anterior lateral motor cortex (ALM) and remained localized to ALM until movement onset. A large proportion of neurons in L2/3 and especially L5 showed preparatory activity, though the temporal structure was not the same among all cells (Li et al., 2015, Chen et al., 2017). The researchers were able to separate the neural preparatory patterns in to 3 types of cell responses: the first showing selective preparatory activity only during the sample and delay periods, the second type showing direction selective activity during both the delay and during movement onset, and the third showing direction selective activity only at movement onset. While many neurons are direction

selective, the ALM contains equal proportions of intermingled neurons predicting ipsi- or contralateral movements. However, unilateral inactivation of this cortical region during movement planning disrupts contralateral movements and produces and ipsiversive bias (Li et al., 2015). Further examinations using cell-type-specific electrophysiology, cellular imaging and optogenetic perturbation have shown that layer 5 neurons projecting within the cortex have unbiased laterality (Economo et al., 2017). Further activity with a contralateral population bias arises specifically in layer 5 neurons projecting to the brainstem, and only late during movement planning (Economo et al., 2017). While these results reveal the transformation of distributed preparatory activity into movement commands within hierarchically organized cortical circuits, the origin and maintenance of this preparatory activity is unknown, but both basal ganglia and cerebellar circuits have been hypothesized to contribute to the ramping activity in preparation to move. The origin of preparatory activity in the cortex remains elusive. Previous work in the primate basal ganglia found preparatory neural activity in nearly a third of neurons in the caudate and putamen as well as the globus pallidus in a delayed reaching task (Jaeger et al., 1993). In a recent study by Guo and colleagues, preparatory activity was found in the motor thalamus including both basal ganglia and cerebellar receiving areas (Guo et al., 2017). This preparatory activity was similar to that found in the ALM such that when the thalamus was inactivated it produced an ipsiversive bias.

Movement Initiation

Disentangling neural activity underlying movement preparation and initiation is difficult as the two are not mutually exclusive in many scenarios. Several studies have begun to parse neural circuits responsible for preparatory activity compared to initiation

signals finding that populations of neurons that show activity before, during, and or after movement initiation suggesting that preparatory and initiation activity is shared within and across individual neurons (Li et al., 2015, Economo et al., 2017). The brain areas responsible for movement initiation have been extensively examined through recordings techniques that provide insights in to the neural activity around the initiation and execution of movements as well as electrical and optical stimulation techniques that are able to artificially drive movements by activating specific brain areas. Like the primary sensory cortex, the motor cortex is considered to be organized in a topographical fashion, with different areas of motor cortex responsible for initiating movements across different parts of the body, particularly in lateral extremities that require complex coordination (as opposed to axial muscle systems that do not receive as much innervation from the pyramidal system). However, there is considerable debate on the localization of different muscles or movements within motor cortex. Recent micro-stimulation experiments in monkeys have found that instead of specific muscle innervation (simple movements) being triggered by localized micro-stimulation, stimulating different areas of motor cortex triggered different types of complex behavior (Graziano et al., 2002). Additionally, the distance between stimulation sites corresponded to the similarity of the triggered behaviors, suggesting that instead of specific areas of motor cortex innervating specific muscles, motor cortex is instead controlling the initiation of complex motor programs or behaviors.

Though several hypotheses emerged early on proposing models for how neural activity in the motor cortices leads to movement initiation after decades of extensive research, the fundamental model of cortical function remains elusive. There exist

numerous models for neural control of movement initiation, several of which will be highlighted here. One of the popular model classes has existed since the 1970s and is known as the class of “accumulator” models (Thura and Cisek, 2016). In accumulator models, a movement is triggered when a signal that represents the decision process grows over time to reach a threshold level. From this larger group, two alternative models elaborate on the basic concept of the accumulator model: a variable rate model, where the reaction time depends on the rate of increase of activity before reaching the threshold; and a variable threshold model, where the reaction time depends on a changing threshold value that must be reached to initiate movement (Hanes and Schall, 1996).

In the context of licking or orofacial behavior in mice, a number of cortical areas have been implicated in the control of movement initiation. Guo and colleagues used a photoinhibition technique (silencing small cortical areas by optically stimulating inhibitory interneurons expressing ChR2) (Guo et al., 2014c). They found a relatively large region of pre-motor cortex extending from 1.5-3mm anterior and 0.5-1.5mm lateral of bregma, that when silenced using photoinhibition prevented voluntary licking to the contralateral direction. In another recent study, researchers used micro-stimulation and found a similar territory of pre-motor and primary motor cortex (though quite variable between individual mice) that triggered orofacial and specifically tongue movements (Komiyama et al., 2010).

Movement Suppression

While it is typically considered that the cortex acts to initiate movements, firing rates in cortex do not only increase around movement preparation and initiation events, but can also exhibit decreased activity during movement (Ebbesen et al., 2017). This suggests that motor cortex may play a more complicated role in motor control by also

actively coordinating movement suppression. In addition, the tonic, powerful inhibitory nature of the basal ganglia output to ascending and descending motor systems has provided support for the notion that the basal ganglia act as a “gate” on movements: constantly inhibiting motor activity and only allowing movements to occur with pauses in the output activity (Hikosaka, 2007).

1.2.3 Control of Voluntary Licking Behavior

In the context of this thesis, it is important to take a critical look at the motor systems involved in directed licking behavior. Goal directed licking movements are controlled via a motor cortical circuit where pyramidal tract neurons from layer 5B of ALM project to the contralateral intermediate nucleus of the reticular formation, which then projects to the hypoglossal nucleus. The hypoglossal nucleus then controls both the intrinsic and extrinsic muscles of the tongue (Travers and Jackson, 1992, Travers et al., 1997). The layer 5B pyramidal tract neurons in ALM show directional selectivity relating to the direction of licking movements and silencing the ALM prevents contralateral licking behavior. Additionally, optical stimulation of these neurons biases mice to lick to the contralateral direction, regardless of the rewarded spout direction (Li et al., 2015).

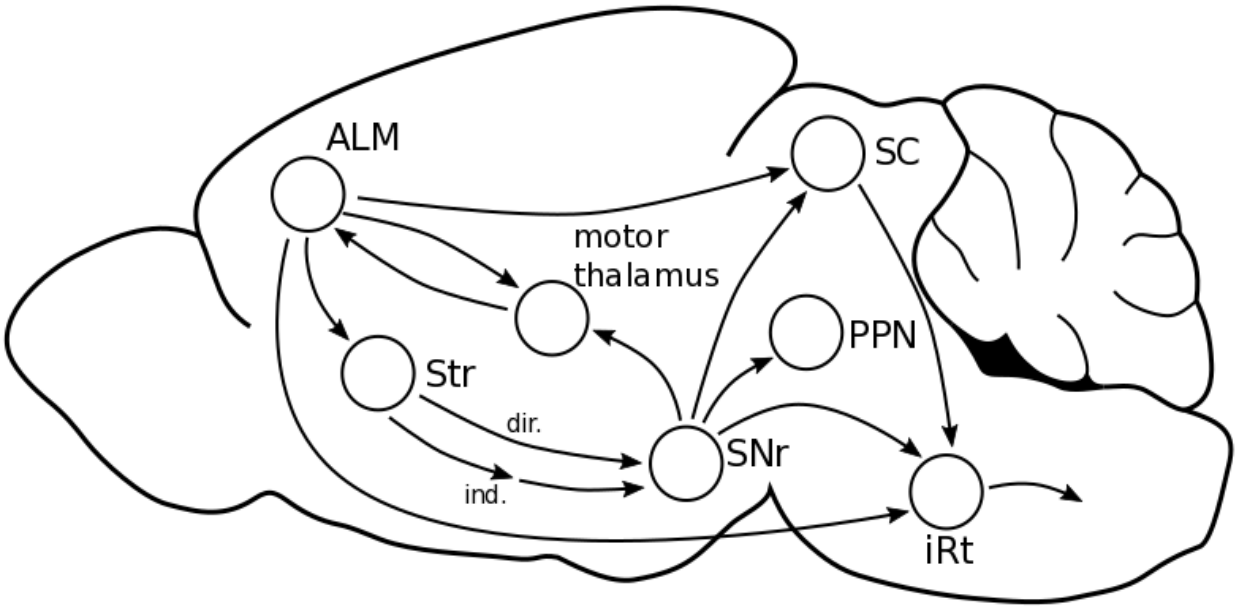

Figure 1.3. Neural circuits for preparation and initiation of directed licking in mice
The circuits underlying the preparation and execution of directed (left/right) licking behavior has been extensively studied in the mouse. The anterior lateral motor (ALM) cortex is thought to be a primary center where both preparatory and initiation signals emerge. The ALM then projects to many cortical targets such as the superior colliculus (SC), the striatum (Str), the motor thalamus, and finally the intermediate nucleus of the brainstem reticular formation (iRt). The iRt is one of the final output nuclei as it then projects to the hypoglossal nucleus that directly innervates the intrinsic and extrinsic muscles of the tongue. There are indirect pathways as well to the iRt such as those from the basal ganglia output nucleus (substantia nigra pars reticulata – SNr) as well as the SC. The recurrent projections between the motor thalamus and the ALM are thought to maintain neural activity amongst each other in preparation for a future movement. The basal ganglia are well situated to influence this thalamo-cortical preparatory activity via the output from the SNr to the motor thalamus.

Basal Ganglia-Thalamocortical Circuits and Directed Licking

While the motor cortical pathway to initiate voluntary licking has been established, the role of the basal ganglia and basal ganglia-receiving thalamus is less clear. There is however, recent evidence suggesting basal ganglia-thalamocortical circuits are especially

suited to shape directed licking behavior. In Guo et al., 2017, the motor thalamus was demonstrated to control directed licking behavior through maintenance of recurrent interactions with ALM (Guo et al., 2017). Optically inhibiting the motor thalamus (including both basal ganglia and cerebellar receiving regions) disrupts neural preparatory activity in the ALM and impairs licking performance on trials contralateral to the side of thalamic inhibition. Additionally, they found that inhibiting ALM activity disrupted similarly observed preparatory activity in the motor thalamus demonstrating the mutual reliance exhibited by the ALM and thalamus in planning and executing licking movements.

Another study has also implicated the SNr pathway to the superior colliculus on the internal generation of licking behavior. The superior colliculus also receives input from ALM and inactivation of this nucleus impairs licking behavior in both rats and mice (Redgrave et al., 1980, Taha et al., 1982, Rossi et al., 2016, Toda et al., 2017, Svoboda and Li, 2018). Activating the inhibitory SNr projections to the SC by stimulating the GABAergic SNr terminals expressing ChR2 at the level of the SC bilaterally disrupts licking behavior, but does not entirely suppress licking (Rossi et al., 2016). Instead, the pattern of licking is primarily disrupted and the ability of the mouse to time the interval of rewards is impaired (Toda et al., 2017). While the context of this type of licking behavior is different from sensory-guided licking responses, these experiments place the SC and especially SNr projections to the SC within the complex brain network orchestrating licking motor behaviors.

1.3 Thesis Organization

While the cortical input circuits to the basal ganglia have been extensively studied, little is known about how output from the basal ganglia influences neural activity and animal behavior. In this thesis, I use a combination of genetically targeted optical and electrophysiological techniques in the mouse model system to examine how the basal ganglia and downstream thalamo-cortical regions influence sensory-guided licking behavior. In Chapter 2, I use optogenetic manipulations of basal ganglia output activity to examine how output from the basal ganglia broadly and specifically to the motor thalamus influences performance in a directed licking behavioral paradigm previously shown to require both the cortex and motor thalamus. In order to comprehensively record from these areas of cortex, we utilized wide-field cortical imaging, using a large macro-scope to measure changes in tissue fluorescence that represents fluctuations in voltage. In Chapter 3, I characterize the voltage activity across cortex underlying behavior states and arousal (i.e. changes in pupil diameter) in awake mice. In Chapter 4, I further utilize wide-field imaging to examine cortical activity related to movement preparation, suppression, and initiation in mice performing the same directed licking paradigm used in Chapter 2. In Chapter 5 I discuss the implications of these studies and outline future experiments to address limitations of current approaches and remaining gaps in knowledge.

Chapter 2: Unilateral optogenetic inhibition and excitation of basal ganglia output show opposing effects on directional lick choices and movement initiation in mice

**This paper was initially submitted for review to J. Neuroscience on Aug. 15, 2018 with co-authors Morrissette AE, Chen PC, Bhamani C, Borden PY, Waiblinger C, Stanley S, Jaeger D. I designed and conducted experiments, analyzed results, and wrote the manuscript.*

2.1 Abstract

Models of basal ganglia function predict that tonic inhibitory output to motor thalamus suppresses unwanted movements, and that a decrease in such activity leads to action selection. A direct test of these outcomes of thalamic inhibition has not been performed, however. To conduct such a direct test, we utilized rapid optogenetic activation and inactivation of the GABAergic output of the substantia nigra pars reticulata (SNr) to motor thalamus in mice that were trained in a sensory cued left/right licking task. Directional licking tasks have previously been shown to depend on a thalamocortical feedback loop between ventromedial motor thalamus and antero-lateral premotor cortex (Li et al., 2015, Guo et al., 2017). In confirmation of model predictions, we found that 1s of unilateral optogenetic inhibition of GABAergic output from the SNr biased decision making towards the contralateral lick spout with ipsilaterally cued trials while leaving motor performance intact. In contrast, 1s of optogenetic excitation of SNr terminals in motor thalamus resulted in an opposite bias towards the ipsilateral direction confirming a bidirectional effect of tonic nigral output on directional decision making. In a second

variant of the task we disallowed anticipatory licking and found that successful suppression of anticipatory licking was also impacted by our optogenetic manipulations in agreement with the suppressive effect of tonic nigral output. Nevertheless, direct unilateral excitation of SNr cell bodies resulted in bilateral movement suppression, suggesting that pathways projecting bilaterally from the SNr to superior colliculus may also play an important role in the control of licking behavior.

2.2 Significance Statement

This study provides the first evidence that basal ganglia output to motor thalamus can control decision making in left/right licking choices and suppress anticipatory movement initiation. Unilateral optogenetic inhibition or excitation of basal ganglia output via the substantia nigra resulted in opposite changes of directional lick choices and could override the sensory information on lick direction provided by a whisker stimulus. These results suggest that basal ganglia output gates activity in a thalamo-cortical feedback loop previously shown to underlie the control of forced choice directional licking behavior. The results substantiate models stating that tonic inhibition of motor thalamus from the basal ganglia directs action selection and suppresses unwanted movements.

2.3 Introduction

The basal ganglia (BG) are thought to influence the control of movement by inhibiting and facilitating selected motor programs to accomplish and reinforce goal-directed behavior (Albin et al., 1989, DeLong, 1990). Our long-standing understanding of the BG's role in the control of movement suggests that the output nuclei of the BG provide tonic inhibition over motor areas of the thalamus and brainstem to suppress unwanted movements; pauses in the inhibitory output would therefore facilitate movement initiation (Deniau and Chevalier, 1985, Mink, 1996, Hikosaka, 2007). In support of this general basal ganglia functional model, optogenetic activation of the basal ganglia direct pathway has been found to be pro-kinetic, leading to a reduction in the inhibition of the SNr (Freeze et al., 2013), the primary basal ganglia output nucleus in the rodent, and disinhibition of downstream targets (Oldenburg and Sabatini, 2015). Additionally, pauses in SNr activity preceded initiation of orienting movements in rats performing an auditory-cued Go-Stop task (Schmidt et al., 2013). It remains unclear, however, how cortical planning activity and motor initiation is affected by output from the basal ganglia.

Recent studies have shown that in mice directional (left vs. right) licking in delayed choice tasks is initiated from an anterolateral premotor area named ALM (Guo et al., 2014a, Li et al., 2015, Chen et al., 2017). ALM expresses ramping activity in a feedback loop with the ventromedial thalamus (VM) during preparation of directional licking, and inhibition of either area reduces task performance to chance (Guo et al., 2017). The VM thalamus is a major part of the motor thalamus receiving strong input from the basal ganglia (BGMT, which also includes a portion of the anterior VA/VL nuclei) (Kuramoto et al., 2011). The basal ganglia are thus well positioned to control this corticothalamic

feedback loop through their strong inhibitory projection to motor thalamus from the substantia nigra reticulata (SNr) and the globus pallidus internus (GPi). Directional licking behavior as planned and initiated by ALM presents therefore an ideal model system to study how the basal ganglia exert motor effects in cortically initiated movements in rodents. To address this question, we trained mice to perform a licking task where they must lick a left or right positioned lick spout following a left or right air puff, respectively. In order to further parse the contributions of BG output on cognitive control of movement preparation and suppression, we trained the same mice to perform two variations of this task: first allowing mice to lick before the response window and anticipate the reward delivery ('anticipatory' task variant) and later a variant that required mice to actively withhold licking until the onset of the response window ('withholding' task variant). By training the mice to perform these task variants one after another, we were able to parse the basal ganglia contributions to initiating or suppressing anticipatory movements and the control of rewarded choice preparation and initiation. Using optogenetic methods to inhibit SNr neurons unilaterally, we found that silencing the inhibitory output of the basal ganglia triggered licking contralateral to the side of inhibition, irrespective of the rewarded licking direction. In contrast, exciting SNr projections to the motor thalamus and inhibiting thalamic activity suppressed contralateral licking and biased licking towards ipsilateral direction. These results suggest that the basal ganglia output via SNr to the motor thalamus exerts powerful unilateral control over movement preparation and initiation in the context of sensory guided motor behavior.

2.4 Methods

Animals:

For optogenetic stimulation and electrophysiological experiments, male and female Vgat-IRES-Cre mice (*Slc32a1*) aged 6-12 months at the start of experiments were used. Mice were maintained on a 12h:12h reverse light cycle and all experiments and behavioral training was performed during the dark portion of the cycle. Mice undergoing behavioral training were provided *ad libitum* food access and were kept on 1-1.5 ml/day water restriction 6 days a week starting at least 3 days prior and for the duration of handling, training, and experimental testing. On day 7 of each week, mice were given free access to water. During behavioral training and testing, mice were given 10% sucrose solution with 0.1% grape Kool-Aid powder. Liquid consumption was measured during testing and mice were supplemented with water to reach the 1-1.5 ml/day volume. All experimental procedures were approved by the Emory University Institutional Animal Care and Use Committee.

Surgery:

Viral Vector Injection and Fiber Placement. For optogenetic AAV vector injection, mice were anesthetized with isoflurane (induction at 3-4%, maintained at 1-2%) and head-fixed on a stereotaxic frame (Kopf). Craniotomies were made unilaterally above the SNr. For somatic SNr inhibition, 200nL of AAV5-EF1a-DIO-eARCH3.0-eYFP (ARCH; n = 5, 3 male) or for excitation, 200nL of AAV5-EF1a-DIO-hChR2(E123T/T159C-EYFP (ChR2(ET/TC) or ChR2; n = 4, 2 male) was injected with a nano-injector (Nanoject II, Drummond Scientific) at the rate of 0.46nl/s into the SNr targeting the coordinates (in mm from Bregma): AP -3.2, ML 1.6, DV -4.2). For somatic SNr excitation and SNr-BGMT

terminal excitation 200µm, 0.22NA optic fibers (Thor Labs) each with a 1.25mm steel ferrule were then implanted targeting the SNr and the ventromedial thalamus (AP -1.5, ML 0.9, DV -4.0). Following surgical implantation, mice were kept in single housed cages. All optogenetic manipulations were performed unilaterally on the right side of the animal, and hence 'ipsilateral' (IPSI) in this paper always refers to the right and 'contralateral' (CONTRA) refers to the left side of the body.

Acute Electrode/Optrode Recordings:

To record and/or optogenetically manipulate neural populations in the right SNr or downstream projection targets, a craniotomy was made above the site targeting these areas and the dura was kept intact. A 4mm diameter and 1mm tall plastic tube was glued in place above the craniotomy and the area was filled with a removable elastomer (Kwik-Cast, World Precision Instruments) to allow for access to the tissue for future experiments.

Behavior:

Prior to behavioral training, a custom stainless-steel head-post was attached posterior to lambda by placing a thin layer of cyanoacrylate adhesive on the skull, followed by a thin layer of dental acrylic (Metabond; C&B Associates). Following recovery, mice were head-fixed and placed within the behavioral training setup consisting of two 2mm diameter lick spouts placed 5mm apart and two 2mm diameter air-puff tubes that were directed at the C row of whiskers. The lick spouts were connected to a custom capacitive lick sensor circuit that recorded time and duration of licks at 200 Hz. Air-puff intensities were

calibrated such that whisker deflection was apparent under high-speed video monitoring without signs of freezing or startle behavior from the mouse.

Behavioral Task:

Animal training protocols and behavioral paradigm are adapted from previously reported procedures (Guo et al., 2014b). The behavioral paradigm is illustrated in Figure 1A. Left and right air-puff/lick trials were selected pseudo-randomly such that the probability of a right/left trial was adjusted based on the ratio of left/right rewarded trials (e.g. for the trial history of the current session consisting of 8 correct right trials and 4 correct left trials, the probability that the next trial would be left was set to right rewards/total rewards = 66%). Each trial was made up of 3 discrete intervals: a “pre-stimulus” period, a “sensory” period where mice received either a left or right air-puff for 1-1.5 s, followed by a 5 s “response” period where the mice lick the left or right spout to indicate which spout they believe will be rewarded and then consume the reward if the correct choice was made. Trials were separated by a variable inter-trial period. During the sensory period, mild non-aversive air-puff stimuli were directed through 2mm-diameter steel tubes towards the whiskers. The tubes were angled at 15 degrees away from the mouse center to isolate air-puff stimuli to the whiskers, avoiding the face of the mouse. The stimuli lasted for 1-1.5 s during training, though for optogenetic experiments during the withholding task, the sample period was held constant at 1 s.

Training for the behavioral task began after a minimum of 10 days following surgery and 5 days following the start of water restriction. Mice were handled during initial days of water restriction to acclimate with handling. On the first day of head-fixation and training,

mice were secured in the holder and placed in the behavioral setup with the two lick spouts positioned and centered in front of the mouth of the mouse. During the first day of training, mice could lick both the left or right spout and would receive a sucrose reward following licks at a minimum interval of 10 s. This was primarily used to acclimate the mouse with head-fixation and the positions of the lick spouts. The positions of the spouts were manually adjusted relative to the center of the mouth to promote equal licking of both lick spouts. During subsequent days of training, mice were transitioned to a task where the air-puffs signifying the rewarded spout were active, though the reward was automatically triggered ("Auto-Reward"). This typically lasted 1 day of training (~4 50 trial blocks) until the mice became acclimated to the puffs and would display anticipatory licking towards the correct lick spout before the reward was triggered, demonstrating that the mice had built the association between air-puff location and rewarded lick spout. In the next step of training, typically occurring on days 2-3, mice received the air-puffs and were then allowed to lick freely towards both spouts in the Response period and were only rewarded on licks to the correct spout ("Free-Lick"). Mice during this time learned to make the correct perceptive decision (signified by licking the rewarded spout exclusively during trials). Mice were then introduced to the 'anticipatory' variant of the task (Fig 2.1C). This variant of the task now penalized incorrect decision licks during the reward period by transitioning straight into a lengthened inter-trial delay period (6-10 s vs. 2-4 s for passed trials). To minimize licking outside of the response interval of the trials, each trial began with a pre-stimulus period where the mouse was required to withhold licking for at least 2-3 s before air-puff onset. Licking during the last second of this period led to a trial fail and mice were placed back in the inter-trial period awaiting the start of the next trial.

Training mice to perform the anticipatory task occurred over 2-5 days. Finally, mice were trained on the second variant of the task that required the mice to withhold licking ('withholding' variant) during the air-puff stimulus period until the offset of the air-puff (Fig 2.1D). To train mice to begin withholding licks during the air-puff stimulus period, any lick activity during the air-puff triggered an "early lick" fail and was penalized with an extended inter-trial period. At the beginning, the air-puff was shortened to 0.5 s and gradually increased in steps of 0.25 s until the mice were able to withhold licking and achieve 60% performance with a variable sample period duration between 1-1.5 s. This training typically took an additional 1-2 weeks. Of the 12 mice that were trained in the anticipatory variant of the task, 8 mice were able to subsequently learn the withholding variant.

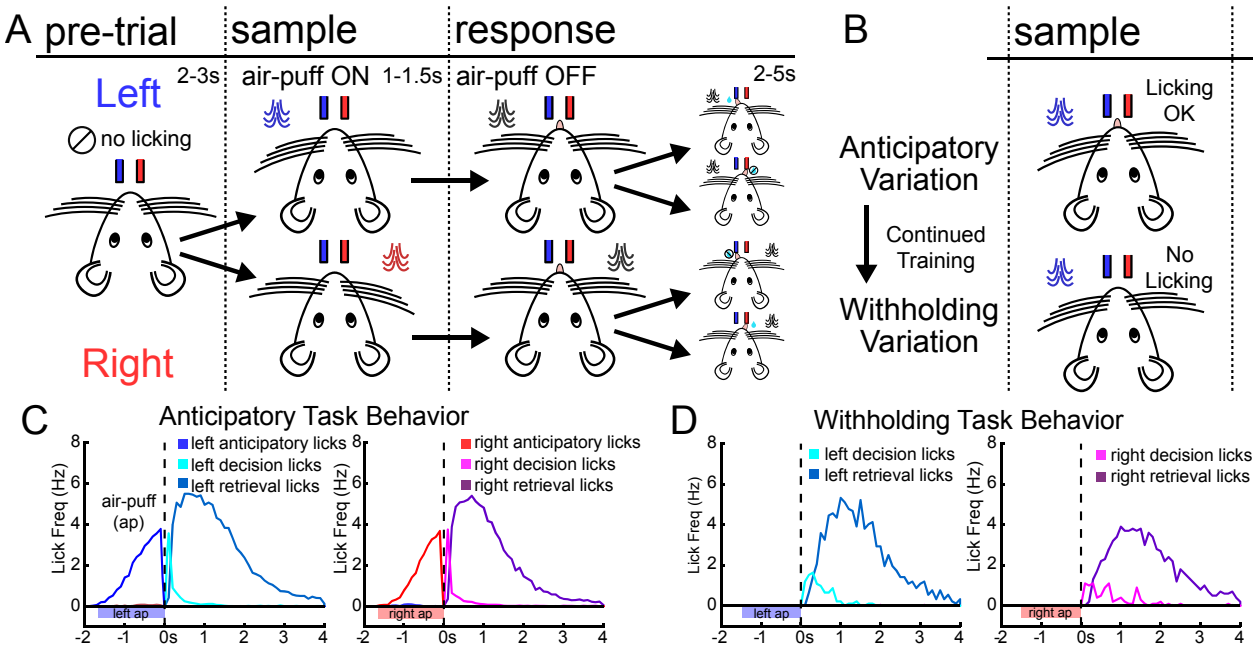

Figure 2.1 Mice learn to perform anticipatory and withholding variants of a forced choice licking task.

A. Illustration of the forced choice licking task. Each trial begins with a pre-trial period lasting 2-3 s where the mouse cannot lick either spout. During the sample period, an air-

puff is directed at either the left or right whiskers and remains on for 1-1.5 s. The response period begins after the offset of the air-puff and the first lick during this period is counted as the decision lick. If the decision lick is correct (towards the left spout for left air-puff or right lick spout for right air-puff) the mouse is provided a liquid reward from the correct spout. If the mouse does not provide a lick for the duration of the response period (2-5 s) or licks the incorrect spout no reward is provided. **B.** Mice were trained in two subsequent variations of the licking task. First, they are trained in the anticipatory variation where they are allowed to lick towards either spout during the air-puff in anticipation of the response period and potential reward delivery. After they have learned this task, the same mice are further trained in the withholding variation of the task where the must suppress licking during the duration of the air-puff. **C.** Average lick frequency traces for correct trials from mice performing the anticipatory variant of the task (N = 12 mice). **Left.** For left trials (n = 1151 trials), Mice begin to show anticipatory licking (middle blue) after the onset of the air-puff and the first lick after the offset of the air-puff is counted as the decision lick (light blue). The retrieval licks (dark blue) are the licks corresponding to the mouse retrieving the sucrose reward after a correct decision lick. **Right.** Same format as left trials, but instead showing right trials (n = 1098). Anticipatory, decision, and retrieval licks are depicted as middle red, light red, and dark red, respectively. **D.** Average lick frequency traces for correct trials from mice performing the withholding variant of the task (N = 8 mice). **Left.** For left trials (n = 397 trials), mice successfully withhold licking activity during the air-puff and once again the first lick after the offset of the air-puff is counted as the decision lick (light blue). The retrieval licks (dark blue) are the licks corresponding to the mouse retrieving the sucrose reward after a correct decision lick. **Right.** Same as for left, but now for right lick trials (n = 403 trials).

Optogenetic stimulation:

Before and after each session the output intensity of the light source (either LED or laser) was determined using an optical power meter and sensor (PM100D and S121C, ThorLabs). For SNr inhibition experiments, we used a 593nm yellow laser (Shanghai

Dream Lasers) collimated and coupled to a 200micron, 0.22 NA patch cable (Doric Lenses) leading to 8-12mW output from the fiber tip. For somatic SNr excitation we used a 470nm LED (Doric Lenses) coupled to the same patch cable with output power between 1-3mW from fiber tip. Finally, for SNr-BGMT terminal excitation, we used a 470nm blue laser (Shanghai Dream Lasers) with the same patch cables with output power between 8-12mW from the fiber tip. Trials with optogenetic stimulation were randomly intermixed with control trials for a total proportion between 25-50% of trials with light exposure. The optical stimulation trials were also all executed with a fixed 1 s air-puff duration in order to avoid inconsistent relations between stimulation and the timing of anticipatory licking.

Electrophysiology:

During surgical preparation, a craniotomy was made over the future right SNr/BGMT recording sites (-4 to 1mm AP, 0.5 to 2.5mm ML) and covered with Kwik-cast (WPI Inc.). The dura was left intact. A stainless-steel reference skull screw (#19010-10, Fine Science Tools) was placed over the contralateral sensory cortex. A 0.01” diameter steel wire was soldered between the screw and a gold pin to connect to the acquisition system during recording. The mice were allowed at least 3 days to recover. Following recovery, mice were acclimated to being head-fixed and recording sessions began (one session per day, 2 hours per session). Within the first session of head-fixation, mice showed no overt signs of stress and appeared relaxed. During recording, mice were maintained on a randomized interval reward paradigm where mice were provided with a sucrose reward via right or left lick spout every 30-60 s to encourage quiet wakefulness during the session. At the start of the session, the Kwik-cast cover over the craniotomy was removed. Custom optrodes

consisting of a 50-100 micron optic fiber (ThorLabs) attached 200-300 microns above a micro-electrode (FHC) were lowered into the SNr or BGMT. Raw signals (0.1–10 kHz band-pass filtered) were acquired at 20 kHz, amplified and digitized (RHD2132 headstage, Intan Technologies) and saved (RHD2000 Evaluation System/Interface Software, Intan Technologies). Once unit activity was detected in the SNr or BGMT, optical stimulation with either a yellow (593 nm) or blue (473 nm) laser was delivered for 1 or 2 s continuous pulses every 10 s to stimulate ARCH3 or ChR2 expressing neurons, respectively. For some recordings, the optic fiber was placed in the SNr with a separate electrode lowered in to the BGMT for recording activity downstream of the site of optogenetic stimulation. After each session, the craniotomy was covered with Kwik-cast and following the final recording session, the mouse was perfused with PBS followed by perfusion with 4% paraformaldehyde and 15% sucrose. The brain was then removed and transferred to a 4% paraformaldehyde/30% sucrose solution for later histological processing.

Data Analysis:

Analysis of behavioral and electrophysiological data was performed in MATLAB (MathWorks). Only behavioral sessions where baseline performance was above 60% were included in analysis. Behavioral trials in which the mouse licked <1 s before the start of the trial (onset of the air-puff) were caught and sent to inter-trial delay. These trials were rare (<2% in trained mice and excluded from analysis). Lick data was pre-processed to remove “artifact licks” (spout contacts shorter than 10 ms and contacts lasting longer than 200 ms typically caused by electrical noise and paw touches, respectively). Trials

where the decision lick (first lick during the response period) was classified as an artifact lick were removed from subsequent analyses. To calculate average lick frequencies for the various behavioral and experimental conditions, the onsets of lick contacts were marked and lick contacts across each trial were summed in 50 ms bins and divided by the length of the bin duration. Significance of the performance change in each optogenetic stimulation condition was determined using bootstrapping to account for variability across mice, sessions, and trials. We tested against the null hypothesis that the performance change caused by optogenetic stimulation was due to normal behavioral variability. In each round of bootstrapping, we replaced the original data set with a re-sampled set in which we resampled with replacement from: 1) animals; 2) sessions performed by each animal; and 3) the trials within each session. We then computed the change in performance on the re-sampled data set. Repeating this procedure 10,000 times produced a distribution of performance changes that reflected the behavioral variability. The P value observed performance change was calculated as the fraction of times bootstrapping produced an inconsistent performance change (for example, if a performance decrease was observed during optogenetic stimulation, the P value is the fraction of times a performance increase was observed during bootstrapping, one-tailed test). Error bars represent the +/- SEM generated from bootstrapping unless noted otherwise.

2.5 Results

Mice learn to perform 'anticipatory' and 'withholding' variants of a forced choice licking task.

In order to understand how the basal ganglia output influences directed licking behavior, we employed a forced choice behavioral task. In order to further parse the contributions of BG output on cognitive control of movement preparation and suppression, we trained the same groups of mice to perform two variations of this task: first, allowing mice to lick before the response window and anticipate the reward delivery, and second, a new variant that required mice to actively withhold licking until the onset of the response period (Fig 2.1B). By training the same mice to perform these task variations in sequence, we were able to parse the basal ganglia contributions to anticipation and initiation of licking movements (anticipatory task) as well as the control of movement preparation and suppression (withholding task).

Unilateral inactivation of the SNr biases towards contralateral licking behavior.

We began assessing the role of basal ganglia output in the anticipatory variant of the forced choice licking task using fast, reversible optogenetic inactivation of the SNr through nigral ARCH3 activation (Fig 2.2A). Cre-dependent ARCH3 was injected to the SNr of VGAT-cre mice that express cre in GABAergic populations. Extent of expression was well localized to the SNr with axon terminals extending towards known projection targets of the SNr such as the substantia nigra compacta, brainstem and thalamus (typical example shown in Fig 2.2A, right). In awake mice at rest, yellow (593nm) light stimulation of SNr neurons expressing ARCH3 abolished nearly all firing activity for the duration of

the stimulation (mean firing rates 17.2Hz baseline vs. 2.61Hz with ARCH inhibition, n = 10 single units, Fig 2.2BC). Following the offset of the optogenetic stimulation, the firing rate quickly returned to baseline levels. In behaving mice, we optogenetically manipulated the SNr unilaterally in the right hemisphere (Fig 2.2D). To examine the role of the SNr in anticipatory licking activity, the SNr was inhibited from 0.5 s before the offset of the air-puff until 0.5 s into the response period of the 'anticipatory' variant of the task. Inhibiting the right SNr during this period biased licking activity towards the contralateral direction (Fig 2.2E,H). A striking increase in ipsilateral air-puff trials with contralateral decision licks was observed and the overall success rate of ipsilateral trials was decreased (Fig 2.2H). Additionally, the decrease in successful trial performance with ipsilateral air-puffs was due to an increase in no-response trials (Fig 2.2H, $P<0.001$). In contrast, contralateral air-puff trials showed an increase in successes associated with a decrease in mistaken decision licks to the ipsilateral direction (5 mice, 36 sessions, $P<0.001$ (left), $P<0.001$ (right), bootstrap, Fig 2.2H). Importantly, successful trials showed the same amount and timing of anticipatory licking and the same consummatory lick rate in trials with air-puffs on either side with or without SNr inhibition (Fig 2.2F). This suggests that the lateralization of decision making towards the spout contralateral to SNr inhibition was not due to a slowing of movement, but rather a categorical change in the decision process. In control mice expressing injected with an EYFP virus without ARCH3, light stimulation had no effect on licking behavior or task performance (2 mice, 11 sessions, data not shown).

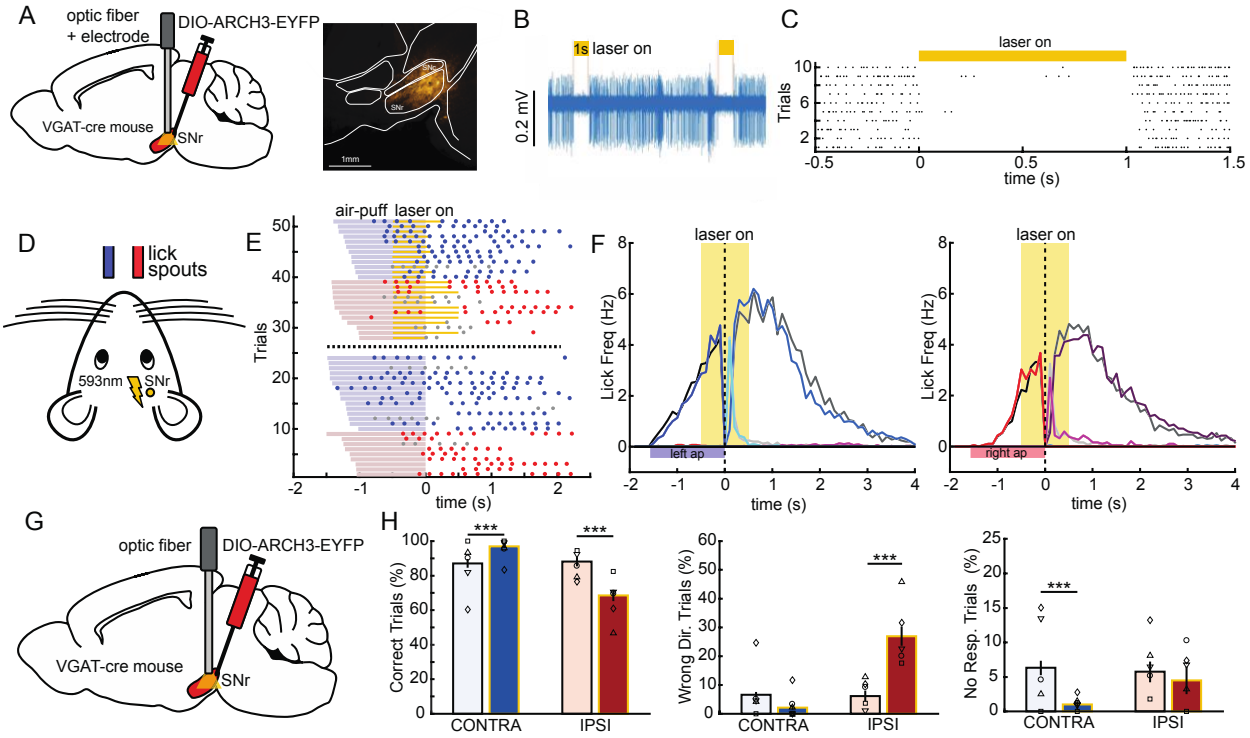

Figure 2.2 Unilateral inactivation of the SNr biases towards contralateral licking behavior

A. Diagram of optogenetic vector injection and optic fiber targeting. Cre-dependent AAV2-DIO-ARCH3-EYFP was injected in the right SNr of VGAT-cre transgenic mice and optic fiber attached to a microelectrode was lowered into SNr. Example of ARCH3-EYFP (yellow) expression in SNr (right). **B.** Example single-unit recording of an SNr neuron expressing ARCH3. 593nm laser stimulation silences firing activity for the duration of the light pulse and firing quickly resumes following the offset of the light stimulation. **C.** 10 stimulation trials aligned to the onset of stimulation that show the consistency of ARCH3 inhibition of SNr activity. **D.** Illustration showing mouse orientation with respect to ipsilateral (red) and contralateral (blue) lick spouts positioned in front of the mouse and optogenetic illumination through fiber implanted over the SNr. **E.** Example behavioral session showing licking activity for ipsilateral and contralateral optogenetic and baseline trials. Trials are arranged by optogenetic stimulation condition (stim trials top, baseline below) and length of air-puff presentation. Blue and red horizontal lines depict the presentation of the air-puff during the sample period and yellow lines are the periods of optogenetic SNr inhibition. In this example, optogenetic inhibition of right SNr disrupts

right (ipsilateral) licking behavior such that the mouse is biased towards licking the contralateral spout. **F.** Average lick frequency traces for correct trials with (colored lines) and without (gray lines) optogenetic SNr inhibition. For contralateral trials (n = 300 opto, 247 baseline, **left**) and ipsilateral trials (n = 185 opto, 301 baseline, **right**) mice show anticipatory licking activity towards the correct spout that increases until the start of the response period. Anticipatory licks are depicted by the middle colored line, followed by decision licks (light color) and retrieval licks (dark colored line). **G.** Behavioral effects of unilateral SNr optogenetic inhibition in the anticipatory task. **H.** Changes in performance between contralateral (blue) and ipsilateral (red), off (light) and on (dark) stimulation. Bar height represents mean across all sessions (n = 35 sessions), with shapes representing the mean for each mouse (5 mice). Error bars represent SEM (bootstrap, 10000 iterations) and p values based on bootstrap (see methods, ***p<0.001, **p<0.01, *p<0.05). **Left.** B Compared to interleaved baseline trials (light blue/red columns), licking performance during unilateral SNr inhibition (dark blue/red columns) produced a significant increase in the percent of contralateral trials correct (p<0.001) and significant decrease in the percent of ipsilateral trials correct (35 sessions, 5 mice). **Middle.** Optogenetic inhibition of the SNr caused a significant increase (P<0.001) in the percent of ipsilateral wrong direction fail trials (incorrectly lick contralateral spout during ipsilateral trials). **Right.** For contralateral lick trials, SNr inhibition significantly reduced the number of no response trials (P<0.001).

Unilateral inhibition of the SNr increases anticipatory licks and decreases reaction time towards the contralateral direction.

To test the hypothesis that SNr optogenetic inhibition interferes with the ability to withhold unwanted anticipatory movements, we activated ARCH during the 2nd half of the air-puff stimulus in the same mice after further training them to perform the ‘withholding’ variant of the task. A subset (3 of 5) of the mice were able to learn this variant of the task. After achieving 60% performance, we again tested the effect of optogenetic manipulation starting 0.5 s before the offset of the 1 s air-puff. This manipulation again lateralized the

execution of trials, but with additional features compared to the ‘anticipatory’ task (Fig 2.3). Ipsilateral air-puff trials again resulted in a significantly increased proportion of wrong direction decision licks (Fig 2.3E, P<0.01, bootstrap). Nevertheless, overall correct performance in the withholding version of the task was slightly increased in ipsilateral air-puff trials with optogenetic SNr inhibition (3 mice, 17 sessions, P=0.041, bootstrap), opposite of the observed change in the anticipatory task. By further examining the breakdown of failure types (Fig 2.3E), we found a reduction of failures due to early licking (P<0.001, bootstrap), indicating a higher success rate of suppressing anticipatory licking in the ‘withholding’ task when SNr was inhibited. In contrast, contralateral air-puff trials were associated with a significant increase in such early licks (P<0.01, bootstrap). This supports the hypothesis that inhibiting SNr output did not only have direct consequences for on the decision of lick direction, but also impaired the ability to withhold licks towards the direction contralateral to optogenetic stimulation and facilitated withholding to the ipsilateral direction. The average lick frequency traces from correct trials (Fig 2.3C) with optogenetic stimulation were again similar to control trials, suggesting that the licking process when initiated was not itself disrupted. However, success trials did show a shorter reaction time for contralateral licks and a longer reaction time for ipsilateral licks compared to baseline trials (Fig 2.3FG, P<0.01 (left), P<0.01 (right), bootstrap). This suggests that when the mice were able to withhold licking during the optogenetic stimulation, suppressing basal ganglia output biases preparation of movement or motor readiness, such that the mouse was able to respond more quickly to the contralateral spout and more slowly towards the ipsilateral direction. Control mice expressing EYFP in

the SNr but no ARCH (n = 2 mice, data not shown), showed no significant changes in trial outcomes between baseline and optogenetic stimulation trials.

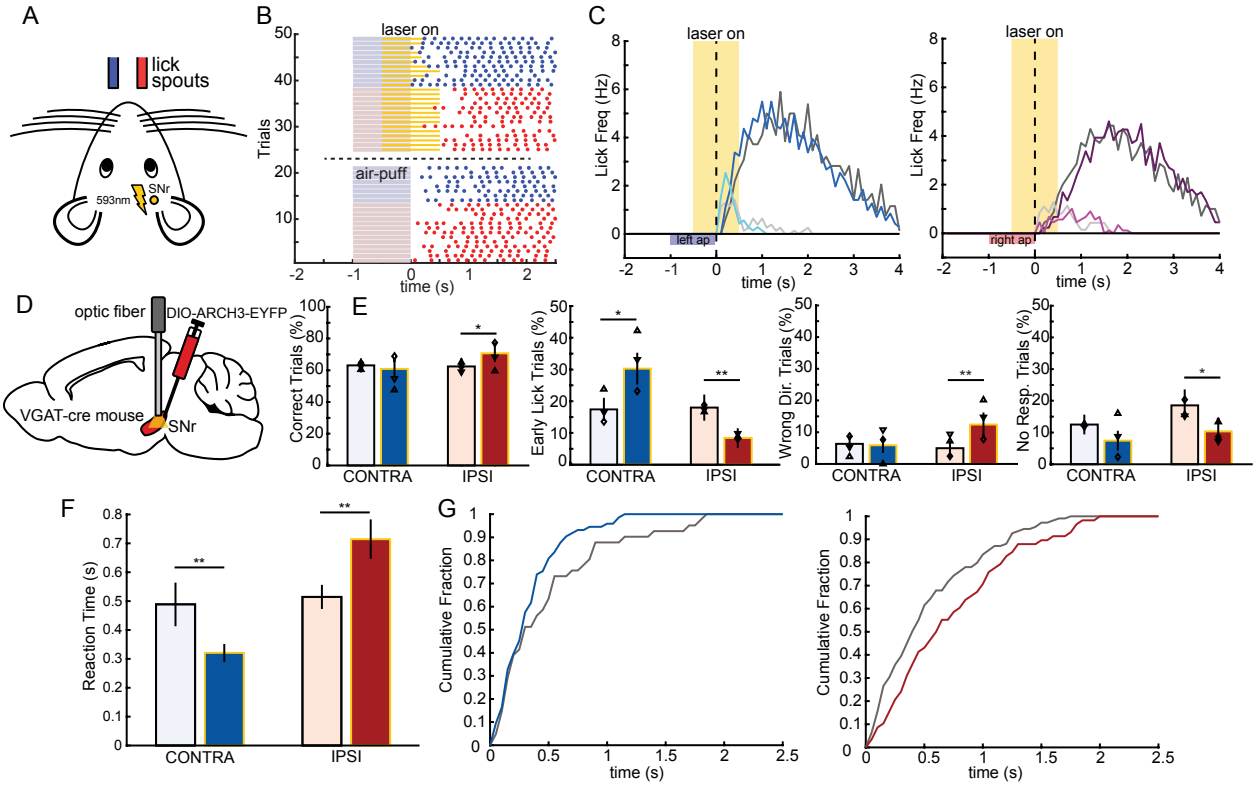

Figure 2.3 Unilateral inhibition of the SNr increases anticipatory licks and decreases reaction time towards the contralateral direction

A. Illustration showing mouse orientation with respect to ipsilateral (red) and contralateral (blue) lick spouts positioned in front of the mouse and optogenetic illumination through fiber implanted over the SNr. **B.** Example behavioral session showing trial-by-trial licking activity (early lick trials excluded) for ipsilateral and contralateral optogenetic and baseline trials. Trials are arranged by optogenetic stimulation condition (stim trials top, baseline below). Blue and red horizontal lines depict the presentation of the air-puff during the sample period and yellow lines are the periods of optogenetic SNr inhibition. In this example, optogenetic inhibition of SNr shifts lick onset for contralateral trials closer to the start of the response window appears to slightly delay ipsilateral licking behavior. **C.** Average lick frequency traces for correct trials with (colored lines) and without (gray lines) unilateral optogenetic SNr inhibition. For contralateral trials (n = 71 opto, 140 baseline, **left**) and ipsilateral trials (n = 89 opto, 127 baseline, **right**) mice show faster decision

licking activity on contralateral trials compared baseline lick decisions. Decision lick activity is depicted by the light shaded lines and retrieval licks by the dark shaded lines. **D.** Behavioral effects of unilateral SNr optogenetic inhibition in the withholding task. **E.** Changes in performance between contralateral (blue) and ipsilateral (red), off (light) and on (dark) stimulation. Bar height represents mean across all sessions (n = 16 sessions), with shapes representing the mean for each mouse (3 mice). Error bars represent SEM (bootstrap, 10000 iterations) and p values based on bootstrap (see methods, **p<0.01, *p<0.05). **Left.** Compared to baseline trials (light blue/red columns), licking performance during SNr inhibition (dark blue/red columns) produced a marginally significant increase in the percent of ipsilateral trials correct (p=0.0418, 16 sessions, 3 mice). **Middle Left.** Optogenetic inhibition of the SNr caused a significant increase in the percent of contralateral early lick fail trials (P=0.016) and a significant decrease in the percent of ipsilateral early lick trials (P<0.01). **Middle Right.** Optogenetic inhibition of the SNr increased the percentage of wrong direction ipsilateral trials (P<0.01). **Right.** SNr inhibition produced a slight trend and a marginally significant decrease percentage of no response trials for contralateral (P=0.23) and ipsilateral (P=0.048) trials, respectively. **H.** Mean reaction times for contralateral and ipsilateral trials with and without optogenetic SNr inhibition. Reaction times for contralateral trials were significantly decreased (P<0.01) and for ipsilateral trials were significantly increased (0.01) during SNr inhibition trials. **I.** Cumulative distribution plots showing the changes in the distribution of reaction times for contralateral (**left**) and ipsilateral (**right**) lick trials. Optogenetic stimulation trials are colored blue/red and baseline distributions are gray. The reaction time distribution shifts towards shorter reaction times for contralateral trials (**left**) and towards longer reaction times for ipsilateral trials (**right**).

Unilateral excitation of the SNr impairs both contra- and ipsilateral licking activity.

Since inhibiting basal ganglia output resulted in a contralateral bias in movement initiation and preparation, the classic model of basal ganglia rate coding leads to the prediction that increasing basal ganglia output would exert an opposite effect on licking activity, namely a reduction of correct decisions to lick in the direction contralateral to

optogenetic stimulation. To test this prediction, we used the neural activator, ChR2(ET/TC), to increase output activity from the SNr (Fig 2.4A). The extent of the ChR2(ET/TC) opsin expression was again well localized to the SNr and SNr terminals observable in the VM thalamus and brainstem (typical example shown in Fig 2.4A, right). In awake mice, blue light (473 nm) stimulation of the SNr using a 1 s continuous pulse increased the already highly active SNr to approximately double the baseline firing rate for the duration of the light stimulation (mean firing rate at baseline = 13.9Hz vs. opto = 49.9Hz, n = 8 single units, Fig 2.4BC). In mice performing the anticipatory variant of the behavioral task (n = 4 mice, 16 sessions, Fig 2.4D-F), exciting the right SNr suppressed both contralateral and ipsilateral licking activity for the duration of the optogenetic stimulation after anticipatory licking had already started in the first 0.5 s of the air-puff (Fig 2.4EF). Following the offset of the optogenetic perturbation, mice often resumed licking towards the correct spout (Fig 2.4EF), indicating that they remembered the air-puff direction through the period of movement inhibition. However, successful task performance significantly decreased in both contralateral and ipsilateral lick trials with ChR2 stimulation (Fig 2.4H, $P<0.01$ (left), $P<0.01$ (right), bootstrap). This decrease in performance was both a result of licking the wrong spout direction (Fig 2.4H, $P<0.01$ (left), $P<0.001$ (right), bootstrap) and not licking during the response period (Fig 2.4H, $P<0.05$ (right), bootstrap), suggesting a partial loss of the neural representation of lick direction during the motor inhibition. In control mice injected with an EYFP virus without ChR2, blue light stimulation had no effect on licking behavior or task performance (n = 2, data not shown). These results give a more complex picture of bidirectional motor control with SNr inhibition or excitation than predicted by the classic rate model. Particularly striking was

a complete bilateral lick cessation during ChR2 induced SNr rate increases, which was distinctly different from the lateralized effects of ARCH inhibition.

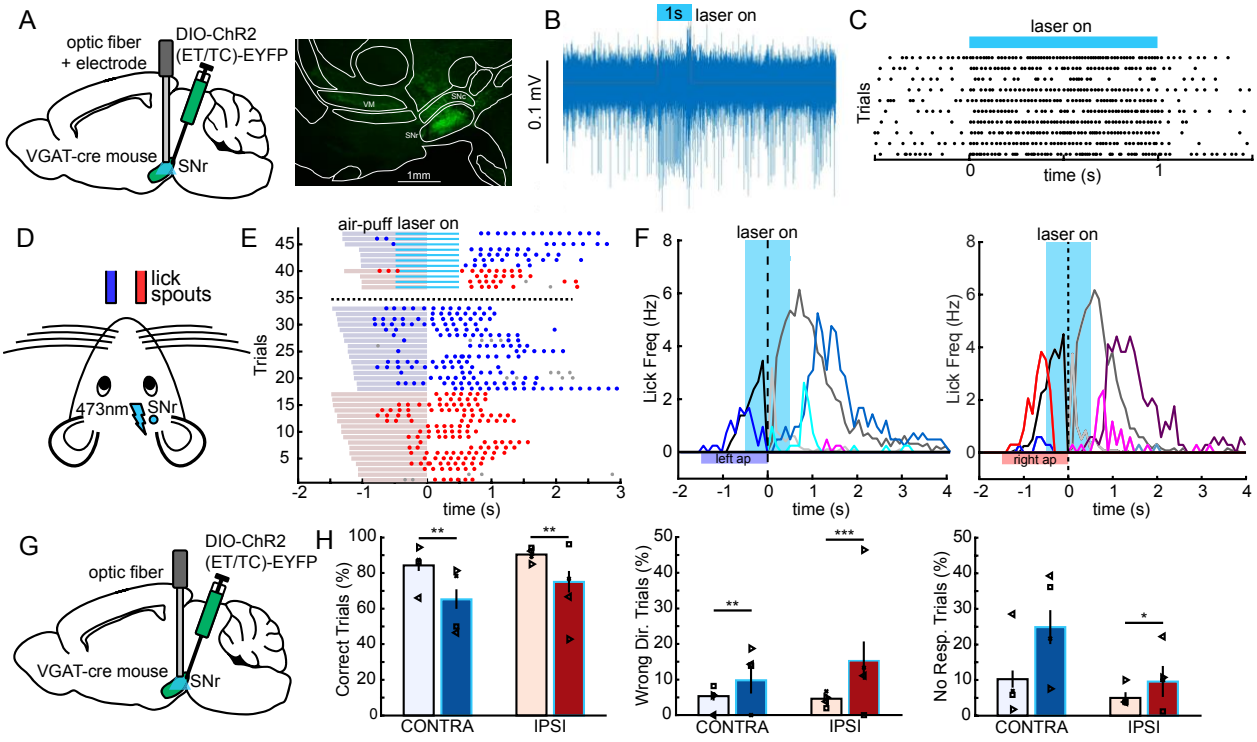

Figure 2.4 Unilateral excitation of the SNr impairs both contra- and ipsilateral licking activity

A. Diagram of optogenetic vector injection and optic fiber targeting. Cre-dependent AAV2-DIO-hChR2(E123T/T159C)-EYFP was injected in the right SNr of VGAT-cre transgenic mice and optic fiber attached to a microelectrode was lowered in to SNr. Example of ChR2(ET/TC)-EYFP expression (green) in SNr and axonal projections in VM thalamus and brainstem areas (right). **B.** Example multi-unit recording of an SNr neuron expressing ChR2(ET/TC). 473nm laser stimulation increases firing activity for the duration of the light pulse and firing quickly resumes following the offset of the light stimulation. **C.** 10 stimulation trials aligned to the onset of stimulation that show the excitation of SNr activity across trials (single unit isolated from recording shown in B). During ChR2 excitation, mean firing rate increased from 13.9Hz to 49.9Hz (n=10 neurons). Firing rate increase of example neuron is 14.4Hz vs. 46.3Hz during optogenetic stimulation. **D.** Illustration showing mouse orientation with respect to right and left lick spouts positioned in front of

the mouse and optogenetic illumination through fiber implanted over the SNr. **E.** Example behavioral session showing licking activity for ipsilateral and contralateral optogenetic and baseline trials. Trials are arranged by optogenetic stimulation condition (stim trials top, baseline below) and length of air-puff presentation. Blue and red horizontal lines depict the presentation of the air-puff during the sample period and light blue lines are the periods of optogenetic SNr excitation. In this example, optogenetic excitation of SNr disrupts licking behavior both ipsilateral and contralateral to the side of optogenetic stimulation, though licking resumes following the offset of the light. **F.** Average lick frequency traces for correct trials with (colored lines) and without (gray lines) optogenetic SNr excitation. For contralateral trials (n = 96 opto, 168 baseline, **left**) and ipsilateral trials (n = 103 opto, 153 baseline, **right**) mice show anticipatory licking activity towards the correct spout that increases until the start of the response period for baseline licking, though is suppressed following the onset of light stimulation for optogenetic trials. Anticipatory licks are depicted by the middle colored line, followed by decision licks (light color) and retrieval licks (darkest color). **G.** Behavioral effects of unilateral SNr optogenetic excitation in the anticipatory task. **H.** Changes in performance between contralateral (blue) and ipsilateral (red), off (light) and on (dark) stimulation. Bar height represents mean across all sessions (n = 16 sessions), with shapes representing the mean for each mouse (4 mice). Error bars represent SEM (bootstrap, 10000 iterations) and p values based on bootstrap (see methods, ***p<0.001, **p<0.01, *p<0.05). **Left.** Compared to baseline trials (light blue/red columns), licking performance during right SNr excitation (dark blue/red columns) produced a significant decrease in the percent of contralateral and ipsilateral trials correct (p<0.01, 16 sessions, 4 mice). **Middle.** Optogenetic excitation of the SNr caused a significant increase in the percent of wrong direction fail trials for both contralateral (P<0.01) and ipsilateral (P<0.001) trials. **Right.** For contralateral lick trials, SNr excitation showed a trend towards increase percentage of no response trials (P=0.094) and a marginally significant increase in no response trial percentage for ipsilateral lick trials (P<0.014).

Unilateral excitation of the SNr in 'withholding' task variant improves contralateral withholding of anticipatory licks and suppresses licking bilaterally.

A subset of the ChR2 expressing mice (3 of 4) were further trained to perform the withholding version of the task. In agreement with the results for the anticipatory task, licking was generally suppressed until after the offset of the optogenetic stimulation (3 mice, 11 sessions, Fig 2.5BC. Unlike for the anticipatory variant of the task, however, SNr excitation led to an increase in percent correct for contralateral trials (Fig 2.5E, $P<0.05$). While this effect seems opposite to our hypothesis, examining the failure outcomes shows that this change was driven primarily by a decrease in the percent of contralateral early lick fails (Fig 2.5E, $P<0.001$), indicating an improvement in the ability to withhold premature licking predominantly to the contralateral side. Optogenetic excitation of the SNr also led to an increase in no response trials towards the direction contralateral to optogenetic stimulation (Fig 2.5E, $P<0.05$) and a trend towards decision licks in the wrong direction (Fig 2.5E, $p=0.071$). However, wrong decision licks were much reduced compared to the anticipatory variant of the task, suggesting that the additional training during the withholding stage had strengthened the neural representation of air-puff direction and made it more resilient to the ChR2 induced period of lick suppression. On trials where the mice did lick following the offset of the optogenetic stimulation, reaction time was significantly increased compared to control trials for both the ipsilateral and contralateral lick directions (Fig 2.5FG) due to the suppression of licking in the initial 0.5 s after air-puff offset when light stimulation was still on. Mice expressing EYFP, but no ChR2 in SNr did not demonstrate any changes in licking performance (n=2, data not

shown). Overall, these results give further support to the strong bilateral motor suppression of unilateral SNr excitation.

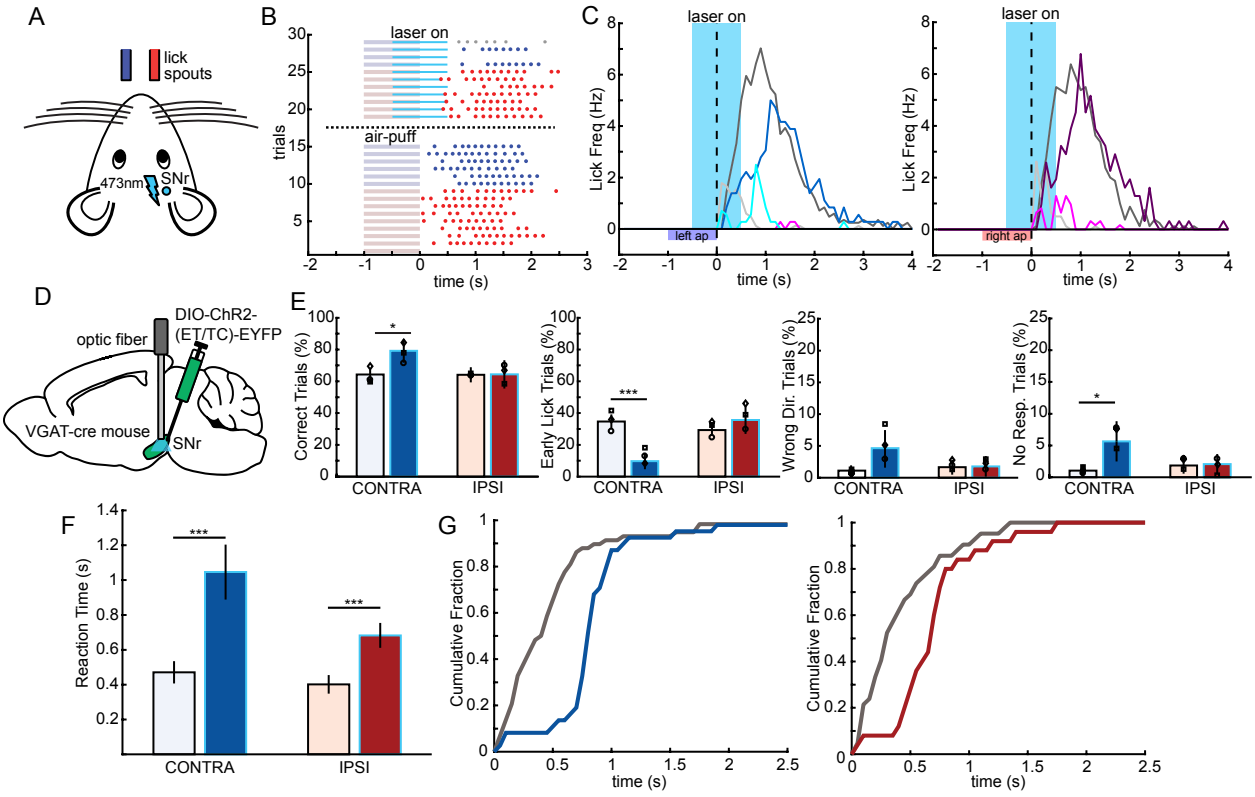

Figure 2.5 Unilateral excitation of the SNr increases reaction time towards both lick directions

A. Illustration showing mouse orientation with respect to right and left lick spouts positioned in front of the mouse and optogenetic illumination through fiber implanted over the right SNr. **B.** Example behavioral session during the withholding task showing trial-by-trial licking activity (early lick trials excluded) for ipsilateral and contralateral optogenetic and baseline trials. Trials are arranged by optogenetic stimulation condition (stim trials top, baseline below). Blue and red horizontal lines depict the presentation of the air-puff during the sample period and light blue lines are the periods of optogenetic SNr excitation. In this example, optogenetic excitation of right SNr delays lick onset for both ipsilateral and contralateral licking behavior. **C.** Average lick frequency traces for correct trials with (colored lines) and without (gray lines) optogenetic right SNr excitation. For contralateral trials (n = 63 opto, 132 baseline, **left**) and ipsilateral trials (n = 53 opto, 127 baseline, **right**) mice show delayed decision licking activity towards both spouts

compared to baseline lick decisions. Decision lick activity is depicted by the light shaded lines and retrieval licks by the dark shaded lines. **D.** Behavioral effects of unilateral SNr optogenetic excitation in the withholding task. **E.** Changes in performance between contralateral (blue) and ipsilateral (red), off (light) and on (dark) stimulation. Bar height represents mean across all sessions (n = 12 sessions), with shapes representing the mean for each mouse (3 mice). Error bars represent SEM (bootstrap, 10000 iterations) and p values based on bootstrap (see methods, ***p<0.001, **p<0.01, *p<0.05). **Left.** Compared to baseline trials (light blue/red columns), licking performance during SNr excitation (dark blue/red columns) produced a significant decrease in the percent of contralateral and ipsilateral trials correct (p=0.023, 12 sessions, 3 mice). **Middle Left.** Unilateral optogenetic excitation of the SNr caused a significant decrease in the percent of contralateral early lick fail trials (P<0.001). **Middle Right.** Optogenetic excitation SNr did not produce any changes in direction licking behavior. **Right.** For contralateral lick trials, SNr excitation produced a significant increase percentage of no response trials (P=0.014). **H.** Mean reaction times for contralateral and ipsilateral trials with and without optogenetic SNr excitation. Reaction times for both contralateral and ipsilateral trials were significantly during SNr excitation (P<0.001). **I.** Cumulative distribution plots showing the changes in the distribution of reaction times for contralateral (**left**) and ipsilateral (**right**) lick trials. Optogenetic stimulation trials are colored blue/red and baseline distributions are gray. Both ipsilateral and contralateral lick responses are primarily delayed until after the offset of the optogenetic stimulation, shifting the distribution towards the ipsilateral spout compared to baseline responses.

Unilateral excitation of nigrothalamic terminals in BGMT biases licking towards the ipsilateral direction in the anticipatory task variant.

The differences in effects described for somatic SNr inhibition and excitation may be due to descending projections from the SNr towards the brainstem as well as ascending projections to BGMT. To begin to resolve the functional differences between these projection pathways, we selectively targeted the ascending pathway from the SNr

to the BGMT. To achieve this, we stimulated ChR2 expressing SNr terminals in BGMT in the same mice used for somatic stimulation through a second fiber implanted over the BGMT. In contrast to somatic stimulation we found that SNr terminal stimulation in BGMT in the anticipatory variant of the task suppressed only contralateral licking behavior and did not affect ipsilateral licking (4 mice, 25 sessions, Fig 2.6BC). Successful trial execution was significantly impaired for contralateral lick trials but remained unchanged for ipsilateral licks (Fig 2.6E, P<0.001 (left), bootstrap). This change in performance was due to an increase of contralateral air-puff failed trials both by not responding (Fig 2.6E, P<0.001, bootstrap) as well as licking the wrong direction (Fig 2.6E, P<0.001, bootstrap). This last effect in particular was in stark contrast to the results with somatic SNr excitation, suggesting that the ascending thalamic pathway leads to a lateralized effect on motor preparation, whereas descending outputs may globally suppress the brainstem lick pattern generator.

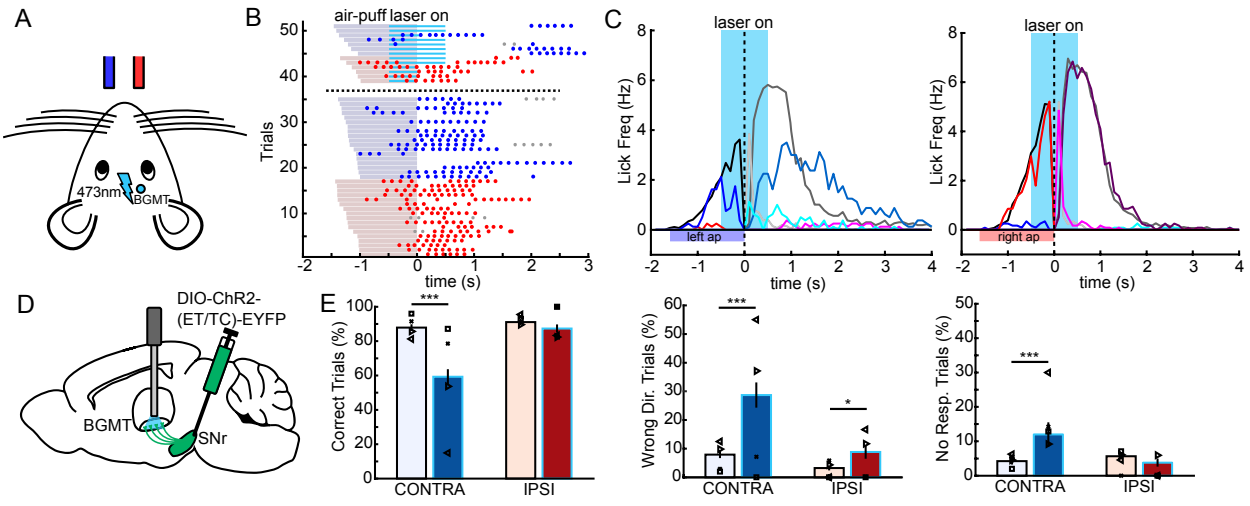

Figure 2.6 Unilateral excitation of SNr projections to the BGMT biases licking towards the ipsilateral direction

A. Diagram showing mouse orientation with respect to right and left lick spouts positioned in front of the mouse and optogenetic illumination through fiber implanted over the BGMT.

B. Example behavioral session showing licking activity for ipsilateral and contralateral optogenetic and baseline trials during the anticipatory task. Trials are arranged by optogenetic stimulation condition (stim trials top, baseline below) and length of air-puff presentation. Blue and red horizontal lines depict the presentation of the air-puff during the sample period and blue lines are the periods of optogenetic SNr-BGMT excitation. In this example, optogenetic excitation of right SNr-BGMT projections disrupts only contralateral licking behavior during optogenetic stimulation trials. **C.** Average lick frequency traces for correct trials with (colored lines) and without (gray lines) optogenetic right SNr-BGMT terminal excitation. For contralateral trials (n = 95 opto, 310 baseline, **left**) and ipsilateral trials (n = 128 opto, 297 baseline, **right**) mice show anticipatory licking activity towards the correct spout that increases until the start of the response period for baseline licking, though anticipatory licking is suppressed following the onset of light stimulation for contralateral optogenetic trials. Anticipatory licks are depicted by the middle colored line, followed by decision licks (light color) and retrieval licks (dark color). **D.** Behavioral effects of unilateral SNr-BGMT optogenetic excitation in the anticipatory task. **E.** Changes in performance between contralateral (blue) and ipsilateral (red), off (light) and on (dark) stimulation. Bar height represents mean across all sessions (n = 25 sessions), with shapes representing the mean for each mouse (4 mice). Error bars represent SEM (bootstrap, 10000 iterations) and p values based on bootstrap (see methods, ***p<0.001). **Left.** Compared to baseline trials (light blue/red columns), licking performance during right SNr-BGMT terminal excitation (dark blue/red columns) produced a significant decrease in the percent of contralateral trials correct (p<0.001, 25 sessions, 4 mice). **Middle.** Optogenetic excitation of the right SNr-BGMT terminals caused a significant increase in the percent of contralateral (P<0.001) and ipsilateral (P=0.02) wrong direction fail trials. **Right.** For contralateral lick trials, SNr-BGMT terminal excitation caused a significant increase in the percentage of no response trials (P<0.001).

Unilateral excitation of nigrothalamic terminals in BGMT in the withholding task variant facilitates suppression and increases reaction time for contralateral licking.

Lastly, we again compared changes in the withholding task to those in the anticipatory variant. Licking activity was similarly impaired towards the contralateral direction while it remained intact towards the ipsilateral direction (3 mice, 13 sessions, Fig 2.7BC). The proportion of successful task performance in the 'withholding' variant was almost unchanged with SNr-BGMT terminal stimulation. However, there was a significant decrease in withholding failures (early lick trials) towards the contralateral direction (Fig 2.7E, $P<0.05$, bootstrap). This suggests SNr output to BGMT also contributes to the ability of the mouse to withhold movement, though only towards the contralateral direction. In this version of the task, lick reaction times in the response period to the contralateral direction were significantly longer than baseline (Fig 2.7FG, $P<0.001$, bootstrap). Ipsilateral reaction times were not significantly changed. This supports the conclusion that exciting SNr output specifically in BGMT exerted a lateralized influence on motor preparation and initiation.

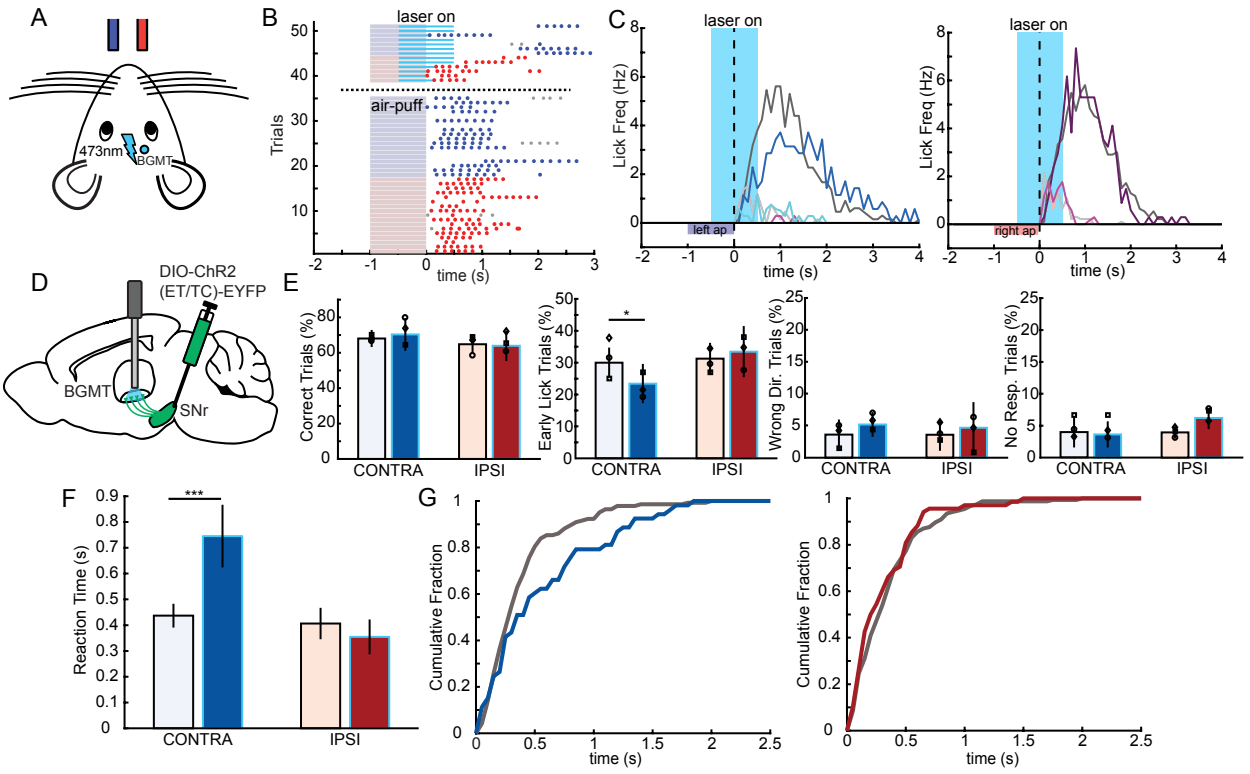

Figure 2.7. Unilateral excitation of nigrothalamic terminals facilitates suppression and increases reaction time for contralateral licking

A. Illustration showing mouse orientation with respect to right and left lick spouts positioned in front of the mouse and optogenetic illumination through fiber implanted over the SNr. **B.** Example behavioral session during the withholding task showing trial-by-trial licking activity (early lick trials excluded) for ipsilateral and contralateral optogenetic and baseline trials. Trials are arranged by optogenetic stimulation condition (stim trials top, baseline below). Blue and red horizontal lines depict the presentation of the air-puff during the sample period and light blue lines are the periods of optogenetic SNr-BGMT terminal excitation. In this example, optogenetic excitation of right SNr projections to BGMT delays lick onset of contralateral licking behavior. **C.** Average lick frequency traces for correct trials with (colored lines) and without (gray lines) optogenetic right SNr-BGMT terminal excitation. For contralateral trials (n = 87 opto, 245 baseline, **left**) and ipsilateral trials (n = 91 opto, 197 baseline, **right**) mice show similar licking activity during baseline trials, though during left optogenetic trials, decision and retrieval licking appears delayed. Decision lick activity is depicted by the light shaded lines and retrieval licks by the dark

shaded lines. **D.** Behavioral effects of unilateral SNr-BGMT optogenetic terminal excitation in the withholding task. **E.** Changes in performance between contralateral (blue) and ipsilateral (red), off (light) and on (dark) stimulation. Bar height represents mean across all sessions (n = 13 sessions), with shapes representing the mean for each mouse (3 mice). Error bars represent SEM (bootstrap, 10000 iterations) and p values based on bootstrap (see methods, *p<0.05). **Left.** Compared to baseline trials (light blue/red columns), performance in optogenetic stimulation trials (dark blue/red columns) remains unchanged. **Middle Left.** Unilateral optogenetic excitation of the SNr projections to BGMT caused a significant decrease in the percent of contralateral early lick fail trials (P=0.023). **Middle Right.** Optogenetic excitation of SNr-BGMT did not produce any changes in percentage of wrong direction fail trials. **Right.** No response fail percentages were not altered by optogenetic stimulation of SNr projections to the BGMT. **H.** Mean reaction times for contralateral and ipsilateral trials with and without optogenetic SNr excitation. Reaction times for contralateral, but not ipsilateral trials were significantly increased during SNr excitation (P<0.001). **I.** Cumulative distribution plots showing the changes in the distribution of reaction times for contralateral (**left**) and ipsilateral (**right**) lick trials. Optogenetic stimulation trials are colored blue/red and baseline distributions are gray. Contralateral lick responses are delayed during optogenetic stimulation trials (**left**) while the response distribution for ipsilateral trials is unchanged compared to baseline (**right**).

2.6 Discussion

Our results demonstrate that optogenetic excitation and inhibition of basal ganglia output from the SNr in mice drives lateralized and opposing influences on the control of directional licking. Specifically, unilateral inhibition of the SNr with ARCH activation leads to a decrease in performance of ipsilateral but an improvement in contralateral lick choices. The opposite performance effects were observed with activation of SNr terminals in BGMT (summarized in Fig. 2.8A,C). These findings indicate that the SNr firing rate decreases/increases are bidirectionally controlling lick direction choice. In mice performing a similar directional licking task, suppressing activity in either the VM thalamus, which is a major component of BGMT, or the ALM premotor cortex, through either optogenetic or muscimol inactivation selectively disrupts contralateral licking, while leaving ipsilateral licking unaffected (Chen et al., 2017, Guo et al., 2017, Svoboda and Li, 2018). Our results therefore suggest that this thalamo-cortical motor planning process can be gated by basal ganglia output in agreement with traditional rate coding concepts of basal ganglia – cortical loops (Alexander et al., 1990). According to this model, inhibiting the SNr with ARCH unilaterally leads to disinhibition of ipsilateral BGMT, and thus allows ipsilateral thalamocortical activity to develop and cause contralateral movement initiation. The opposite is expected for unilateral activation of the SNr with ChR2, and was observed in our study, but only if SNr terminals were activated in BGMT. Direct unilateral activation of GABAergic SNr cell bodies resulted in strong bilateral movement inhibition instead (Fig. 2.8B). A recent set of studies have implicated the SNr projection to the superior colliculus (the nigrotectal pathway) in the control of non-directional licking behavior (Rossi et al., 2016, Toda et al., 2017). In Rossi et al. 2016,

researchers optogenetically bilaterally excited SNr projections at the level of the superior colliculus which led to diminished, though not completely suppressed, licking towards the lick spout positioned in front of the mouse. Our results showing that unilateral excitation of the SNr near completely suppressed licking could therefore be explained via projections to the SC. Consistent with this explanation, anatomical tracing experiments demonstrate that the SNr projects to SC bilaterally, while projections to the thalamus are ipsilateral (Deniau and Chevalier, 1992, Liu and Basso, 2008). Why somatic inhibition of the SNr did not facilitate licking bilaterally (opposite of SNr excitation) requires further examination but may suggest that the thalamic pathway is more susceptible to disinhibition than the nigro-collicular pathway.

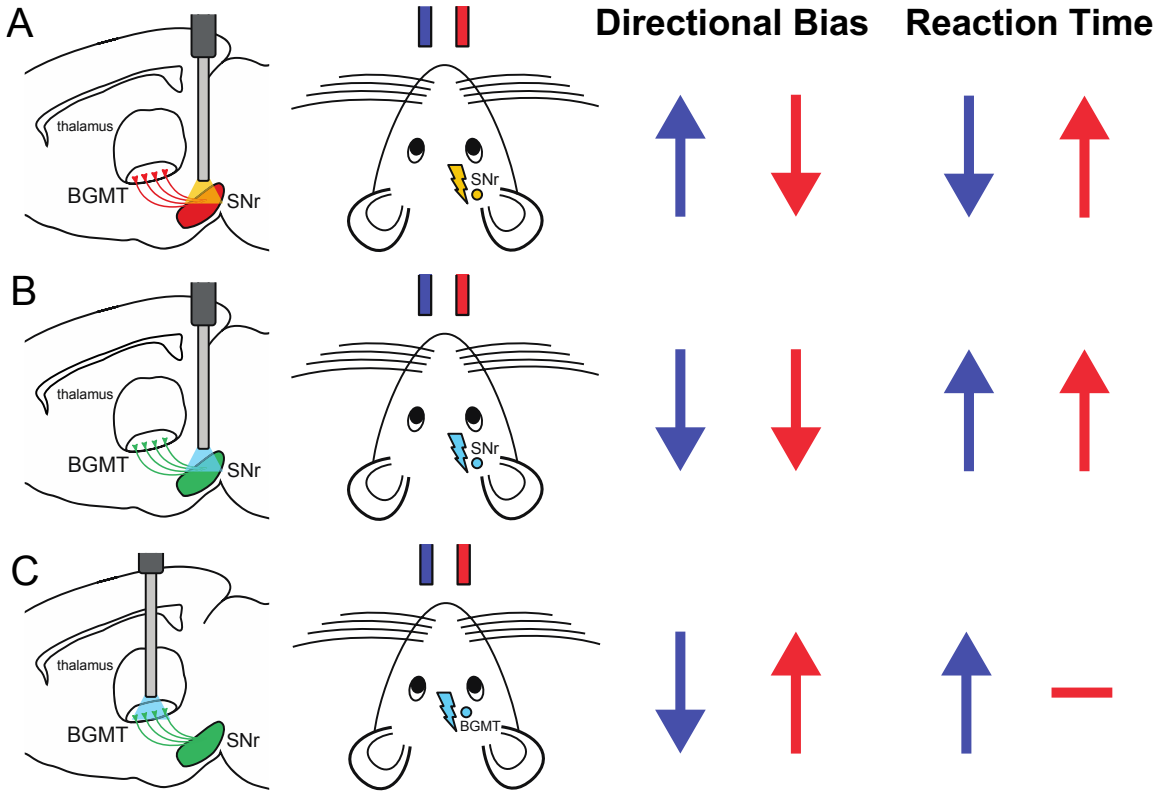

Figure 2.8. Summary of optogenetic manipulations and main results

A. Diagram depicting unilateral optogenetic inhibition of SNr expressing ARCH3 and orientation of lick spouts and mouse. SNr optogenetic inhibition is contralateral to the blue

spout (left) and ipsilateral to the red spout (right). Optogenetic inhibition of the SNr produced a change in directional bias towards the contralateral spout (blue arrow) and away from the ipsilateral lick spout (red arrow). With respect to reaction time, optogenetic SNr inhibition reduced the reaction time towards the contralateral spout (blue) and increased time to respond towards the ipsilateral spout (red). **B.** Same as A., but for experiments with unilateral optogenetic excitation of SNr expressing ChR2(ET/TC). Optogenetic excitation of the SNr produced a bilateral change in directional bias; decreasing licking activity towards both the contralateral (blue) and ipsilateral (red) lick spouts. Additionally, optogenetic SNr excitation increased reaction times towards both contralateral and ipsilateral spouts. **C.** Same as A. and B., but for terminal excitation of SNr projections to the BGMT. Optogenetic excitation of SNr terminals in the BGMT produced a change in directional bias towards the ipsilateral spout (red) and away from the contralateral spout (blue). Excitation of SNr projections to BGMT also increased the reaction time towards the contralateral spout (blue) and did not affect reaction times towards the ipsilateral spout (red).

An important feature of our behavioral task training was the use of two different task variants that entailed different cognitive demands (Fig 2.1). The 'anticipatory' task mice were taught first, did not require lick withholding during air-puff delivery and indeed we observed a steady increase in anticipatory licking activity as the start of the response period was approached. This licking was in in the direction of the correct target (Fig 2.1C), therefore revealing the completion of air-puff stimulus evaluation and motor preparation as early as 1 s before air-puff offset (Fig 2.1C). Importantly, the prevalence of anticipatory licking was not affected by nigral ARCH activation (Fig. 2.2F), suggesting that tonic nigral inhibition in BGMT during reward anticipation was low when anticipatory licking was allowed, and therefore disinhibition had little effect on anticipatory licking. In contrast, a slowing of anticipatory licking was seen upon the onset of ChR2 activation of SNr

terminals in BGMT for contralateral trials with a subsequent slowing of contralateral reward licks as well (Fig. 2.6C). This finding indicates that increased nigral activity in BGMT results in a lateralized slowing of movement. Several previous studies have shown that the basal ganglia exert lateralized control of motor circuits (Sakamoto and Hikosaka, 1989, Hikida et al., 2010, Tai et al., 2012, Dominguez-Vargas et al., 2017) and our results support this general concept. A slowing in licking is congruent with both the concepts of direct involvement of basal ganglia output in controlling movement velocity (Barter et al., 2015, Yttri and Dudman, 2016) or motor vigor (Dudman and Krakauer, 2016).

The 'withholding' variant of our lick task required mice to actively suppress licks for the duration of the air-puff (Fig 2.1D). By adding this withhold demand, we were able to investigate the role of the SNr in movement suppression and movement initiation by measuring early lick fail trials and reaction time following the offset of the air-puff, respectively. All mice preferred to lick in anticipation of directional choice behavior during initial training, and the suppression of this licking clearly required a cognitive effort. After the mice had learned this suppression, unilateral optogenetic inhibition of the right SNr suppressed anticipatory licking towards the ipsilateral lick spout, while it increased such licking to the contralateral spout (Fig. 2.3E). As described above, the same optogenetic inhibition of SNr activity in the same mice had not affected anticipatory licking in the 'anticipatory' variant of our task. In combination, these findings suggest that the mouse used increased nigral output to suppress anticipatory licking in the 'withholding' variant, and this increased nigral activity was inhibited with ARCH activation, which thus effectively undid the withhold learning. In addition, unilateral excitation of SNr terminals in the right BGMT now suppressed licking contralaterally (Fig 2.6E). These findings are

in agreement with the active suppression of movement as a function of the indirect pathway in the basal ganglia (Nambu et al., 2002, Ozaki et al., 2017). Movement suppression is hypothesized to result from an activation of D2 receptor expressing GABAergic striatal projection neurons (SPNs), which then leads to increased activity in SNr and GPi via inhibition of the external pallidum (GPe) (Albin et al., 1989, Nambu et al., 2002). Cortical activity elicits excitation of GPi neurons more widely than inhibition, which is congruent with a center surround model of movement initiation and suppression (Ozaki et al., 2017). Optogenetic activation of D1 or D2 SPNs also supports the general principle that the indirect pathway causes movement suppression through SNr rate increases (Freeze et al., 2013), though optogenetic activation of either D1 or D2 SPNs resulted in excitation or inhibition of different SNr neurons.

Many studies have implicated the rodent SNr in the control of behavior other than licking, including for example locomotion (Roseberry et al., 2016) and head movement (Schmidt et al., 2013, Barter et al., 2015). To determine whether our manipulations inadvertently triggered extraneous movements, we recorded high-speed video of the mouse pupil and face for a subset of trials across mice. Interestingly, we did not observe any movements (including eye, whisker, fore-limb) associated with our optogenetic manipulations (data not shown). This suggests that the behavioral impact seen with SNr optogenetic manipulations may be limited to behaviors trained in a reward-based task.

The BGMT with VM as its core component is well situated anatomically to influence ipsilateral cortical activity, with single-cell tracing studies in rodents depicting large projections branching across ipsilateral layer 1 of sensory and motor cortices (Kuramoto et al., 2009, Kuramoto et al., 2015). We showed here that activity in BGMT could be

changed by inhibitory basal ganglia input and through this effect switch lateralized cortical decision-making processes about whisker stimulation dependent directional licking. Control of this behavior has previously been linked to a VM – ALM thalamocortical feedback loop (Li et al., 2015, Chen et al., 2017, Guo et al., 2017). Further, we also showed that lick movement vigor and reaction time can be impacted as well. The widespread axonal efferents of BGMT suggest that similar effects are likely for a multiplicity of other behaviors, though we saw no impact on spontaneous behavior. Because it is unlikely that a uniform optogenetic inhibition or excitation across SNr codes for any specific behavioral event, it seems most likely that our optogenetic stimulation interfered with endogenous population coding, which in a highly trained mouse will be quite specific to the trained behavior. However, even for certain behavioral events such as a stop-signal in a countermanding task, a relatively uniform activity increase has been observed across SNr neurons (Schmidt et al., 2013). The detailed mechanism by which SNr mediated activity changes in BGMT impact cortical decision making remains unclear, especially since layer 1 is far removed from the activity of cell bodies in L5/6 providing output from cortex. A likely candidate mechanism for amplifying such distal input is given by active distal dendritic properties such as NMDA spikes in L2/3 (Palmer et al., 2014) and calcium spike dependent BAC firing in L5 pyramidal neurons (Larkum et al., 1999, 2001, Larkum and Zhu, 2002). Similar active properties are also seen in the apical dendrites of L6 pyramidal neurons (Ledergerber and Larkum, 2010), which have a strong projection back to BGMT (Yamawaki and Shepherd, 2015). In addition, BGMT input could also act on L1 interneurons (Cruikshank et al., 2012), which provide a powerful inhibition of pyramidal neuron dendrites (Palmer et al., 2012, Palmer et al., 2013). The exact impact

of BGMT input on these mechanisms and its integration into cortico-cortical information processing awaits future studies.

Chapter 3: Wide-Field Imaging of Spatiotemporal Cortical Voltage Activity Underlying Arousal During Spontaneous Behavior

3.1 Abstract

Changes in pupil diameter have long been associated with cognitive aspects of neural processing and arousal (Kahneman and Beatty, 1966). Recent studies have further demonstrated that the pupil closely resembles sub-threshold voltage activity and arousal levels in awake mice. While it is clear that the pupil provides important insights in neural processing as a proxy for arousal, it is unknown how arousal signals as measured by pupil diameter are represented spatially and temporally within spontaneous changes in cortical activity. To uncover the dynamics of the functional coupling of cortical activity and pupil diameter, we recorded wide-field voltage activity across the extent of dorsal cortex while acquiring video of the face and pupil in mice expressing the voltage indicator, VSFP-Butterfly 1.2 in excitatory cortical neurons. We found that pupil diameter is tightly coupled to global changes in cortical voltage with distinct coupling patterns across different cortical regions and frequency components. This coupling is dependent on both frequency and the spatial location in cortex, with lower frequency signals more strongly related to pupil diameter changes and medial areas of the sensory-motor cortex most strongly coupled with arousal especially during periods of orofacial movements. These insights further our understanding of how different areas of cortex are coupled to alertness or arousal related signals and the temporal properties where this coupling occurs.

3.2 Introduction

The state of brain activity and behavior are constantly varying across both fast and slow timescales. Two of the main contributors to the ongoing animal state are changes in arousal and animal movement. Many studies have used pupil dilations as a measure for animal arousal, such that heightened arousal would lead to an increase in pupil diameter and small pupil diameter would characterize periods of low arousal (Reimer et al., 2014, McGinley et al., 2015a, McGinley et al., 2015b, Vinck et al., 2015, Shimaoka et al., 2018). Additionally, animal movements, often measured by periods of locomotion has also been observed to influence animal arousal with periods of running leading to long dilations in pupil diameter and periods of desynchronized neural activity (Niell and Stryker, 2010, Polack et al., 2013, McGinley et al., 2015b, Vinck et al., 2015, Shimaoka et al., 2018). Recent work has shown that arousal changes due measured primarily via locomotion can have differential effects across sensory and motor cortices with each area linked to arousal through complex temporal profiles (Shimaoka et al., 2018). While locomotion provides an insightful measure of arousal, it provides an incomplete picture, as pupil fluctuations relating to arousal changes can be observed in the absence of locomotion. Additionally, there appears to be different frequency components of arousal, potentially mediated by differential influence of the cholinergic and adrenergic neuromodulatory systems (Reimer et al., 2016). In the anesthetized mouse, pupil dilations have been found to be differentially coupled to cortical electrocorticogram activity across different frequencies, though the frequency dependence of cortical coupling to arousal in the awake cortex are unclear (Yuzgec et al., 2018).

In order to address these questions, we used wide-field imaging to record changes in membrane voltage activity in mice expressing a voltage-sensitive fluorescent protein (VSFP) Butterfly 1.2 in excitatory neurons across the dorsal cortex in awake, spontaneously behaving mice (Carandini et al., 2015). By simultaneously monitoring changes in pupil diameter and orofacial movements we were able to parse the spatial and temporal contributions of arousal to cortical activity. We found that the pupil is differentially coupled to cortex based on the frequency with lower frequencies exhibiting stronger coupling to the global cortical signal that exhibits a peak correlation when the pupil lags behind the voltage signal by ~1s. Finally, during periods of orofacial movements, pupil coupling to cortical activity was greatest in the medial sensory-motor cortices and auditory cortex. In contrast, cortical activity in lateral sensory and prefrontal areas were more negatively correlated with pupil during periods of movement.

3.3 Methods:

Mice:

Mice expressing the voltage sensitive fluorescent protein (VSFP) Butterfly 1.2 in excitatory cortical neurons were generated by crossing the transgenic mouse lines including the cre/tTa dependent VSFP-Butterfly reporter line (Madisen et al., 2015, Ai78-Jax 023528), a CamK2a-tTa line expressing tTa in excitatory neurons (Jax 007004), and an Emx1-cre line expressing cre in excitatory neurons across all cortical layers (Jax 005628). The result of this triple cross were mice expressing VSFP-Butterfly 1.2 in excitatory neurons in all layers of cortex (Fig 3.1A-C).

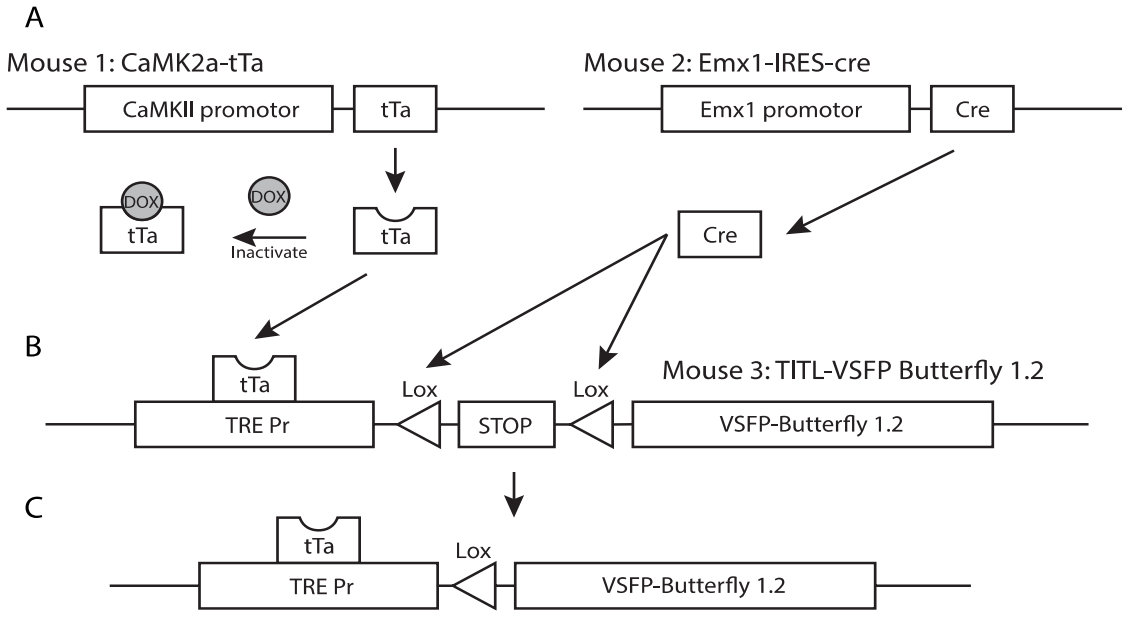

Figure 3.1. Transgenic expression of a genetically encoded voltage indicator

In order to express the voltage sensor, VSFP Butterfly 1.2, in select cortical cell populations, we crossed three different mouse lines to target only excitatory cells in cortex. **A.** Two transgenic driver lines were used, including a CaMK2a-tTa mouse and the Emx1-IRES-cre mouse to selectively target excitatory neurons in the cortex. **B.** The genetically induced cre expression allows for the STOP codon from the voltage indicator sequence to be cleaved and removed and the tTa expression binds to the TRE promotor

allowing the sequence containing the voltage indicator (**C.**) to be transcribed in specific cell excitatory cortical cell types.

Surgery:

For voltage imaging, 8 mice were implanted with a head-post and a through-skull dual-hemisphere cranial window (Silasi et al., 2016) over the dorsal cortex. The cranial window consisted of a custom-cut #1 glass coverslip cemented over the cleaned skull surface. A thin layer of cyanoacrylate glue was placed in between the bone and cement interface. Mice were administered 0.1mg/kg of buprenorphine as an analgesic and 1-2% isoflurane (prior to 3-4% for induction) for the duration of the surgery. For simultaneous imaging and electrophysiology experiments, small ~1mm diameter craniotomies were additionally made over the left motor and sensory cortices and covered with Kwik-Cast elastomer to protect the tissue until recordings. For these mice (n = 2), imaging was performed through the clear cement covering the skull without an added coverslip. A thin layer of cyanoacrylate glue was applied over the areas of cement to improve the optical clarity. Mice were aged 3-12 months at the start of experiments and maintained on a 12h:12h reverse light cycle for the duration of behavior training and imaging. During behavioral training, mice were provided ad libitum food access and were kept of 1-1.5mL/day water restriction protocol for 6 days a week starting 3 days prior to handling and imaging. On the 7th day of each week, mice were given free access to water. During behavioral testing and imaging sessions, mice were given 10% sucrose solution with 0.1% grape Kool-Aid powder. Liquid consumption was measured during testing and mice were supplemented with water to reach their 1-1.5mL daily volume. All experimental procedures were approved by the Emory University Institutional Animal Care and Use Committee.

Voltage Imaging:

We imaged VSFP signals with a macroscope (MiCAM Ultima, Brainvision Inc.) based on the tandem lens and epi-illumination system design (Ratzlaff and Grinvald, 1991). Excitation light was provided by a blue LED (LEX2-B, Brainvision Inc.), through a band-pass filter at 482nm (FF01-482/35, Semrock Inc.) and a dichroic mirror (FF506-Di03, Semrock Inc.). VSFP-Butterfly FRET chromophores (mKate2 and mCitrine) were imaged through two CMOS cameras (MiCAM-Ultima). The first camera recorded the emitted fluorescence from mCitrine, which was reflected by a second dichroic mirror (FF593-Di03, Semrock, Inc.), passed through an emission filter (FF01-543-50-25, Semrock Inc.). The second camera recorded the emitted fluorescence from mKate2, passed through the second dichroic mirror and an emission filter (BLP01-594R-25, Semrock Inc.) (Fig 3.2A). The camera acquisition was controlled by the MiCAM Acquisition Software. Acquisition frames rates varied between 25-200Hz with a spatial resolution of 100μm/pixel. The blue LED remained on for the duration of each imaging session that lasted 60 minutes on average to maintain constant illumination at the start of image acquisition.

Imaging During Different Behavioral Contexts:

All mice in this study were imaged during two different behavioral contexts: light isoflurane anesthesia and awake, spontaneous behavior. During anesthetized imaging, mice were induced with 3-4% isoflurane and maintained at 1-2% isoflurane for the duration of imaging. To monitor respiration and heart-rate during anesthesia, a pulse oximeter cuff (Starr Physiology) was placed on a hindlimb.

Pupil and Behavioral Monitoring Videography:

In order to monitor and record changes in behavioral state and pupil diameter, we captured moderate-speed (10-25Hz) videography of the mouse acquired simultaneously during imaging sessions. The first camera was positioned to the front and side of the mouse, capturing the left side of the mouse face as well as the left eye and the area where the forelimbs often rest underneath the mouse body (Fig 3.2C). An additional camera was occasionally positioned in front of the mouse and reflected off of a mirror to capture the whiskers, snout, and mouth from underneath of the mouse.

Behavioral State Classification:

Moving and quiet periods were based on video capturing the side of the mouse face including snout, whiskers, jaw. The onset and offset of movement periods were detected based on average changes in pixel intensity between frames. Mean orofacial movement signals were differentiated and squared, then thresholded using a low threshold (0.5-2SD) to reliably detect short or small movements. For analysis of voltage/pupil signals based on movement/quiet periods, we detected and analyzed epochs of continuous behavioral states lasting at least 4s. The middle 4s of each epoch was used for analysis.

VSFP Image Processing:

Raw images from both cameras were first aligned and registered to the first frame of the donor camera for any given trial. The signals from the two cameras were analyzed using the gain-equalization method (Akemann et al., 2012, Carandini et al., 2015, Shimaoka et al., 2018), by equalizing the gains at the heart beat frequency between the two cameras.

The gain equalization factors were obtained once per recording for each pixel, using the first trial of the session. The ratio of the two cameras captures FRET signals linked to membrane potential variations (Carandini et al., 2015) while the sum of the two signals captures large co-fluctuations linked to the hemodynamic response (Shimaoka et al., 2018). To exclude possible residual contamination of the hemodynamics in the ratiometric signal, the sum (hemodynamic) signal was filtered below 5Hz and then scaled by the regression coefficient with the ratiometric signal, then subtracted out from the ratiometric signal (hemodynamic signal regression, HSR). To perform analyses across trials and mice, the base image used to register within-trial frames was aligned to a template cortical map derived from the Allen Brain Mouse Atlas v3 (brain-map.org). A 2D top projection of the annotated Allen Brain Atlas volume was created in MATLAB (MathWorks) and a template image from one mouse was registered to the atlas using an affine transformation computed from two control points that were selected manually: the mid-point at the top of the front portion of dorsal cortex and the base of the cortex at the midline of the retrosplenial cortex.

Behavioral Video Processing (Pupil Diameter):

To determine the pupil diameter, frames were first cropped from video of the side of the mouse face or from videos of the pupil exclusively. To determine periods of orofacial movement, we estimated movement between frames by calculating the average of the squared derivative of each pixel across each frame. Periods when the frame movement was 2SD above the motion estimate were classified as periods of orofacial movement. In our imaging setup, pupil diameter was often acquired through the whisker field with

whisker motion in front of the pupil preventing us from using existing methods for determining pupil diameter (Reimer et al., 2014, Stringer et al., 2018). We developed a fast pupil detection method that uses two steps to determine diameter of pupil frame-by-frame: first, the pixel intensity threshold is set through an interactive user interface to before binarization of the darkest regions representing the pupil; then the edges of the pupil (which may be composed of multiple objects if whiskers obstruct continuous object isolation) are determined and the distances between all of the edge points are used to calculate the maximum projection across the object(s) representing the pupil diameter. This method is both fast and robust to objects crossing the pupil and creating discontinuities in the ellipse shape of the pupil. Lastly, the pupil diameter trace was smoothed with a 100ms median filter. This removed artifacts such as a portion of the whiskers occluding the pupil across 1-2 frames during diameter detection.

Laminar Electrophysiology:

To record LFP and multi-unit activity in motor cortex during voltage imaging, a ~1mm diameter craniotomy was drilled at coordinates 2mm A/P and 1mm M/L for M1. A 32-channel silicon probe electrodes (Neuronexus, Inc) was inserted 1mm deep into cortex at a 30deg angle and allowed to stabilize for 30 minutes before recordings began. The exposed tissue was kept hydrated by warm sterile saline solution. Contacts on the probes had 25μm spacing and extended ~750 μm from L2/3 to L5. Spike sorting was conducted using KlustaKwik software in python and by manual inspection and classification of the units following clustering with Klusta. For multi-unit firing rate analyses, all spikes not classified as noise were grouped together and all spike times

were binned in 5ms blocks and smoothed over 100ms. For LFP analyses, the signals across all 32 channels were band-pass filtered between 0.01 and 50Hz and the mean across all channels was regressed out of the signal for each channel. Definitions of layer ⅔ and 5 were determined and classified by visually inspecting the inverting polarity of the mean-subtracted LFP signals across channels. Electrodes were dipped in DiI before the last recording in a given area and locations were verified during histological processing.

Region Identification:

Cortical regions were assigned based on registration to the Allen brain atlas cv3 (brain-map.org). One template VSFP image from a sample mouse was aligned using manual placement of control points to the Allen brain cortical map. An example image from all other mice was then aligned to the control point-aligned VSFP image using rigid and translation alignment in Matlab. For subsequent processing, the base image from each imaging session was aligned to the mouse-specific template image and all following frames were transformed using the same alignment specifications. Inter-trial registration was performed using a sub-pixel rigid registration of frames up-sampled to 10000x10000 pixels in the frequency space (Guizar-Sicairos et al., 2008).

Frequency Analysis:

To examine the frequency changes in voltage, hemodynamic and pupil diameter activity over the course of recording trial, we calculated wavelet spectrograms depicting the changing frequency power over time. To compute the continuous wavelet transform, we

used the morlet wavelet. To measure the time-varying correlations between the voltage or hemodynamic signal and pupil diameter as a function of frequency, we calculated the wavelet-based coherence using morlet wavelets.

Data Analysis:

To determine statistical significance between correlation maps at rest or movement, we used Mann-Whitney U-tests and when able further performed Bonferroni corrections calculate adjusted p-values. Since statistical comparisons were calculated for the extent of the imaging area (10000 pixels), in order to guarantee a global error probability at a given threshold (0.05, 0.01, etc.) the significance level for a single test (pixel) is obtained by dividing the global error probability by the number of independent tests. For example, if the p-value was initially significant at $p<0.05$, the p-value corrected for multiple comparisons (e.g. new threshold for judging significance) would be $p<0.05/10000$ or $p<0.000005$. Regression coefficients were cross-validated such that the initial coefficient would be determined using the first half of the data ('training set') and would then be tested on the remaining half of the data ('test set'). Correlation maps were tested against chance correlations by shuffling the pupil data series among trials and recalculating correlation coefficients on the shuffled data. The original data was then tested against the shuffled data using Wilcoxon Rank Sum test.

3.4 Results

Wide-Field Cortical Imaging of Voltage Activity Across Dorsal Cortex

In order to comprehensively observe cortical voltage activity across multiple functional territories and both hemispheres we implemented a technique for wide-field voltage imaging to record from excitatory neural populations through the intact cortex during spontaneous and task-oriented behavior. This imaging technique relies on a combination of optics sensitive enough to record changes in faint fluorescent signals at high speed (200Hz) while spanning large areas and genetic tools for expressing voltage dependent fluorescent proteins (VSFPs) throughout the cortex (Ratzlaff and Grinvald, 1991, Ferezou et al., 2009, Carandini et al., 2015, Madisen et al., 2015).

To image cortical activity from excitatory neurons exclusively, we created a triple-transgenic mouse expressing VSFP-Butterfly 1.2 in a cre/tTa dependent manner (Fig 3.1A-C). Cre expression was limited to cortical excitatory neurons (Emx1-cre) and tTa expression was also limited to excitatory neurons more broadly via the CaMK2a promotor (CaMK2a-tTa). We next exposed the skull above the dorsal cortex and covered the area with clear cement with a glass coverslip attached to the surface and focused the macro-scope slightly below (~100μm) the most superficial blood vessels (Fig 3.2B). Wide-field optical signals are very sensitive to physiological variables such as blood flow, blood oxygenation, and intrinsic autofluorescence (Ma et al., 2016a, Ma et al., 2016b, Pisauro et al., 2016). Using a ratiometric equalization technique (Carandini et al., 2015) we were able to compare or combine fluorescent signals from both the acceptor and donor channel of VSFP Butterfly to estimate local membrane voltages separate of the hemodynamic signals, respectively.

Pupil Diameter Is Tightly Coupled to Global Cortical Voltage Signal

Recent wide-field imaging studies have found that activity related to arousal and movement can be observed across large extents of cortex, even in areas not directly considered to be related to movement such as visual auditory and somatosensory cortical areas (Ferezou et al., 2007, Niell and Stryker, 2010, Musall et al., 2018, Shimaoka et al., 2018). For each animal and imaging session, we obtained measures of global voltage or hemodynamic signals by averaging the z-scored signal from each pixel within a mask of the cortex encompassing pre-frontal, motor, somatosensory, retrosplenial, and visual areas Fig 3.2D. We used z-scored signals to ensure each pixel contributed equally to the calculation of global signal and that large transients of activity (either noise or physiological) did not bias the global signal calculation.

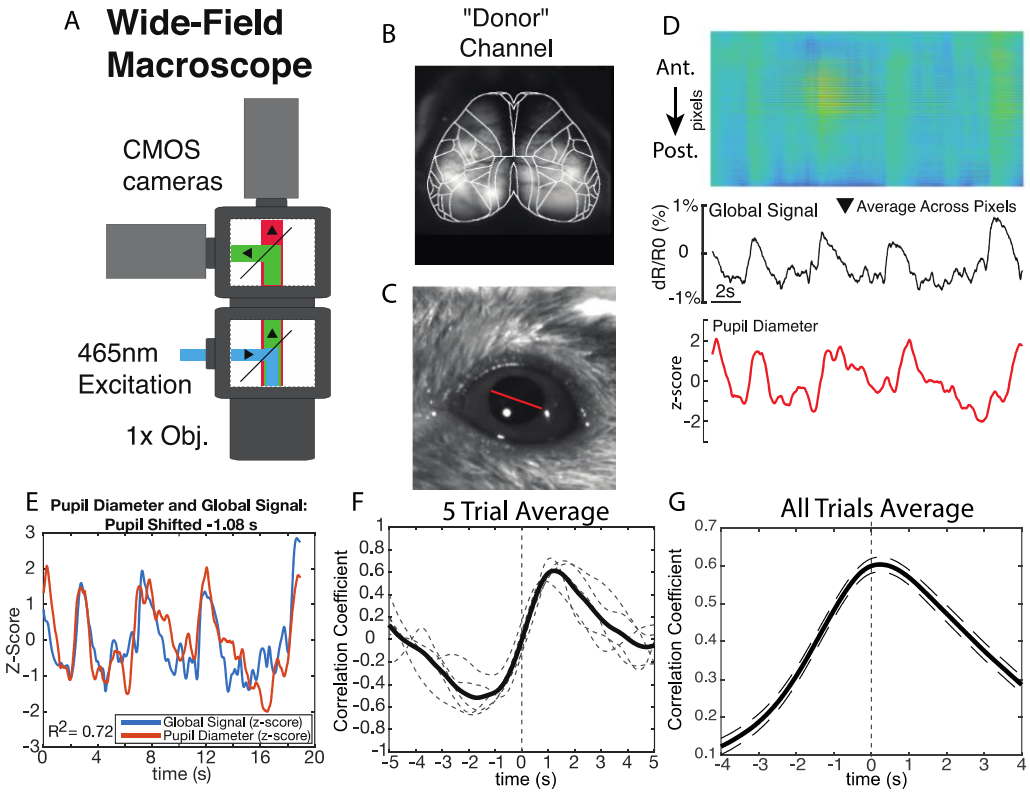

Figure 3.2 Cortical global signal from wide-field voltage imaging is tightly coupled to pupil diameter

A. To record voltage activity across wide extents of the dorsal cortex, we used an epi-illumination macroscope containing a 465nm excitation LED and two cameras to capture fluorescent light in the green and red wavelengths, corresponding to the donor and acceptor fluorophores of the VSFP-Butterfly1.2 protein. **B.** example image of the donor channel from the green receiving CMOS camera. Surface vasculature can be seen across the cortex and the Allen brain atlas surface map is overlaid. The macroscope was focused slightly beneath the superficial blood vessels to acquire surface fluorescent signals from cortex. **C.** Example frame from video recording of pupil diameter. For each frame the maximum diameter across the pupil was calculated (red line) and used to calculate spontaneous fluctuations in the pupil diameter over time. **D.** Pixels from the cortical surface are re-arranged in a 2d plane such that the y-axis contains every pixel covering the cortex and the x-axis is the voltage activity in the given pixel over time. By taking the z-score for each pixel and averaging together we are able to calculate the "global signal." The global voltage signal fluctuates in a similar pattern to that of the pupil diameter. **E.** When the pupil diameter was shifted ahead ~1.2s, the global voltage signal (blue) and the pupil diameter (red) are closely overlaid and have a correlation coefficient of 0.72. **F.** The time-delay between the pupil diameter and global voltage signal is consistent across trials within a given session. Dashed lines indicate individual trials while the solid line represents the average of the cross-correlations. **G**. When averaging the cross-correlations across all mice, sessions, and trials, the correlation coefficient remains high, but the time-delay for the max correlation is now widened and centered at ~0s. The breadth of the total cross-correlation suggests high variability among mice and trials.

While recording cortical fluorescent activity, we also recorded video of the mouse to obtain measures of orofacial movement and pupil diameter. Pupil diameter has been found to be tightly related to subthreshold membrane voltage activity and population firing rates in several cortical and subcortical areas including the auditory and visual cortices

as well as the hippocampus (Reimer et al., 2014, McGinley et al., 2015a, McGinley et al., 2015b, Stringer et al., 2018). During periods of locomotion or increased arousal, the pupil rapidly dilates, with pupil constriction observed during quiescent or low arousal periods. To efficiently determine pupil diameter across hours of video recordings, we applied a binary threshold to isolate the dark pixels representing the pupil and then determined the maximal projection across the outer boundary of the pupil. This method was robust against partial occlusion of the pupil from whiskers or the bright reflection spot from the IR led used to illuminate the face of the mouse.

By plotting the global signal and pupil diameter activity together, it is clear that the signals are similar, though the pupil appears to change at a lagged interval compared to the voltage signals (Fig 3.2D,E). To quantify and examine the variability of the time lag between the pupil diameter and the global voltage, we performed cross-correlation between the global signal and the pupil diameter. Within an example mouse across multiple trials, the pupil consistently lagged behind the global voltage signal by approximately 1s, peaking at a 0.75 correlation average across all mice (Fig 3.2F). The dynamics of this delayed pupil coupling can be further examined by visualizing the changing correlation patterns across cortex across the different lag times (Supplemental Movie 1). However, while clear peaks emerge across lag times within a single mouse across trials, there was variability in the exact delay times between pupil and delay activity across all mice and trials (6 mice, 65 trials) (Fig 3.2G). One such source of this variability could be the primary frequency components within the global signal.

Cortical Laminar Local Field Potential Recordings Are Closely Related to the Wide-Field Voltage Signals

To determine the relationship between voltage imaging signals and electrophysiological activity across cortical layers, we performed simultaneous voltage imaging with laminar silicon probe local field potential (LFP) recordings from pre-motor and primary sensory cortex in awake mice (Fig 3.3A). Using 32-channel laminar probes, we were able to record LFP activity from multiple cortical layers (Fig 3.3B). LFP signals showed the strongest coupling with voltage imaging signals in the superficial layers of cortex. The deeper layers (L5) showed anti-correlated activity of similar magnitude to the superficial layers (Fig 3.3B). This suggests that activity from both layers is depicted in the voltage imaging signals measured from the cortical surface. This is in agreement with a previous calcium imaging study reporting that superficial calcium signals measured in widefield imaging are most representative of input to apical dendrites and dendritic calcium activity (Allen et al., 2017). Since neurons from both layer 2/3 and 5 both have extensive apical dendritic networks that receive subcortical and cortico-cortical input. Additionally, a previous report combining voltage recordings from mice with VSFP-Butterfly1.2 in either all excitatory cortical neurons (Emx1-cre) or only layer 2/3 pyramidal neurons (Rasgrf-cre) found no significant differences in activity patterns related to arousal or sensory evoked activity, further suggesting that the voltage signal measured consists of voltage changes due to inputs to layer 2/3 neurons (Shimaoka et al., 2018). Thus we suggest that voltage imaging of excitatory neural activity in cortex is best represented by synaptic inputs to superficial layers of cortex and primarily the apical dendrites of layers

2/3 and 5 neurons. Further supporting the wide-field voltage measurements were related to functional connections, we created correlation maps between example LFP traces in L2/3 and L5. L2/3 activity in motor cortex showed strong functional connectivity with the contralateral motor cortex as well as sensory cortex bilaterally (Fig 3.3B right, top). In L5, similar strength of connectivity was observed, but the LFP was instead negatively correlated with ipsilateral and contralateral motor and sensory cortices (Fig 3.3B right, bottom).

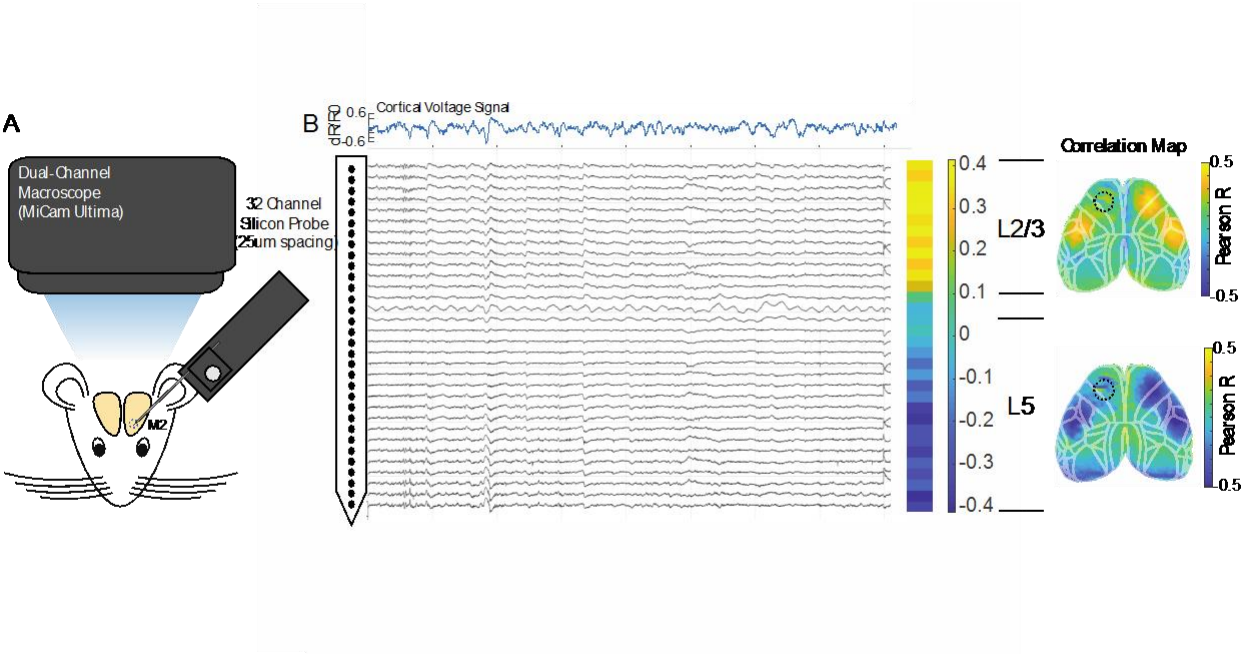

Figure 3.3 Cortical Voltage Imaging Is Correlated with Laminar LFP Activity in Awake Mice

A. Simultaneous wide-field voltage imaging with laminar LFP recordings in M2 of the awake mouse cortex. To avoid occluding imaging area, the laminar probe is inserted from an 30deg. angle lateral to the mouse cortex using a micro-manipulator. **B.** Comparing cortical voltage activity and laminar LFP signals. The signals depicted correspond to the positioning on the laminar probe to the left such that the top traces are from layer 2/3 with the bottom traces extending in to layer 5 of cortex. Notice the polarity of the signals switch as the probe crosses the boundary between layer 2/3 and 5. The cortical voltage trace

(top) is taken from the an M2 pixel contralateral to the laminar recording site due to loss of signal from slight bleeding around probe insertion point. Correlation maps (far right) show that motor and sensory areas are highly correlated with an example L2/3 LFP trace (top) and negatively correlated with an example trace from L5 (bottom). Center of dashed circle represents location of cortical LFP insertion.

Global signal is differentially coupled to pupil diameter across multiple frequencies

We previously observed that pupil coupling to global voltage signals appears to occur across multiple timescales over the course of a 20s trial. To examine how pupil diameter and global voltage and hemodynamic activity are coupled across wider timescales, we acquired simultaneous imaging and pupil video recordings over several minutes (Fig 3.4A). To determine the frequency components present in each of the recorded signals, we calculated wavelet scalograms for voltage activity, hemodynamic activity, and pupil diameter (Fig 3.4B). Across the course of several minutes, each of these signals exhibited dynamic fluctuations across multiple frequency bands. While the voltage activity and pupil diameter exhibited fluctuations in the <0.1Hz range, the global hemodynamic signal did not show similar low-frequency fluctuations. To determine how these signals covaried with one another, we calculated wavelet coherograms on the same example trial between voltage and hemodynamic, voltage and pupil, and hemodynamic and pupil activity (Fig 3.4C). These coherograms shows that the co-fluctuations in global voltage and hemodynamic signals occur across higher frequencies (above 0.1Hz) at specific times throughout the course of the trial (Fig 3.4C, top). Voltage activity shows strong coupling with pupil diameter across multiple frequencies, with low-frequency coherence present throughout the entire trial and more sparse coupling at higher

frequencies (Fig 3.4C, middle). Finally, hemodynamic activity also shows periods of coupling to pupil diameter, but is sporadic and strongest at even higher frequencies around 0.5Hz with little coupling at low frequencies in contrast to voltage/pupil coherence (Fig 3.4C, bottom). To further determine how the pupil diameter changes related to the global voltage across multiple animals and trials, we calculated and plotted the average cross-correlations between global voltage signal and the pupil diameter across the original full frequency spectrum as well as separately for low frequency (<0.1Hz) and high frequency (>0.1Hz) filtered components (Fig 3.4D). Across the observed lag times (+/- 4 seconds), the average correlation coefficients were all positive, with the low-frequency signal components showing the maximum correlation at a lag time of ~1s (n = 6 mice, Fig 3.4D). The variability of the peak correlation was relatively small for the un-filtered and low-frequency filtered signals within mice and as a group (Fig 3.4E). The same was true for the pupil lag times for the low-frequency and original unfiltered signals with the peak coupling between pupil and voltage activity occurring at ~1s and ~0.5s delays, respectively. Interestingly, the high-frequency lag times were extremely variable within and between mice ranging from the pupil lagging behind or ahead of voltage activity between -1 to +1s. Cross-correlations between the global hemodynamic signal and pupil diameter showed similar trends as seen between pupil and global voltage, though at generally lower correlation strengths (Fig 3.4G). Low frequency components showed peak correlations with the pupil diameter of ~0.3 (Fig 4H) and lag times for all frequency components varied between 0 to 2s (Fig 3.4I). As we observed earlier when the two signals were plotted together, the pupil diameter was tightly correlated with the global

signal with peak correlations around 0.5-1s pupil lag times, consistent with previous observations of pupil and intracellular membrane recordings (McGinley et al., 2015a).

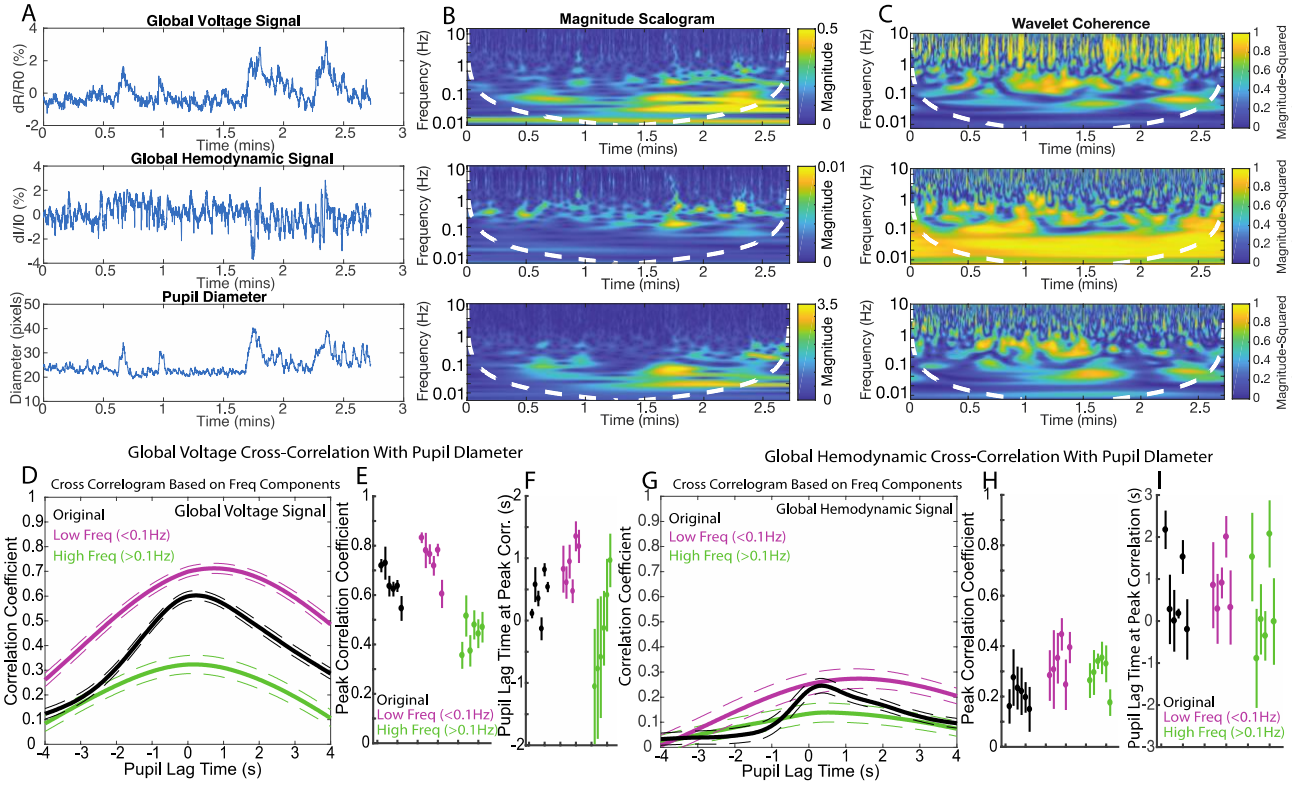

Figure 3.4 Global Cortical Signals Are Differentially Coupled to Pupil Diameter Across Multiple Frequencies

A. Examples of global voltage (top), global hemodynamic (middle), and pupil (bottom) signals from a single 180s trial. **B.** Frequency wavelet scalograms of the signals depicted in A. Over the course of the trial, clear peaks are present across infra-slow and slow frequency ranges in the voltage and pupil signals, but are largely absent in the hemodynamic signal. **C.** Wavelet coherograms comparing global voltage and global hemodynamic signals (top), global voltage and pupil diameter (middle) and global hemodynamics with pupil diameter (bottom). White dashed lines indicate confidence boundaries. The global voltage and hemodynamic signals show periods of coherence above 0.1Hz. The voltage signal shows high coherence with the pupil diameter throughout the course of the trial and across measured frequencies while the hemodynamic signal shows coherence with pupil to a lesser extent across limited frequencies (~0.05-1Hz). White dashed lines indicate confidence boundaries **D.** Cross

correlations between global voltage signal and pupil diameter across original traces (black), low-frequency (magenta), and high frequency (green) filtered traces. The amplitude of the cross correlations is highest between the low-frequency signals with the peak delay between the global signal and pupil diameter at 1s. The original and high frequency signals show a peak correlated with pupil diameter at 0s, suggesting minimal delay between pupil diameter and the global signal. Dashed lines represent standard error (n = 6 mice; 65 trials) **E.** Variability in the peak correlations of individual mice (n=6) across different frequency components. Mice shown consistent coupling amplitudes across the three frequency conditions. **F.** Lag times corresponding to the peak of the cross-correlations. For the original and low-freq filtered signals, pupil lags behind the voltage signal by ~0.5s and 1s, respectively. The high frequency filtered activity displays highly variable lag times both within and across mice. **G.** Same as D, but for global hemodynamic cross-correlations with pupil diameter. Global hemodynamic signal shows decreased correlations across all frequencies compared to voltage signal. **H.** Variability in the peak correlations of individual mice (n=6) for hemodynamic activity. Low-frequency filtered hemodynamic signals show the strongest coupling to pupil diameter with peak correlation coefficients between 0.2 and 0.4. **I.** Pupil lags behind the hemodynamic signal at close to a 0s lag on average for non-filtered signals and high-frequency activity. Low-frequency signals are show a peak correlation when pupil lags by ~1s (n=6).

Cortical Activity and Pupil Diameter Are Differentially Coupled Across Functional Cortical Areas

While it is clear that arousal as measured by pupil diameter and global fluctuations in voltage signal are related across certain frequencies (Fig 3.4C), it is unclear how the pixel-wise voltage signals across different areas of cortex are influenced by arousal. To determine the spatial correlations with arousal, we calculated correlation maps depicting the correlation coefficients of voltage activity at each pixel with the pupil diameter. To examine the spatial aspects of cortical coupling to arousal, we calculated the cross-

correlations between activity in each pixel with the pupil diameter. For cortical voltage activity, we found that the maximum correlation coefficients were highest around medial sensory cortices as well as secondary somatosensory and auditory cortex (Fig 3.5A). The medial aspects of frontal cortex corresponding to parts of secondary motor and anterior cingulate cortex were also strongly coupled.

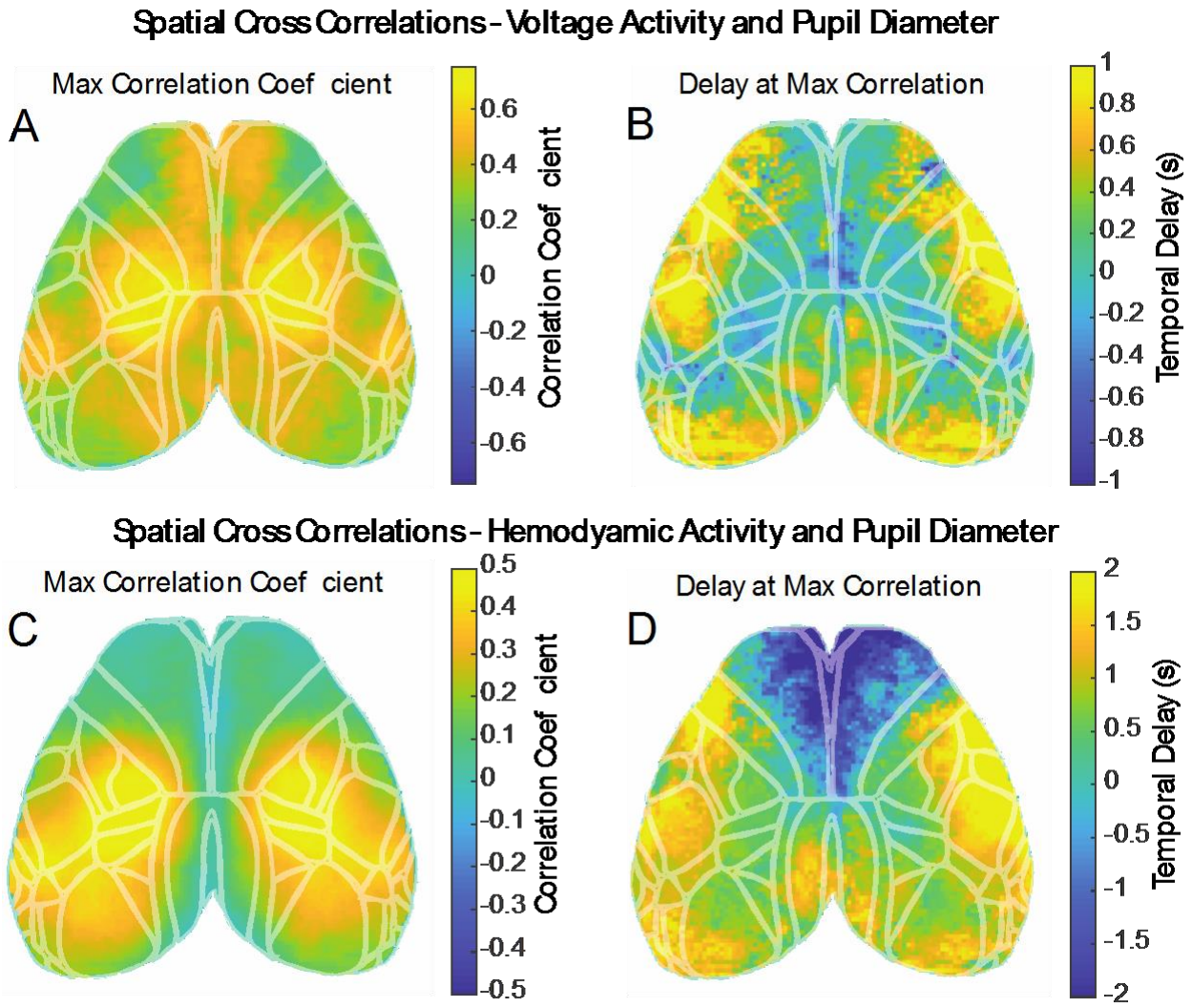

Figure 3.5 Cortical Activity and Pupil Diameter Are Differentially Coupled Across Functional Cortical Areas

Peak Correlation maps and time delay (time lag) at the peak correlation value are plotted across the cortical space for voltage and hemodynamic signals. **A.** Voltage activity is most strongly coupled to pupil diameter changes within medial sensory-motor cortical areas

(exhibiting maximum correlation coefficients above 0.75s) as well as secondary sensory/auditory cortices. Strong correlations also extend in to medial pre-frontal/pre-motor areas of cortex, though lateral areas of motor cortex show slight negative correlations with the pupil. **B.** Temporal delay maps showing the delay time with peak correlation from cross-correlation of voltage activity and pupil diameter. Lateral sensory and posterior visual cortical areas show maximum coupling between voltage and pupil activity when the pupil is delayed over 1 second behind the voltage signal. Medial sensory areas that exhibited the strongest coupling with pupil diameter exhibit peak correlations near 0s delays (6 mice, 65 trials). **C.** Map of maximum coupling between hemodynamic signals and pupil from cross-correlations. Hemodynamic signals share similar pupil correlation patterns as seen in voltage activity, though medial frontal regions no longer show increased pupil coupling. **E.** Temporal delay maps showing the delay time with peak correlation from cross-correlation of hemodynamic activity and pupil diameter. Lateral sensory areas again show maximum coupling between hemodynamic and pupil activity when the pupil is delayed over 2 seconds behind the hemodynamic signal, however pupil diameter actually precedes frontal cortex by up to 2 seconds.

To examine the spatiotemporal aspects of these correlations, we also calculated the lag time that produced the maximum correlation maps for each pixel across dorsal cortex (Fig 3.5B). Interestingly, the cortical areas with the highest coupling to arousal showed the highest coupling at -0.2 to 0.2s lag times, while the lateral sensory-motor areas were most correlated with pupil at over 1s lag times. Similarly, when looking at spatial aspects of hemodynamic coupling to arousal, we find the medial somatosensory, visual, and auditory cortices have the strongest peak correlations (Fig 3.5C). However, the temporal aspects of hemodynamic coupling to arousal slightly differed compared to voltage activity such that the medial frontal cortex is most coupled to pupil diameter when the pupil is sped up ahead of the hemodynamic signal up to 2s (Fig 3.5D). These patterns

of coupling in the observed cortical areas closely resemble cortical areas found to be co-activated with movement, raising the question of exactly how the cortical coupling with arousal is influenced by the presence or absence of animal movement (Musall et al., 2018).

Patterns of Cortical Coupling to Pupil Diameter Are Dependent on Behavioral State

Previous studies have found large effects of behavioral state on membrane voltage across multiple brain regions (Ferezou et al., 2007, Poulet and Petersen, 2008, Shimaoka et al., 2018). In order to characterize the effects of behavioral state on the coupling of cortical voltage activity to pupil diameter, we calculated cortical voltage/pupil correlation maps during periods of movement or rest. During the course of a single 160s trial, mice display periods of spontaneous orofacial movements (Fig 3.6C). Based on our video acquisition setup, these orofacial movements consist of changes in whisker, jaw, or snout movements (Fig 3.6AB). In average correlation maps generated over the course of a single trial, we can observe stark differences in voltage/pupil coupling between rest and movement states with movement periods showing increased coupling to arousal within medial sensory cortex and auditory cortex (Fig 3.6DE). Correlations between voltage and pupil diameter appear to become more negatively correlated in lateral motor areas during movement (Fig 3.6E). When calculating the same average correlation maps combining all mice and trials, we find that at rest, cortical coupling to arousal is relatively even across cortex (Fig 3.6F). However, during periods of movement, correlations greatly increased primarily in medial sensory and auditory as observed before and additionally medial frontal cortex with correlation coefficients in these areas near or exceeding 0.5. Voltage

coupling to pupil diameter in these areas was all significantly increased even when accounting for multiple comparisons (Fig 3.6H).

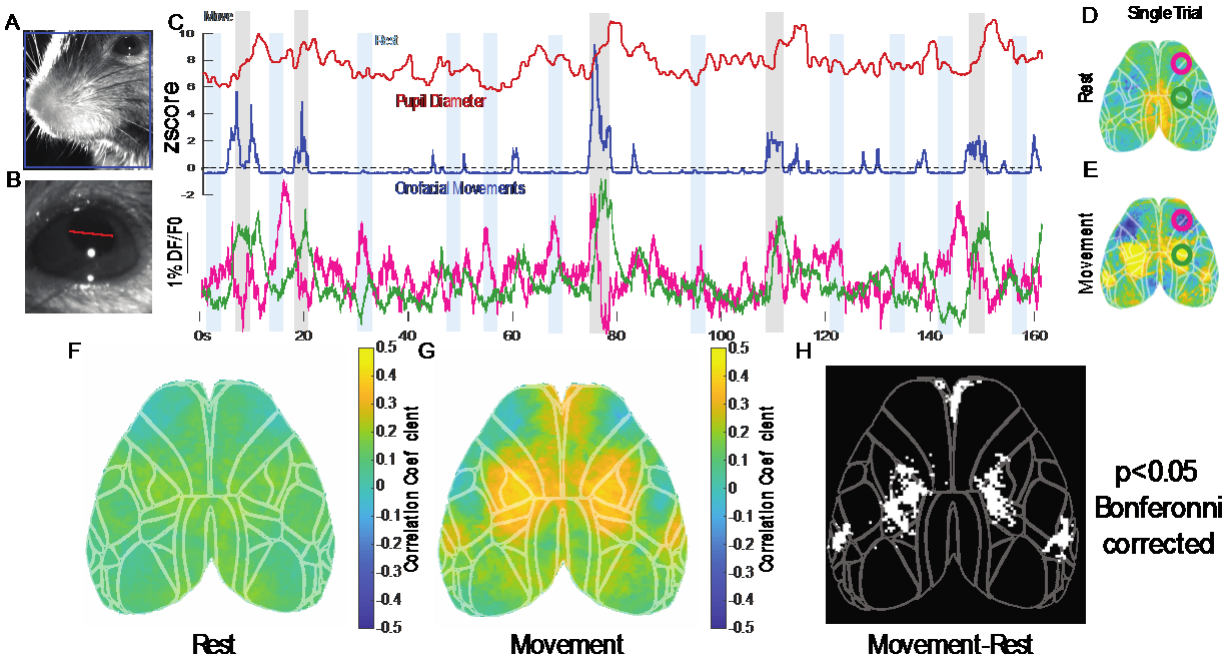

Figure 3.6 Patterns of Cortical Coupling to Pupil Diameter Are Dependent on Behavioral State

A. Example frame from video acquisition of the mouse face during cortical imaging. Region of interest for movement analysis is depicted by the surrounding blue box. Visible areas of the mouse face contributing to movement signal include the nose, snout, jaw, and whiskers of the mouse. **B.** Cropped region of interest for calculating the pupil diameter during cortical imaging. The red line represents the maximum width across the pupil used as the measure of pupil diameter. **C.** Example trial showing pupil diameter (red), orofacial movement (blue), and two regions of interest from cortex including primary motor (red) and sensory (green) cortical areas from the right hemisphere. Movement periods (shaded gray) were classified based on the movement signal remaining above the threshold (dashed line) for at least 4s. Periods of rest were instead identified when the movement signal remained below the threshold for at least 4 seconds. **D.** Correlation map from the single trial shown in C. between voltage activity and pupil diameter during periods of rest. Correlations between sensory area activity and pupil diameter are slightly negative while retrospenial cortex is the only area showing strong positive correlations with pupil activity.

E. Same as D, but for periods of movement. During orofacial movements, cortical activity is strongly correlated with the medial sensory-motor areas and auditory cortex, while the frontal motor areas are strongly negative correlations with pupil diameter. **F.** Average correlation map for cortical voltage activity and pupil diameter for periods of rest. Cortical coupling is uniform across cortex with a maximum Pearson correlation coefficient around 0.2. **G.** On average, during movement periods voltage and pupil correlations are increased in medial sensory-motor areas and decreased in lateral motor and sensory areas. **H**. Statistical maps showing significantly different areas between movement and rest at $p<0.05$ adjusted for multiple comparisons (Bonferroni correction). Map highlights significance across medial sensory-motor areas and auditory cortex as well as medial pre-frontal cortical areas.

3.5 Discussion

In this study, we examined the temporal and spatial components of cortical coupling to arousal measured through changes in pupil dilation. Using wide-field imaging of the voltage sensitive fluorescent protein Butterfly 1.2, we were able to record membrane voltage activity bilaterally across a large extent of dorsal cortex. While the voltage sensitive fluorescent protein was expressed across all cortical layers, our electrophysiological experiments suggest that the population membrane voltages recorded most closely resemble layer 2/3 activity. This finding is in agreement with a recent study that utilized both cortical wide and layer 2/3 excitatory neural targeting of the same GEVI and found no significant differences between the two transgenic mouse lines (Shimaoka et al., 2018). However, another study using both wide-field and 2-photon calcium imaging techniques found that the wide-field signals measured from the epi-fluorescent microscope most closely resembled superficial neuropil activity from layer 1 of the cortex (Allen et al., 2017). Since their targeting of the calcium signals was similarly restricted to excitatory neurons (excluding contributions from layer 1 inhibitory interneurons), they suggest the calcium signals measured in the neuropil and wide-field imaging represent inputs to apical dendrites of both layer 2/3 and 5 pyramidal neurons.

In this study, cortical voltage imaging provides several important advantages over alternative imaging strategies. Most importantly, population membrane voltage fluctuations do not necessarily translate to changes in neural firing rates, especially since the particular voltage sensor used in this study is optimized to show the greatest changes in fluorescence in the sub-threshold voltage range (Akemann et al., 2012). This is advantageous for studying influence of pupil diameter on cortical activity since they may

be primarily coupled across sub-threshold fluctuations as observed in intracellular recordings (McGinley et al., 2015a, McGinley et al., 2015b). Additionally, voltage imaging provides faster temporal resolution than the more commonly used calcium imaging sensors, allowing us to observe neural activity fluctuations on the scale of milliseconds to minutes. Though there are also limitations to voltage imaging, especially with the sensor used in this study. While the ratiometric calculation used to estimate voltage is largely immune to the confounds of hemodynamic activity, the methods used assume that the ratiometric voltage signal is uncorrelated with signals due to hemodynamic activity which is not always true and likely an oversimplification (Carandini et al., 2015).

The term “arousal” is often used to imply changes in the global brain state, which we show is a valid interpretation based on strong coupling of pupil diameter with the global voltage and to a lesser extent hemodynamic signals calculated from cortex-wide global signal regression. Though the concept of arousal reflecting global changes in brain state is incomplete, which we demonstrate by showing that the pupil is differentially coupled to various cortical areas across different behavioral states. While often considered a nuisance variable in MRI imaging, we found that the global signal (the voltage or hemodynamic signals fluctuating together throughout cortex) was tightly coupled to arousal as measured by pupil dilations. Previous work has also shown that the hemodynamic signal shared across visual cortex was coupled to pupil diameter/arousal while local V1 signals coded for details of visual processing (Pisauro et al., 2016). Additionally, one study measuring cortical V1 firing activity at a massive scale (~10,000 neurons) found that the main principal component of the population activity in visual cortex was tightly correlated to measures of arousal such as pupil diameter and

locomotion (Stringer et al., 2018). Thus, the removal of global signal during pre-processing should be carefully considered as it may provide important information or serve as a covariate for changes in arousal or attention.

Using pupil diameter as a proxy, arousal signals fluctuate across fast and slow timescales, and have a drastic, though complex, influence on ongoing cortical activity. Given what we already know about the effect of arousal on sensory and cognitive processing, pupil diameter and animal movements should be routinely monitored as complementary measures of arousal that carry the potential to account for large amounts of neural and behavioral variability. We additionally found that arousal also influences frontal motor/cognitive cortical areas such that are negatively correlated with arousal especially during periods of orofacial movement. Few studies have examined the influence of arousal-related systems on motor cortex, though in one recent report, researchers found that by blocking adrenergic input from the locus coeruleus to motor cortex, they found a reduction in the membrane voltage distribution, reduced firing activity, as well as impaired contralateral motor coordination, suggesting arousal-related modulation of motor cortex can have drastic influences on motor behavior. It is already known that arousal can have opposing effects on inhibitory compared to excitatory circuits (Reimer et al., 2014) even within the same functional area of cortex further illustrating the complexity of arousal influence on cortex. As such, future studies should examine the influence of arousal measures on cortical circuits with improved cell-type specificity to examine how different neural populations are shaped by arousal state.

Lastly, we found spatial and temporal differences in voltage and hemodynamic coupling to pupil dilations based on the frequency of activity. We broadly divided the signal

components in to lower frequency activity (<0.1Hz, sometimes referred to as “infra-slow”) and higher frequency activity (>0.1Hz). While the higher frequency activity was maximally coupled to the pupil diameter at a 0s lag, lower frequency signals showed peak correlations when the pupil was lagging behind the voltage signal by ~1s. These infra-slow fluctuations are of particular interest, since these oscillations are considered to be the basis of resting state functional connectivity measurements in fMRI studies and depict distinct spatiotemporal trajectories based on the neural state. For example, in anesthetized mice, wide-field calcium imaging shows that infra-slow waves propagate from medial-posterior areas of cortex to lateral-frontal areas, however these waves flip direction when the mouse transitions to the awake state (Mitra et al., 2018). Interestingly, delta oscillations (1-4Hz) exhibit a reversal of direction when transferring between the anesthetized to the awake state, but in the opposite direction as infra-slow activity. Our study builds on these previous findings by demonstrating that arousal changes as reflected by pupil diameter fluctuations are differentially coupled to voltage and hemodynamic activity across distinct frequencies. We further showed that the frequency bands showing strong coupling between pupil diameter to cortical activity are also changing across time courses on the scale of several seconds to minutes. These findings build upon another recent study demonstrating that firing rates in cortex exhibit infra-slow fluctuations that are also linked to changes in pupil diameter (Okun et al., 2018). While the sources of infra-slow fluctuations are unclear, they are considered to be influenced at least in part by neuromodulatory systems underlying arousal (McGinley et al., 2015b, Reimer et al., 2016). Further work will be required to parse the fine temporal scales of

arousal and how these signals emerge and change during quiet wakefulness and goal-directed behavior.

Chapter 4: Cortical Voltage Dynamics Underlying Movement Preparation and Initiation in Awake, Behaving Mice

4.1 Introduction

How animals prepare to move and properly execute these movements is a critical question in neuroscience and while it is widely studied, very few mechanisms are well understood or widely accepted regarding the cortical mechanisms controlling movement. Wide-field imaging of calcium activity in motor cortices has recently uncovered new aspects of cortical processing revealing spatial maps of cortical activity underlying movement planning and execution (Crochet and Petersen, 2014, Guo et al., 2014a, Li et al., 2015, Allen et al., 2017, Chen et al., 2017, Musall et al., 2018). While these studies have provided important details in to the cortical areas underlying proper sensory and motor processing, calcium signals represent firing rate activity at relatively slow timescales (<8-10Hz). Cortical voltage imaging using voltage sensitive dyes or genetically encoded voltage indicators currently has less signal to noise compared to existing Ca indicators, but is advantageous in it's ability to track higher frequency activity (>20Hz) and subthreshold voltage fluctuations (Ferezou et al., 2009, Akemann et al., 2012, McVea et al., 2012, Carandini et al., 2015, Borden et al., 2017, Kyriakatos et al., 2017). Since animal behaviors occur on millisecond timescales, the increased temporal resolution of voltage

indicators can begin to address new questions related to the spatiotemporal processes underlying motor control. To determine how motor preparation is facilitated across sensory-motor cortical areas, we use wide-field imaging of the VSFP Butterfly 1.2 voltage indicator (Akemann et al., 2012, Carandini et al., 2015) to measure the population voltage changes across cortex while mice performed a directed licking task. In this task, mice were presented with variable length (1-1.5s) air-puff stimuli to either the left or right whiskers and upon the offset of the air-puff were allowed to lick towards a left or right spout to obtain a sucrose reward. By observing and comparing cortical activity between correct trials with different preparation and reaction times as well as incorrect trials where the mice licked too early (before the air-puff offset), we are able to examine the cortical dynamics underlying movement preparation/initiation as well as movement suppression, respectively.

While years of research have been dedicated to understanding the cortical neural firing patterns underlying various aspects of motor control, the dynamics of membrane voltage activity within the same motor cortical areas remain unclear. In particular, how synaptic input to sensory-motor cortices influences movement preparation and initiation remains unknown. While individual neurons seem to exhibit diverse relationships with movement that also show variability across trials, a lot of information regarding motor control can be obtained by looking at activity across populations of neurons during motor behavior (Churchland et al., 2006b, Churchland et al., 2012, Kaufman et al., 2014, Seely et al., 2016, Peixoto et al., 2018). Since the population activity in motor cortical areas carries useful information regarding the time-course of movement preparation and initiation, it is possible to extract crucial insights into the mechanisms of movement

preparation and initiation by imaging neural populations using genetically expressed calcium and voltage sensitive indicators (Ferezou et al., 2007, Vanni and Murphy, 2014, Li et al., 2015, Svoboda, 2016, Chen et al., 2017, Kyriakatos et al., 2017). In Chen et al. 2017, authors aimed to map anticipatory activity in the motor cortices using wide-field calcium imaging, finding two areas referred to as ALM and in an area referred to as medial motor cortex (MM; also called frontal orienting field) that showed preparatory activity during the end of the sample and delay periods before the mouse produced a left or right licking response(Chen et al., 2017). Overall they found that activity emerged earliest in MM corresponding to the area of motor cortex that receives strongest input from vibrissal sensory cortex and moved to the ALM later in the delay period as the mouse prepared to move. Using two-photon imaging covering the same areas examined under the prior wide-field imaging, they were able to determine a depth profile of anticipatory activity as well, finding that object location cells in MM (and partially in ALM) were located in superficial layers (L2/3) of motor cortex, with lick direction selective cells located at both superficial, but primarily in deep layers (L5) of ALM. For whisker-based motor planning, they propose that decision related activity flows from vS1 -> MM -> ALM, though decision activity could be distributed through other networks as well including secondary sensory projections to motor cortex (vS1-> S2 -> ALM), or through the basal ganglia (vS1-> BG -> thalamus -> ALM). A later study from the same lab used retrograde labelling techniques to isolate two distinct populations of L5b pyramidal tract (PT) neurons in ALM based on projections to the thalamus (L5upper) or to the medulla (L5lower) (Economo et al., 2017). L5u neurons projecting to thalamic regions that project back to cortex showed early preparatory activity that persisted until the movement, while the L5lower neurons

produced late preparatory activity and motor commands. Together these studies have begun to map the circuitry responsible for transforming sensory input in to decision related preparatory activity and ultimately motor initiation signals.

By imaging voltage activity across dorsal cortex in mice performing a sensory-guided forced choice licking task, we sought to examine the population membrane voltages across sensory cortex and motor cortex while mice prepared, withheld, and finally initiated licking movements towards left and right lick spouts. In contrast to previous studies examining preparatory and initiation activity in the motor cortex, we utilized fail trials when the mice were unable to properly suppress licking before the response window to determine cortical voltage correlates of movement preparation, suppression and initiation across sensory and motor cortices. Compared to correct trials, early lick fail trials provide a direct contrast allowing the identification of neural dynamics when the mouse fails to withhold the prepared movement. Additionally, we attempted to account for the variability in reaction time and withhold fail trials by closely examining the neural and behavioral state of the mouse preceding each trial using both the pupil diameter and local/global measures of synchronized cortical activity. We found that membrane voltage in the contralateral motor cortex before the onset of the response period predicts the reaction time on a trial-to-trial basis such that increased voltage activity preceding the first lick is elevated on faster reaction time trials. In contrast, voltage activity extending across other parts of cortex including primary sensory and visual areas negatively predicts reaction time, such that when voltage is elevated across non-motor areas, the mouse's reaction time is slower. In addition, fail trials where the mouse was unable to properly

withhold licks until the start of the response period were characterized by elevated voltage levels in pre- and primary motor cortices contralateral to the direction of the lick.

4.2 Methods

Mice:

For wide-field imaging, VSFP-Butterfly expressing mice were generated by crossing the cre/tTa dependent VSFP-Butterfly reporter line (Akemann et al., 2012) with both an excitatory neuronal expressing CaMK2a-tTa line as well as a mouse line containing cre in excitatory cortical neurons (Emx1-cre). The result of this triple cross were mice expressing VSFP-Butterfly 1.2 in excitatory neurons in all layers of cortex.

Surgery:

For voltage imaging, 5 mice were implanted with a head-post and a through-skull dual-hemisphere cranial window over the dorsal cortex. These mice were also included in a previously *published* study (Morrissette et al., 2018), though none of the data analyzed for these experiments was included in the prior report. The cranial window consisted of a custom-cut #1 glass coverslip cemented over the cleaned skull surface. A thin layer of cyanoacrylate glue was placed in between the bone and cement interface. Mice were administered 0.1mg/kg of buprenorphine as an analgesic and 1-2% isoflurane (3-4% for induction) for the duration of the surgery. Mice were aged 3-12 months at the start of experiments and maintained on a 12h:12h reverse light cycle for the duration of behavior training and imaging. During behavioral training, mice were provided ad libitum food

access and were kept of 1-1.5mL/day water restriction protocol for 6 days a week starting 3 days prior to handling and imaging. On the 7th day of each week, mice were given free access to water. During behavioral testing and imaging sessions, mice were given 10% sucrose solution with 0.1% grape Kool-Aid powder. Liquid consumption was measured during testing and mice were supplemented with water to reach their 1-1.5mL daily volume. All experimental procedures were approved by the Emory University Institutional Animal Care and Use Committee.

Voltage Imaging:

We imaged VSFP signals with a macroscope (MiCAM Ultima, Brainvision Inc.) based on the tandem lens and epi-illumination system design (Ratzlaff and Grinvald, 1991). Excitation light was provided by a blue LED (LEX2-B, Brainvision Inc.), through a band-pass filter at 482nm (FF01-482/35, Semrock Inc) and a dichroic mirror (FF506-Di03, Semrock Inc.). VSFP-Butterfly FRET chromophores (mKate2 and mCitrine) were imaged through two CMOS cameras (MiCAM-Ultima). The first camera recorded the emitted fluorescence from mCitrine, which was reflected by a second dichroic mirror (FF593-Di03, Semrock, Inc.), passed through an emission filter (FF01-543-50-25, Semrock Inc.). The second camera recorded the emitted fluorescence from mKate2, passed through the second dichroic mirror and an emission filter (BLP01-594R-25, Semrock Inc.). The camera acquisition was controlled by the MiCAM Acquisition Software. Acquisition frames rates varied between 25-200Hz with a spatial resolution of 0.01mm/pixel. The blue LED remained on for the duration of each imaging session that lasted 60 minutes on average.

Behavioral Task:

In order to determine the cortical activity underlying movement preparation, we used a behavioral task previously reported in (Morrissette et al., 2018) (Fig 4.1A). In this behavioral task, the mouse was instructed to lick to 1 of two lick spouts position to the left and right of the mouse based on the presence of a left or right air-puff stimuli, respectively. The mouse was forced to withhold movement for the duration of the air-puff (1-1.5s) and was able to lick to indicate the direction of the stimulus once the air-puff had stopped. During this response window, the mouse had up to 5 seconds to lick to indicate its decision and if correct, was provided with a sucrose reward from the respective spout.

Pupil and Behavioral Monitoring Videography:

In order to monitor and record changes in behavioral state and pupil diameter, we captured moderate-speed (10-25Hz) videography of the mouse acquired simultaneously during imaging sessions. The first camera was positioned to the front and side of the mouse, capturing the left side of the mouse face as well as the left eye and the area where the forelimbs often rest underneath the mouse body. An additional camera was occasionally positioned in front of the mouse and reflected off of a mirror to capture the whiskers, snout, and mouth from underneath of the mouse.

VSFP Image Processing:

Raw images from both cameras were first aligned and registered to the first frame of the donor camera for any given trial. The signals from the two cameras were analyzed using the gain-equalization method (Akemann et al., 2012; Carandini et al., 2015; Shimaoka et

al., 2018), by equalizing the gains at the heart beat frequency between the two cameras. The gain equalization factors were obtained once per recording for each pixel, using the first trial of the session. The ratio of the two cameras captures FRET signals linked to membrane potential variations (Carandini et al., 2015) while the sum of the two signals captures large co-fluctuations linked to the hemodynamic response (Shimaoka et al., 2018). To exclude possible residual contamination of the hemodynamics in the ratiometric signal, the sum (hemodynamic) signal was filtered below 5Hz and then scaled by the regression coefficient with the ratiometric signal, then subtracted out from the ratiometric signal (hemodynamic signal regression, HSR). To perform analyses across trials and mice, the base image used to register within-trial frames was aligned to a template cortical map derived from the Allen Brain Mouse Atlas v3 (brain-map.org). A 2D top projection of the annotated Allen Brain Atlas volume was created in MATLAB (MathWorks) and a template image from one mouse was registered to the atlas using an affine transformation computed from two control points that were selected manually: the mid-point at the top of the front portion of dorsal cortex and the posterior position of the retrosplenial cortex.

Region Identification:

Cortical regions were assigned based on registration to the Allen brain atlas cv3 (brain-map.org). One template VSFP image from a sample mouse was aligned using manual placement of control points to the Allen brain cortical map. An example image from all other mice was then aligned to the control point-aligned VSFP image using rigid and translation alignment in Matlab. Functional sub-regions within the larger atlas defined regions were determined by manually localizing cortical pixels responsive to behavioral

task variables such as licking and air-puff onsets. For subsequent processing, the base image from each imaging session was aligned to the mouse-specific template image and all following frames were transformed using the same alignment specifications. Inter-trial registration was performed using a sub-pixel rigid registration of frames up-sampled to 10000x10000 pixels in the frequency space (efficient sub-pixel registration).

Data Analysis:

To determine statistical significance between correlation maps used to identify voltage correlates of reaction time, we calculated shuffle-corrected correlation coefficients, such that the average of trial-shuffled correlations (averaged over 10 randomized reshuffled samples) was subtracted from the original correlations calculated. In order to determine significant differences in the average voltage activity during different epochs of the trial, we used the Wilcoxon rank-sum test.

4.3 Results

Wide-Field Cortical Imaging in Mice Performing A Forced Choice Licking Task

In order to examine cortical activity with high spatial and temporal resolution across large extents of cortex, we imaged fluorescent activity in behaving mice expressing the voltage indicator VSFP-Butterfly1.2 in excitatory cortical neurons (Fig 4.1B). Prior to imaging, mice (n=5) were trained on a forced choice left/right licking task (*Morrissette et al., 2018*) (Fig 4.1C). During the course of a trial, the mice were presented with an air-puff stimulus to the left or right whiskers for a randomized time between 1-1.5s during which mice were not allowed to lick either spout (Fig 4.1C). After the offset of the air-puff the mouse was allowed to indicate the direction of the air-puff stimulus by licking to either the left or right lick spout. If the mouse selected the correct spout, it was provided with a sucrose liquid reward and entered an inter-trial period before the next trial began. Alternatively, if the mouse licked prior to the offset of the air-puff, the air-puff stopped, no reward was provided and the mouse entered the inter-trial period.

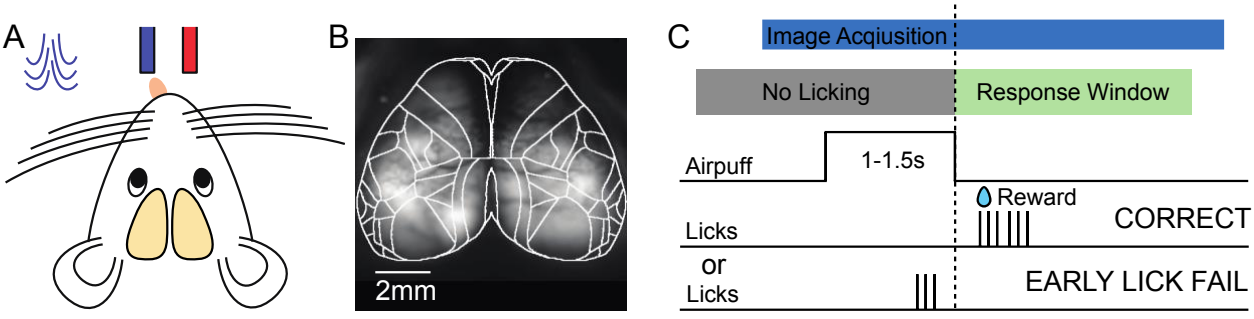

Figure 4.1. Wide-Field Cortical Imaging of Mice Performing Forced Choice Licking Task

A. We trained mice to perform a sensory-guided left/right licking task. In response to a left or right air-puff, mice were required to report the location of the air-puff by licking a left or right positioned lick spout, respectively. In the example graphic, a left air-puff applied to the whiskers requires mice to lick towards the left spout to receive a sucrose

reward. **B.** Example baseline fluorescent image of the camera capturing signal from the donor channel of the voltage sensitive protein, VSFP-Butterfly 1.2. A cortical map generated from the Allen Brain Atlas v3 was overlaid to show the various cortical areas covered by the wide-field imaging macroscope. **C.** Schematic of an example trial with two of the possible outcomes illustrated. Image acquisition begins during the pre air-puff period where the mice must withhold licking. After 3-4 seconds of no licking activity, the mouse is presented with an air-puff stimulus towards the left or right whiskers for a variable time interval between 1 and 1.5s. At the offset of the air-puff, the mouse is then allowed to report the air-puff location by licking the correct spout and receives a sucrose reward if correct ('Correct' trial). Alternatively, if the mouse licks during the air-puff stimulus they fail the trial ('Early Lick Fail' trail).

Spatiotemporal Cortical Voltage Dynamics During Sensory-Guided Licking Behavior

First, we sought to determine the evoked voltage dynamics reflecting decision related activity. Specifically, we wanted to determine the temporal patterns of activity in sensory and motor cortices (Fig 4.2B) around the response lick (first lick during the response period). To do this we aligned and averaged voltage responses in mouse sensory-motor cortex (S1 and M2) in L and R hemispheres centered at the start of the response period (Fig 4.2C). At the onset of the air-puff we found a primary sensory response contralateral to the side of the air-puff followed by a more global secondary response. As the end of the sample period approached, cortical activity across sensory-motor areas increased with the contralateral S1 and M2 increasing even further above the ipsilateral activity just preceding the start of licking activity. To better understand the spatial extent of the cortical activity during the behavioral task, we selected frames from the 10-trial average shown in C to observe activity at the start of the sensory stimulus (Fig

4.2D). At 25ms after the air-puff we saw a clear sensory evoked response in the contralateral barrel cortex. At the start of the response period, we saw an increase in contralateral sensory-motor activity, especially in the contralateral M2 cortex, corresponding to the location of the ALM, the motor cortical area controlling licking movements (Fig 4.2E).

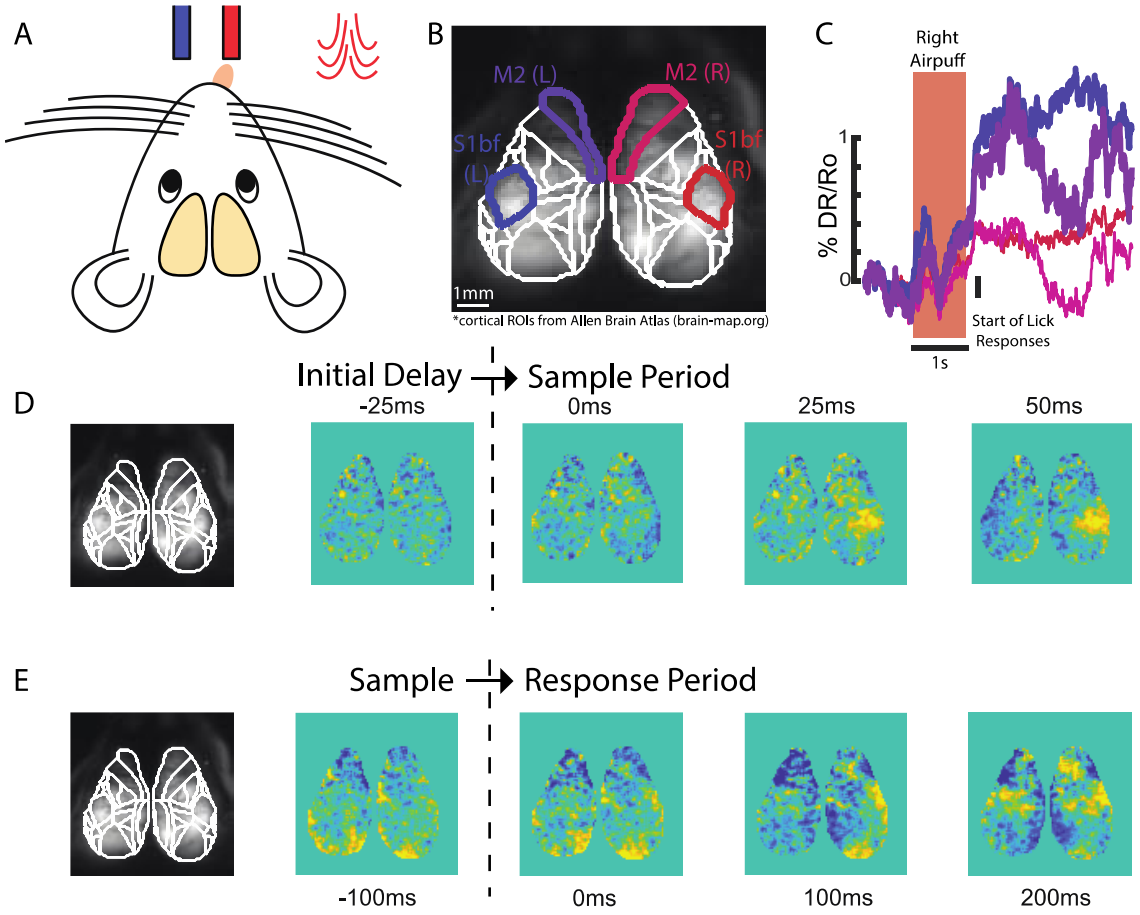

Figure 4.2. Spatiotemporal Cortical Voltage Activity During Sensory-Guided Licking Behavior

A. Illustration of mouse and trial context. In these trials, the air-puff stimulus is directed at the right whiskers and the mouse is required to lick the right lick spout after the offset of the air-puff to receive the sucrose reward. **B.** Allen Brain Atlas map overlaid on the base image from the donor fluorescent channel. Motor cortical areas are colored purple and magenta for left and right M2, respectively and primary sensory barrel cortices are outline

in blue (left) and red (right). **C.** Average cortical activity (n=10 trials) for left air-puff correct performance trials. At the onset of the air-puff, there is a primary sensory response observed in the contralateral sensory cortex (blue) and a secondary response that is cortex wide. During the course of the air-puff period, voltage signals across cortex begin to ramp and at the offset of the sample period, contralateral sensory-motor cortices increase above the ipsilateral hemisphere that precedes the start of licking responses. **D.** Map of cortical activity across imaging frames around the onset of the air-puff stimulus onset. A clear evoked sensory response contralateral to the air-puff can be observed as early at 25ms following the stimulus. **E.** As the trial transitions from the sample to response period, we can observe increased contralateral sensory-motor activity primarily in areas of secondary motor cortex (corresponding to ALM) before the onset of licking activity.

Lateralized Voltage Signals in Anterior Lateral Motor Cortex Underlying Licking Preparation and Initiation

To further examine how voltage activity in ALM was related to directional licking, we recorded fluorescent signals from left and right ALM in mice while performing the forced choice licking task (Fig 4.3A). Previous reports have shown that neural firing activity in ALM is selective for lick direction in sensory-guided licking tasks, though the voltage activity underlying directional licking remains unknown (Li et al., 2015, Economo et al., 2017). To determine how the signals in left and right ALM related to the onset of the response (Fig 4.3B), we aligned and the trials from a single mouse and session (n = 57 trials) to the start of the response period and sorted the trials by reaction time (Fig 4.3C). When aligned to the start of the response period, a clear pattern in activity can be observed of the contralateral neural activity between trials such that the initial peaks in the voltage signals are close to the reaction time of the mouse on any given trial (red

vertical lines). On average, we see the contralateral and ipsilateral activity between contra- and ipsi-lateral ALM areas is similar during the trial until about 100ms before the end of the sample period, at which time the contralateral ALM activity starts to increase above the ipsilateral ALM (Fig. 4.3D). We then aligned the ALM voltage activities to the first lick in the response period for correct left lick trials. When aligned to the first lick, we now see a clear peak in activity at the lick onset across all trials and oscillations representing later time-locked licks in the lick bout for each trial (Fig 4.3E). Looking at the cortical voltage activity averages for contra- and ipsi-lateral ALM, we can see a clear peak in the average contralateral ALM activity at lick onset and additional peaks representing future licking activity. Interestingly, when aligned to the first lick, we can now see that the contralateral and ipsilateral ALM voltages begin to diverge at ~700ms before the first lick with contralateral activity beginning to increase slowly above the ipsilateral ALM activity for 250ms and then beginning to rise faster at around 250ms before the first lick (Fig 4.3F). At this time of ramping increases in contralateral ALM activity, the activity in ipsilateral ALM remains flat, suggesting that direction selective movement preparation signals may emerge in cortical voltage activity over 500ms before the first lick.

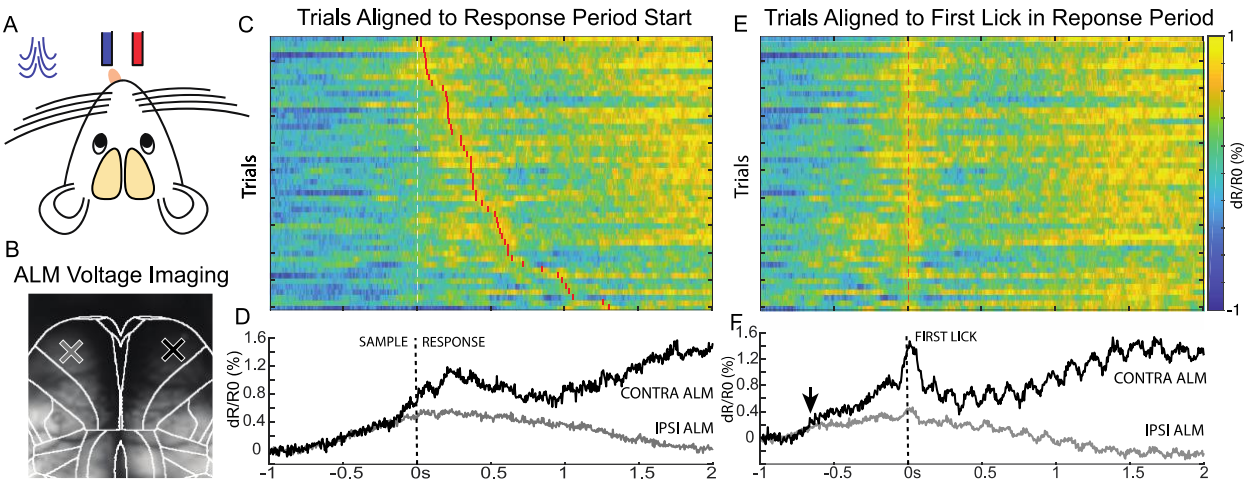

Figure 4.3 Lateralized Voltage Signals in Anterior Lateral Motor Cortex Underlying Licking Preparation and Initiation

A. Diagram of mouse orientation and trial type. In these example trials, the air-puff stimulus is directed at the left whiskers and the mouse is required to lick towards the left spout after the offset of the air-puff to obtain a sucrose liquid reward. **B.** Cropped wide-field image showing the cortical locations used for obtaining voltage signals from ALM ipsilateral to the air-puff (grey) and contralateral to the air-puff (black). **C.** Contralateral ALM voltage activity from correct left lick trials taken from a single imaging session from a single mouse (n = 50 trials). Trials are sorted based on the reaction times (vertical red lines) that are overlaid over the voltage signals. The vertical, white dashed line represents the offset of the air-puff representing the start of the response period. Initial peaks in voltage activity across all trials appear to be tightly locked to the response time for each trial. **D.** Average ALM voltage signal (n = 50 trials) from contralateral cortex (black) and ipsilateral cortex (gray). When aligned to the start of the response period, we can observe the signals from both hemispheres share the same voltage activity until ~200ms before the response period begins. At this point, the contralateral ALM voltage rises faster than the ipsilateral cortex until about 250ms after the start of the response period. **E.** Contralateral ALM voltage activity from correct left lick trials taken from a single imaging session from a single mouse (n = 50 trials). Trials are now sorted based on the first lick during the response period (the reaction time) (dashed red line). Peaks in the voltage signal are now aligned at t=0s and fluctuations of individual subsequent licks are also apparent later in the trial. **F.** Average ALM voltage activity from contralateral (black) and

ipsilateral (gray) ALM. When aligned to the first lick, we can now see that the ALM signals across hemispheres begin to diverge over 500ms before the first lick, with the largest transient occurring in contralateral ALM ms before the first lick. Large fluctuations following the first lick can be observed on the trial-averaged data and is more prevalent in the contralateral ALM, but is also apparent in the ipsilateral ALM activity. Over the course of licking, contralateral ALM activity continues to increase, while voltage in ipsilateral ALM slowly decreases.

Voltage Activity in ALM Underlying Proper Movement Suppression and Initiation

In our behavioral task, we trained mice to withhold movement for the duration of a 1-1.5s sensory air-puff stimulus before licking to indicate their direction decision in order to receive a sucrose reward. While mice learned to perform this task well over the course of training, we still observed many trials where the mice failed to withhold licking movements before the offset of the sample period, causing what we refer to as “early lick fail” trials. To determine the neural activity in ALM relating to the proper withholding of licking during sample period, we compared ALM voltage activity aligned to the first lick in correct trials and early lick fail trials (Fig 4.4A). Looking at the average voltage data for contralateral ALM between correct and fail trials, we can see that early activity in ALM is increased for early lick fail trials compared to correct trials and activity immediately before and after the first lick appears to be increased. However, later in the trial beginning about 500ms after the first lick, ALM activity is actually increased in correct trials compared to early lick fail trials. To better quantify the differences in average voltage activity within specific trial epochs, the 1s to 500ms preceding the movement time is designated as “BASE” activity (shaded gray), the 500ms to 0ms before the lick onset is termed “PRE” (shaded blue), the first 500ms after the onset of the lick is “MOVE” (shaded green), and

finally the period lasting from 500ms to 1s after the first lick is “LATE” activity (shaded red). Within trails taken from the single mouse shown in 4.4A, can observe statistically significant increases in voltage for early lick trials compared to trials where the mouse properly withheld licking across BASE ($p<0.001$), PRE ($p<0.0001$), and MOVE ($p<0.0001$) periods (Fig 4.4B). Voltage activity during the LATE trial period was instead significantly increased in correct trials compared to early lick fail ($p<0.0001$). To account for changes in the baseline voltage level potentially causing the voltage activity differences between subsequent trial epochs, we recalculated voltage the PRE, MOVE, and LATE periods as differences relative to the baseline. After correcting for the baseline offset in the single mouse voltage data, we now see that PRE voltage activity is non-significant between correct and early lick fail trials. MOVE epoch activity when corrected for the voltage just before the first lick is still significantly increased after accounting for the pre-lick voltage. Finally MOVE and LATE epochs adjusted for baseline offsets are also still significantly increased ($p<0.0001$) and decreased ($p<0.0001$), respectively in early lick fail trials compared to correct withhold trials. Across all mice, we observed the same presence of increased voltage activity especially just before and after the onset of the first lick (Fig 4.4DE). Together these results suggest increased excitatory voltage signals in contralateral ALM contribute to the mouse’s inability to properly withhold licking movements.

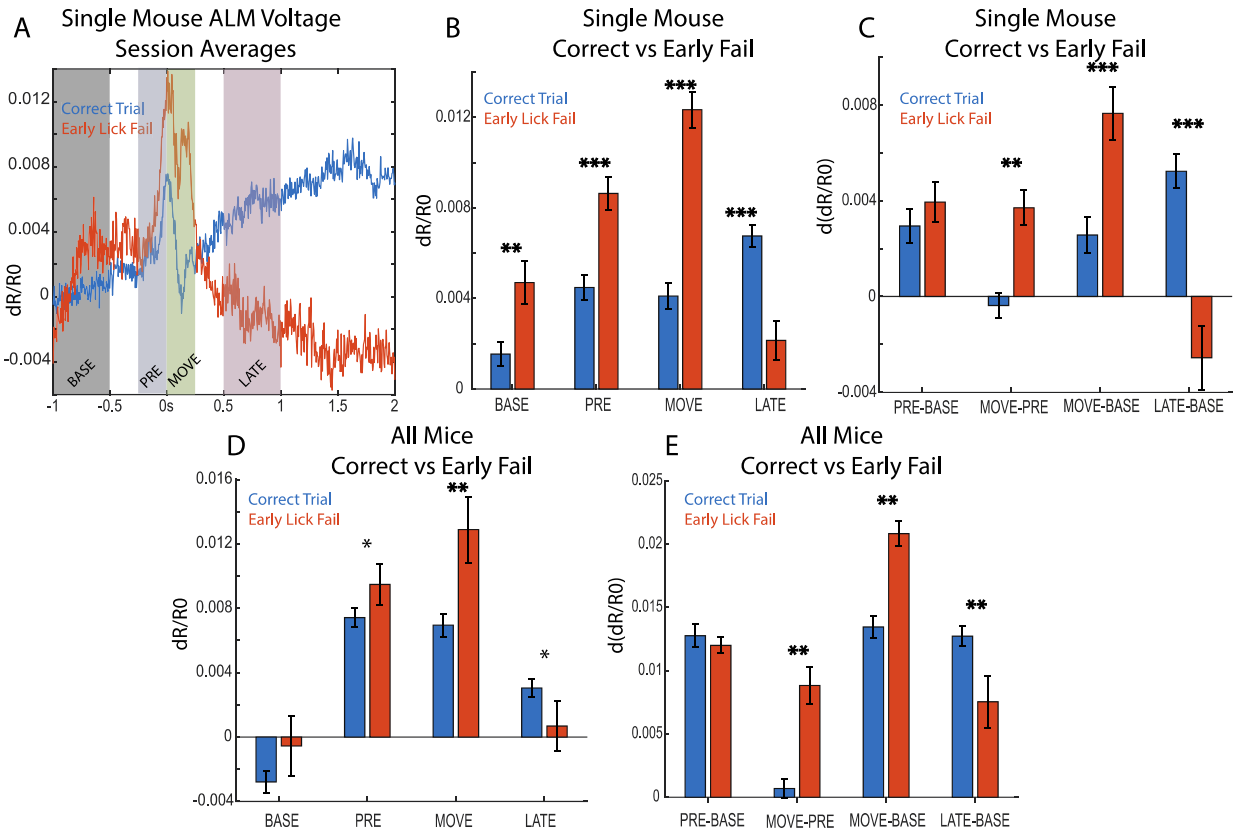

Figure 4.4 Voltage Activity in ALM Underlying Proper Movement Suppression and Initiation

A. Example of average session activity within a single mouse comparing ALM voltage activity in correct trials (blue) and early lick fail trials (red). Activity is aligned to the animals first lick during the trial. The voltage activity for the correct trial averages shows an increase in voltage before the onset of the first lick, followed by a negative transient, that then increases for the remainder of the trial time shown. In contrast, early lick fail trials show elevated voltage early in the trial and increased pre-movement and post-movement voltage activity compared to correct trials. After this increase in activity the voltage decreases back towards baseline levels. For analysis of voltage changes within specific trial epochs, the 1s to 500ms preceding the movement time is designated as "BASE" activity (shaded gray), the 500ms to 0ms before the lick onset is termed "PRE" (shaded blue), the first 500ms after the onset of the lick is "MOVE" (shaded green), and finally the period lasting from 500ms to 1s after the first lick is "LATE" activity (shaded red). **B.** Statistical comparison of ALM voltage levels across the different task epochs between

correct and early lick fail trials for a single mouse (n = 2 sessions). At baseline, the voltage is significantly increased above correct trial activity. Similar significant increases are found for both PRE and MOVE periods where fail trials exhibit increased voltage activity on average. For the LATE period, the correct trials show increased cortical voltage activity (* $p<0.01$, ** $p<0.001$, *** $p<0.0001$). Error bars represent +/- SEM. **C.** Differences in voltage controlling for baseline offsets and relation to movement for the single mouse shown in B. After correcting for the difference in voltage activity observed at baseline levels, the PRE activity is no longer different between correct and early lick fail trials. However, movement activity when corrected by PRE activity remains significantly increased in the early lick fail trials and MOVE activity is still significantly increased compared to correct trials when adjusted for the baseline offset. Finally, when adjusted for baseline differences, correct trials still exhibit increased voltage during the LATE trial period compared to early lick fail trials. **D/E.** Same as B and C., but including sessions from all mice in the analysis (n = 5 mice, 10 sessions).

Cortical Correlates of Reaction Time Are Not Limited to Motor Cortical Areas

To determine how reaction time is reflected in voltage activity across cortex, we aligned trials to the start of the response period and performed pixel-wise correlations between the trial-to-trial voltage level and the trial-to-trial reaction times. We hypothesized that motor cortical areas would show a negative correlation with reaction times as the start of the response period approached such that increased preparatory voltage activity would lead to shorter reaction times. We indeed found that negative correlations emerge early in the contralateral sensory-motor cortical areas with lateral effects most apparent in pre-frontal motor areas and emerging in (Fig 4.5B, left middle). Interestingly, we found striking positive correlations across many brain areas during the withholding period with reaction time, suggesting that increased voltage activity outside of motor pre-motor cortex actually led to slower reaction times (Fig 4.5B middle, right).

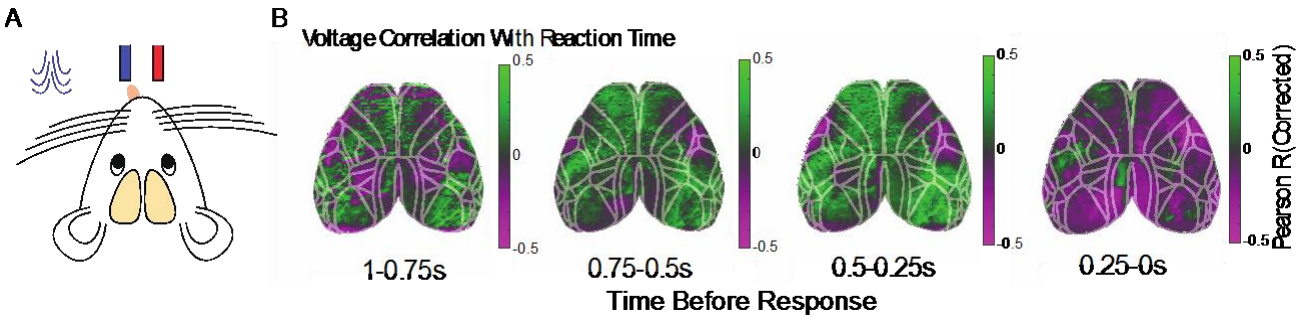

Figure 4.5 Neural Correlates Predicting Reaction Time Emerge in Over 1s Before Onset of Movement Response

A. Mouse graphic indicating the trial direction that informs the cortical activity maps in B. **B.** Single mouse example of voltage correlations with reaction times emerging across the course of the withholding period (n = 1 mouse, 20 correct left lick trials). In this example mouse, right hemisphere sensory and motor areas are negatively correlated with future reaction time beginning at 1s before response (left). As time continues, activity in other cortical areas is positively correlated with reaction time, such that more activity in these areas correlates with longer time to lick (middle left and middle right panels). In the last 250ms before the onset of licking, the right sensory-motor cortical areas are even more negatively correlated as well as other areas across cortex that were positively correlated earlier in the withholding period. Importantly, activity in the ipsilateral sensory cortex and pre-motor cortex are still positively correlated with reaction time, suggesting activity in these areas is competing against the contralateral hemisphere to direct the movement.

4.4 Discussion

Decision making tasks provide a fundamental paradigm in neuroscience used to examine how animals process sensory inputs and use that sensory information to make a behavioral choice and evaluate the outcome of their decision. While considerable research has been devoted to understanding how the brain processes incoming sensory information, less is known about the systems involved in converting sensory cues in to movements to successfully perform the given behavioral task. In this study, we used non-invasive measures of cortical membrane voltage activity to determine how sensorimotor cortical activity accounts for variability in movement preparation and movement suppression in behaving mice. Using single trial analyses of neural activity and mouse reaction times, we were able to correlate neural activity across the course of movement preparation finding that sensorimotor areas primarily contralateral to the upcoming movement were strong predictors of the reaction time, up to 1s before the mouse began to move. In addition, we found that increased cortical activity outside of the sensory-motor cortex was a negative predictor of reaction time, such that increased activity in non-motor cortical areas correlated with slower reaction times early in movement planning. Finally, by comparing trials where the mouse licked too early, failing to suppress movement prior to the response period, were accompanied by increased voltage activity preceding the first lick compared to trials where the mouse correctly licked after the response period began. This increase in voltage activity for early lick trials diverged from the voltage transients observed in correct trials approximately 0.5s before the lick onset, suggesting that movement suppression was facilitated by less excitatory input or increased inhibitory input to the motor cortex during the interval preceding the initial movement.

To our knowledge, this is the first study investigating neural correlates of movement preparation and suppression across sensory-motor circuits in behaving mice. Closely related studies begun to examine the voltage dynamics of sensory integration in sensory-motor cortex in awake mice using voltage sensitive dyes (Ferezou et al., 2007) and intracellular recordings (Poulet and Petersen, 2008, Sachidhanandam et al., 2013, Yamashita and Petersen, 2016). Using Go-NoGo behavioral tasks, these studies have found that proper sensory detection relies upon complex coordination between sensory cortices (S1/S2) and motor cortices (M1/M2). In these detection tasks, mice are only required to withhold licking before the presented sensory stimulus and can respond as quickly as possible following the sensory stimuli to report detection and receive a reward. In this context, sensory activity is quickly followed by activations in motor cortical activity (Ferezou et al., 2007, Kyriakatos et al., 2017) and the motor cortex activity is dependent on S1 with local inactivation of S1 using CNQX-APV (an ionotropic glutamate receptor antagonist) blocking whisker evoked responses in both S1 and M1. The whisker evoked activity in S1 and M1 is also dependent on the behavioral state of the mouse, such that during periods of whisking, whisker stimulation does not evoke a cortical response. This feature of cortical processing suggests that trials in which the mouse was actively whisking during the presentation of the air-puff stimulus would result in less activation of sensory-motor cortices and delay detection and reaction times. Accordingly, we found that when the cortex was more active (as observed during bouts of movement) before and during the sensory stimulus, reaction times were increased.

A main advantage of our study was the ability to monitor membrane potential fluctuations across wide areas of cortex with high spatial and temporal resolution. The

use of voltage imaging to observe this voltage activity overcomes many technical limitations preventing traditional electrophysiological analyses from addressing the questions presented in this study. While LFP recordings provide some insight in to the synaptic input and voltage activity within a neural circuit, the physiological contributions to the LFP signals are difficult to localize and the spatial extent from which one is able to record LFP activity is limited by the invasiveness of inserting physical objects in to the brain. Other techniques such as electrocorticography (ECoG) and electroencephalography (EEG) provide an improved spatial sampling compared to LFP, but significantly sacrifice spatial resolution (Musall et al., 2014).

One limitation of this study was the overlapping of sensory and motor preparatory signals since the sensory period was also used as the period where the mouse must withhold licking movements. Thus, parsing the distinct contributions of the air-puff stimulus and the coordination of choice activity remained difficult. By focusing on the activity preceding the first lick during correct and early lick fail trials, each within trials featuring the same preceding sensory stimulus, we were able to parse contributions neural activity relating to movement with minimal contamination from ongoing sensory activity. It was difficult to teach mice to withhold for extended periods and requires weeks of training to learn to properly withhold movement until the start of a response period. While fail trials that emerge from mice licking before the withhold period is over are often discarded from analyses (Guo et al., 2014a, Li et al., 2015, Guo et al., 2017), this aspect of the task design was used as a feature of the behavioral task in order to parse the cortical voltage correlates of movement suppression.

Chapter 5: General Discussion

Determining how the brain integrates sensory information to instruct future movements is a critical aspect of animal behavior and a core objective in neuroscience. One neural circuit at the center of this question is the basal ganglia-thalamocortical system and while considered to be a fundamental system for voluntary motor control, little is known about how the areas interact to orchestrate movements. The studies described above aim to narrow the knowledge gap regarding how the basal ganglia influences cortical activity in the context of sensory-motor behavior. Selection of a proper behavioral paradigm for our studies is an understated but critical aspect of our studies. We adapted a well described sensory-guided forced choice licking task that has been shown to require coordinated activity between the thalamus and cortex to perform (Guo et al., 2014c, Li et al., 2015, Guo et al., 2017). We first used optogenetic manipulation of the SNr and its projections to the motor thalamus and determined that by optically exciting or inhibiting basal ganglia output, we can facilitate or suppress licking movements, respectively. Interestingly, while increasing activity in the SNr impaired licking towards both the right and left directions, when we instead only excited SNr projections to the motor thalamus, licking was only impaired towards the contralateral direction. The main feature of these experiments was the use of optogenetics to selectively target specific cell-type and projection specific circuits (Luo et al., 2018). In previous studies, one technique used for neural manipulation involved electrically stimulating neural populations which can result in off-target effects due to exciting nearby nuclei or passing fibers. Chemical and chemogenetic alternatives have also been used to selectively silence or excite neural activity within the injected area, however, in addition to potentially affecting off-target cell

populations, this method does not provide fine temporal specificity with effects lasting minutes to hours until the injected chemical is cleared. Optogenetics improves on all of the shortcomings described above by allowing for fine temporal and spatial control by using light pulses delivered through a small optic fiber to the brain area of interest. The affected area is determined by the illuminated area below the optic fiber as well as the genetic strategy used to target the light sensitive protein to the cell population of interest.

This study is the first to directly test the role of basal ganglia output to the motor thalamus on motor (directional licking) behavior. Many neurological disorders are rooted in or partially involve basal ganglia dysfunction including Parkinson's disease, Huntington's disease, Autism Spectrum Disorders, Obsessive Compulsive Disorder, and Tourette Syndrome. Thus, understanding how the basal ganglia influences downstream circuits and animal behavior is critical to understanding the mechanisms by which these disorders impair healthy neural function. In addition, as human therapies advance to allow for cell-type and projection specific interventions, dissecting the contributions of the various basal ganglia output pathways on behavior may inform future development and targeting of therapies or refinement of existing therapies such as deep brain stimulation.

5.1 Establishment of Cortical Voltage Imaging Techniques in Awake, Behaving Mice

The basal ganglia receiving area of the motor thalamus (BGMT) projects across large spatial extents of motor and sensory cortex (Kuramoto et al., 2009, Kuramoto et al., 2015, Svoboda and Li, 2018). In order to comprehensively examine cortical areas receiving input from the BGMT, we adapted and further developed a technique for

imaging cortical voltage activity in behaving mice. Using a wide-field macroscope, we were able to image over a 10x10mm area of the cortex and measure fluorescent changes in a mouse cortical neurons that were genetically engineered to change fluorescence based on the membrane voltage. Compared to calcium imaging, voltage imaging is able to track much faster activity as well as changes in subthreshold voltage levels, though this comes with a large sacrifice in fluorescent signal currently offered by the latest versions of calcium sensors (Luo et al., 2018). Since the available voltage sensors offer relatively low signal, they are increasingly susceptible to noise, including movement artifacts and hemodynamic activity. To get around this limitation, recent studies using voltage imaging techniques have relied on obtaining large numbers of trials and averaging trials around a specific event such as a sensory stimulus (Petersen et al., 2003, Brown et al., 2009, Ferezou et al., 2009, Borden et al., 2017). Many of these studies have been in the anesthetized mouse, where baseline activity is low and steady allowing for low signals to be clearly observed above the signal noise. Due in part to these difficulties, there are not yet any published studies using wide-field imaging of genetically encoded voltage indicators in the behaving mouse. In our imaging studies, we were able to successfully image voltage activity during behavior through several careful considerations and strategic decisions. We used the FRET-based voltage indicator VSFP-Butterfly 1.2 which is uniquely suited for acquiring single trial activity due to the two fluorescent channels emitted from the fluorescent protein: one channel that increases and the other that decreases fluorescence based on membrane voltage (Akemann et al., 2012, Carandini et al., 2015). By utilizing two separate cameras to record the two different wavelengths and then using ratiometric equalization methods we are able to divide the properly scaled

signals from each channel and obtain a voltage signal independent of hemodynamic or movement artifacts.

5.2 Cortical Voltage Dynamics in During Awake, Spontaneous Behavior

Before imaging in the behaving mouse, we wanted to evaluate the voltage activity dynamics in the awake mouse in the absence of a behavioral task, which includes periods of quiescence as well as bouts of spontaneous movement. In the third chapter, I performed initial imaging experiments in awake mice while also obtaining pupillometry video, since recent reports suggested pupil diameter and membrane voltage may share similar activity dynamics related to arousal (McGinley et al., 2015a, McGinley et al., 2015b, Reimer et al., 2016). Through these first experiments aimed at characterizing the cortical voltage activity patterns, we found that pupil diameter even more closely related to the global voltage signal fluctuations (the average voltage shared across cortex) than expected. In some trials, pupil diameter accounted for over 70% of the variance in the global voltage signal and is especially well suited for tracking infra-slow fluctuations in the frequency ranges less than 0.1Hz. The spatial pattern of cortical activity coupling with pupil diameter is also interesting, with medial sensory areas and auditory cortex showing strong coupling with the pupil and frontal motor areas as well as the sensory barrel cortex showing little or even negative coupling. These findings have significant implications for neuroscience and psychology research, suggesting that by measuring a physiological variable as simple as the pupil diameter, one can obtain measure of neural activity accounting for the majority of arousal-related (e.g. global signal) variability. Based on the pupil diameter, we found profound differences in the underlying cortical voltage activity,

which further supports using pupil diameter as covariate in neuroscience experiments to control for arousal related changes in neural activity and/or behavior.

5.3 Cortical Voltage Imaging of Movement Preparation and Initiation

In order to understand how output from the basal ganglia influences the cortex in the context of motor control, it is critical that the cortical mechanisms underlying movement are well characterized as well. Voluntary movement requires complex coordination of activity within motor cortex as well as sensory and cognitive cortical areas that all receive input from the BGMT. Neural representations of movement planning and initiation have been found across sensorimotor cortex with varying relationships to the preparation and onset of movement. Wide-field voltage imaging provides a unique combination of high spatial and temporal resolution strongly suited to examining cortex-wide interactions during sensory-motor behavior in head-fixed animals. Many aspects of the underlying population neural activity have been found to correlate strongly with various aspects of movement, including movement velocity, reaction time, and movement direction (Churchland et al., 2006a, Churchland et al., 2006b, Churchland et al., 2012, Elsayed et al., 2016, Kaufman et al., 2016, Lara et al., 2018a, Lara et al., 2018b, Russo et al., 2018). These studies primarily utilize single-cell recordings over the course of many trials to identify firing rate changes relating to movement. In addition to neural firing rates, our study adds membrane voltage to the large list of neural correlates underlying aspects movement suppression and preparation. Whether the underlying voltages across motor cortex provides unique information in predicting movement parameters remains yet to be determined.

While our correlation analyses allow calculation of metrics for relating neural activity patterns and behavior that are straightforward to interpret, it provides only a limited view of the context and behavioral components that may account for the neural activity. Generalized linear models accounting for specific variations in trial context as well as mouse behavioral state are powerful methods for separating the contributions of many measured variables to the observed neural activity (Musall et al., 2018), though can be difficult to interpret as the regression coefficients to not necessarily map to correlations. In addition, several recently developed techniques have shown promise in identifying lower dimensional latent dynamics in the of population neural activity (Yu et al., 2009, Seely et al., 2016, Pandarinath et al., 2018, Wei et al., 2018)

5.4 Future Directions

While the studies encompassed in this thesis extend our knowledge of basal ganglia, thalamic, and cortical contributions to motor control, there are some limitations to these experiments and unanswered questions that give rise to new experimental paradigms that may be used to further this field of research.

Much of the uncertainty and speculation around the differential contributions of the basal ganglia and cerebellar receiving territories of the motor thalamus stems from our inability to cleanly isolate manipulations to a specific motor thalamic nuclei. While recent research provides support that new genetic markers may one day be developed to specifically target opto- or chemo-genetic manipulation strategies, another method utilizing trans-synaptic anterograde transport of cre recombinase has shown promising preliminary results. This method, adapted from recent reports from Kim et al. 2017, uses the AAV1 viral vector carrying cre recombinase injected in to the initial nuclei of interest

to transport cre recombinase across 1 synapse to the areas receiving projections from the injected nucleus. By injecting 100nL of AAV1-cre in to the SNr in tdTomato cre-reporter mice, we were able to observe strong expression of cre in the VM nucleus of the motor thalamus (corresponding to the BG receiving zone) as well as other regions receiving SNr input such as the CM, PF, and MD thalamic nuclei as well as the midbrain reticular formation, the zona incerta, the superior colliculus, and the pedunculopontine nucleus. Additionally, I injected a cre-dependent ChR2 AAV in the motor thalamus at varying volumes to see if the cre-expressing cells will also express the ChR2. While the larger volumes of ChR2 injections led to expression across multiple thalamic nuclei such as the CM, MD in addition to the VM, the smallest injected volume (60nL) led to more focal expression in just the VM thalamus. In this mouse, we also observed axonal expression of tdTomato and EYFP (tagged to the ChR2 expression) in L1 of the frontal cortex, consistent with previous studies showing that BGMT projects predominantly to L1. Thus, I have developed a novel method for selectively targeting the basal ganglia receiving motor thalamus. This method then provides an experimental platform for several key studies. First, excitatory or inhibitory opsins may be selectively targeted to the BGMT to determine the functional role of the BGMT during mouse licking behavior as performed in this thesis work or within the context of other sensory-motor behavioral tasks such as forelimb reaching, locomotion, or motor learning behavioral paradigms. Second, genetically encoded voltage or calcium indicators can also be selectively expressed in the BGMT to allow for optical imaging of thalamocortical axons in behaving mice. Using two different wavelength GEVI/GECIs, somatic cortical activity can also be imaged in parallel with BG-thalamocortical axonal activity to better understand how axons arising

from the BGMT influence cortical activity across different spatial, laminar, and temporal scales. Finally, cortical imaging may also be performed in conjunction with optogenetic manipulations of the BGMT. Importantly, careful considerations must be taken in to account such that opsin expressing axons from thalamocortical neurons are not inadvertently stimulated during cortical imaging. This may be achieved by using red-shifted opsins and blue light-activated optical indicators in cortex, though cross-talk can still occur even with color shifted opsins and activity sensors. An improved alternative could use recently developed soma-targeted opsins expressed only in the cell bodies of the thalamus that prevent activation of thalamocortical axons during imaging.

References

Ackermann H, Ziegler W (1991) Articulatory deficits in parkinsonian dysarthria: an acoustic analysis. J Neurol Neurosurg Psychiatry 54:1093-1098.

Akemann W, Mutoh H, Perron A, Park YK, Iwamoto Y, Knopfel T (2012) Imaging neural circuit dynamics with a voltage-sensitive fluorescent protein. J Neurophysiol 108:2323-2337.

Albin RL, Young AB, Penney JB (1989) The functional anatomy of basal ganglia disorders. Trends Neurosci 12:366-375.

Alexander GE, Crutcher MD (1990) Preparation for movement: neural representations of intended direction in three motor areas of the monkey. J Neurophysiol 64:133-150.

Alexander GE, Crutcher MD, DeLong MR (1990) Basal ganglia-thalamocortical circuits: parallel substrates for motor, oculomotor, "prefrontal" and "limbic" functions. Prog Brain Res 85:119-146.

Allen WE, Kauvar IV, Chen MZ, Richman EB, Yang SJ, Chan K, Gradinaru V, Deverman BE, Luo L, Deisseroth K (2017) Global Representations of Goal-Directed Behavior in Distinct Cell Types of Mouse Neocortex. Neuron 94:891-907 e896.

Arber S (2017) Organization and function of neuronal circuits controlling movement. EMBO Mol Med 9:281-284.

Arber S, Costa RM (2018) Connecting neuronal circuits for movement. Science 360:1403-1404.

Barter JW, Li S, Sukharnikova T, Rossi MA, Bartholomew RA, Yin HH (2015) Basal ganglia outputs map instantaneous position coordinates during behavior. Journal of Neuroscience 35:2703-2716.

Bergman H, Wichmann T, DeLong MR (1990) Reversal of experimental parkinsonism by lesions of the subthalamic nucleus. Science 249:1436-1438.

Bhatia KP, Marsden CD (1994) The behavioural and motor consequences of focal lesions of the basal ganglia in man. Brain 117 (Pt 4):859-876.

Borden PY, Ortiz AD, Waiblinger C, Sederberg AJ, Morrissette AE, Forest CR, Jaeger D, Stanley GB (2017) Genetically expressed voltage sensor ArcLight for imaging large scale cortical activity in the anesthetized and awake mouse. Neurophotonics 4:031212.

Brown CE, Aminoltejari K, Erb H, Winship IR, Murphy TH (2009) In vivo voltage-sensitive dye imaging in adult mice reveals that somatosensory maps lost to stroke are replaced over weeks by new structural and functional circuits with prolonged modes of activation within both the peri-infarct zone and distant sites. J Neurosci 29:1719-1734.

Canales JJ, Graybiel AM (2000) A measure of striatal function predicts motor stereotypy. Nat Neurosci 3:377-383.

Carandini M, Shimaoka D, Rossi LF, Sato TK, Benucci A, Knopfel T (2015) Imaging the awake visual cortex with a genetically encoded voltage indicator. J Neurosci 35:53-63.

Chen TW, Li N, Daie K, Svoboda K (2017) A Map of Anticipatory Activity in Mouse Motor Cortex. Neuron 94:866-879 e864.

Churchland MM, Cunningham JP, Kaufman MT, Foster JD, Nuyujukian P, Ryu SI, Shenoy KV (2012) Neural population dynamics during reaching. Nature 487:51-56.

Churchland MM, Cunningham JP, Kaufman MT, Ryu SI, Shenoy KV (2010) Cortical preparatory activity: representation of movement or first cog in a dynamical machine? Neuron 68:387-400.

Churchland MM, Santhanam G, Shenoy KV (2006a) Preparatory activity in premotor and motor cortex reflects the speed of the upcoming reach. J Neurophysiol 96:3130-3146.

Churchland MM, Yu BM, Ryu SI, Santhanam G, Shenoy KV (2006b) Neural variability in premotor cortex provides a signature of motor preparation. J Neurosci 26:3697-3712.

Cisek P, Kalaska JF (2005) Neural correlates of reaching decisions in dorsal premotor cortex: specification of multiple direction choices and final selection of action. Neuron 45:801-814.

Crammond DJ, Kalaska JF (2000) Prior information in motor and premotor cortex: activity during the delay period and effect on pre-movement activity. J Neurophysiol 84:986-1005.

Crochet S, Petersen CC (2014) From perception to action: a spatiotemporal cortical map. Neuron 81:5-8.

Cruikshank SJ, Ahmed OJ, Stevens TR, Patrick SL, Gonzalez AN, Elmaleh M, Connors BW (2012) Thalamic Control of Layer 1 Circuits in Prefrontal Cortex. Journal of Neuroscience 32:17813-17823.

Cui G, Jun SB, Jin X, Pham MD, Vogel SS, Lovinger DM, Costa RM (2013) Concurrent activation of striatal direct and indirect pathways during action initiation. Nature 494:238-242.

Cury RG, Fraix V, Castrioto A, Perez Fernandez MA, Krack P, Chabardes S, Seigneuret E, Alho EJL, Benabid AL, Moro E (2017) Thalamic deep brain stimulation for tremor in Parkinson disease, essential tremor, and dystonia. Neurology 89:1416-1423.

Day BL, Rothwell JC, Thompson PD, Maertens de Noordhout A, Nakashima K, Shannon K, Marsden CD (1989) Delay in the execution of voluntary movement by electrical or magnetic brain stimulation in intact man. Evidence for the storage of motor programs in the brain. Brain 112 (Pt 3):649-663.

DeLong MR (1990) Primate models of movement disorders of basal ganglia origin. Trends Neurosci 13:281-285.

Deniau JM, Chevalier G (1985) Disinhibition as a basic process in the expression of striatal functions. II. The striato-nigral influence on thalamocortical cells of the ventromedial thalamic nucleus. Brain Res 334:227-233.

Deniau JM, Chevalier G (1992) The lamellar organization of the rat substantia nigra pars reticulata: distribution of projection neurons. Neuroscience 46:361-377.

Dominguez-Vargas AU, Schneider L, Wilke M, Kagan I (2017) Electrical Microstimulation of the Pulvinar Biases Saccade Choices and Reaction Times in a Time-Dependent Manner. J Neurosci 37:2234-2257.

Dudman JT, Krakauer JW (2016) The basal ganglia: from motor commands to the control of vigor. Curr Opin Neurobiol 37:158-166.

Ebbesen CL, Doron G, Lenschow C, Brecht M (2017) Vibrissa motor cortex activity suppresses contralateral whisking behavior. Nat Neurosci 20:82-89.

Economo M, Viswanathan S, Tasic B, Bas E, Winnubst J, Menon V, Graybuck LT, Nguyen TN, Wang L, Gerfen CR, Chandrashekar J, Zeng H, Looger LL, Svoboda K (2017) Distinct descending motor cortex pathways and their roles in movement. bioRxiv.

Elsayed GF, Lara AH, Kaufman MT, Churchland MM, Cunningham JP (2016) Reorganization between preparatory and movement population responses in motor cortex. Nat Commun 7:13239.

Erlich JC, Bialek M, Brody CD (2011) A cortical substrate for memory-guided orienting in the rat. Neuron 72:330-343.

Essman WD, McGonigle P, Lucki I (1993) Anatomical differentiation within the nucleus accumbens of the locomotor stimulatory actions of selective dopamine agonists and d-amphetamine. Psychopharmacology (Berl) 112:233-241.

Faull RL, Mehler WR (1978) The cells of origin of nigrotectal, nigrothalamic and nigrostriatal projections in the rat. Neuroscience 3:989-1002.

Ferezou I, Haiss F, Gentet LJ, Aronoff R, Weber B, Petersen CC (2007) Spatiotemporal dynamics of cortical sensorimotor integration in behaving mice. Neuron 56:907-923.

Ferezou I, Matyas F, Petersen CCH (2009) Imaging the Brain in Action: Real-Time Voltage- Sensitive Dye Imaging of Sensorimotor Cortex of Awake Behaving Mice. In: In Vivo Optical Imaging of Brain Function(nd and Frostig, R. D., eds) Boca Raton (FL).

Freeze BS, Kravitz AV, Hammack N, Berke JD, Kreitzer AC (2013) Control of basal ganglia output by direct and indirect pathway projection neurons. J Neurosci 33:18531-18539.

Fuxe K, Ferre S, Canals M, Torvinen M, Terasmaa A, Marcellino D, Goldberg SR, Staines W, Jacobsen KX, Lluis C, Woods AS, Agnati LF, Franco R (2005) Adenosine A2A and dopamine D2 heteromeric receptor complexes and their function. J Mol Neurosci 26:209-220.

Gaidica M, Hurst A, Cyr C, Leventhal DK (2018) Distinct Populations of Motor Thalamic Neurons Encode Action Initiation, Action Selection, and Movement Vigor. J Neurosci 38:6563-6573.

Garcia-Munoz M, Arbuthnott GW (2015) Basal ganglia-thalamus and the "crowning enigma". Front Neural Circuits 9:71.

Gent TC, Bandarabadi M, Herrera CG, Adamantidis AR (2018) Thalamic dual control of sleep and wakefulness. Nat Neurosci 21:974-984.

Gerfen CR, Engber TM, Mahan LC, Susel Z, Chase TN, Monsma FJ, Jr., Sibley DR (1990) D1 and D2 dopamine receptor-regulated gene expression of striatonigral and striatopallidal neurons. Science 250:1429-1432.

Gerlach J (1977) The relationship between parkinsonism and tardive dyskinesia. Am J Psychiatry 134:781-784.

Gerlach J, Reisby N, Randrup A (1974) Dopaminergic hypersensitivity and cholinergic hypofunction in the pathophysiology of tardive dyskinesia. Psychopharmacologia 34:21-35.

Godschalk M, Lemon RN, Kuypers HG, van der Steen J (1985) The involvement of monkey premotor cortex neurones in preparation of visually cued arm movements. Behav Brain Res 18:143-157.

Graybiel AM, Ragsdale CW, Jr. (1978) Histochemically distinct compartments in the striatum of human, monkeys, and cat demonstrated by acetylthiocholinesterase staining. Proc Natl Acad Sci U S A 75:5723-5726.

Graziano MS, Taylor CS, Moore T (2002) Complex movements evoked by microstimulation of precentral cortex. Neuron 34:841-851.

Guizar-Sicairos M, Thurman ST, Fienup JR (2008) Efficient subpixel image registration algorithms. Opt Lett 33:156-158.

Guo K, Yamawaki N, Svoboda K, Shepherd GMG (2018) Anterolateral motor cortex connects with a medial subdivision of ventromedial thalamus through cell-type-specific circuits, forming an excitatory thalamo-cortico-thalamic loop via layer 1 apical tuft dendrites of layer 5B pyramidal tract type neurons. J Neurosci.

Guo ZCV, Li N, Huber D, Ophir E, Gutnisky D, Ting JT, Feng GP, Svoboda K (2014a) Flow of Cortical Activity Underlying a Tactile Decision in Mice. Neuron 81:179-194.

Guo ZV, Hires SA, Li N, O'Connor DH, Komiyama T, Ophir E, Huber D, Bonardi C, Morandell K, Gutnisky D, Peron S, Xu N-L, Cox J, Svoboda K (2014b) Procedures for behavioral experiments in head-fixed mice. PLoS One 9:e88678.

Guo ZV, Inagaki HK, Daie K, Druckmann S, Gerfen CR, Svoboda K (2017) Maintenance of persistent activity in a frontal thalamocortical loop. Nature 545:181-186.

Guo ZV, Li N, Huber D, Ophir E, Gutnisky D, Ting JT, Feng G, Svoboda K (2014c) Flow of cortical activity underlying a tactile decision in mice. Neuron 81:179-194.

Haber S, McFarland NR (2001) The place of the thalamus in frontal cortical-basal ganglia circuits. Neuroscientist 7:315-324.

Halassa MM, Chen Z, Wimmer RD, Brunetti PM, Zhao S, Zikopoulos B, Wang F, Brown EN, Wilson MA (2014) State-dependent architecture of thalamic reticular subnetworks. Cell 158:808-821.

Halassa MM, Kastner S (2017) Thalamic functions in distributed cognitive control. Nat Neurosci 20:1669-1679.

Hanes DP, Schall JD (1996) Neural control of voluntary movement initiation. Science 274:427-430.

Hikida T, Kimura K, Wada N, Funabiki K, Nakanishi S (2010) Distinct roles of synaptic transmission in direct and indirect striatal pathways to reward and aversive behavior. Neuron 66:896-907.

Hikosaka O (2007) GABAergic output of the basal ganglia. Prog Brain Res 160:209-226.

Hikosaka O, Takikawa Y, Kawagoe R (2000) Role of the basal ganglia in the control of purposive saccadic eye movements. Physiol Rev 80:953-978.

Hikosaka O, Wurtz RH (1983a) Visual and oculomotor functions of monkey substantia nigra pars reticulata. I. Relation of visual and auditory responses to saccades. J Neurophysiol 49:1230-1253.

Hikosaka O, Wurtz RH (1983b) Visual and oculomotor functions of monkey substantia nigra pars reticulata. IV. Relation of substantia nigra to superior colliculus. J Neurophysiol 49:1285-1301.

Isomura Y, Takekawa T, Harukuni R, Handa T, Aizawa H, Takada M, Fukai T (2013) Reward-modulated motor information in identified striatum neurons. J Neurosci 33:10209-10220.

Jaeger D, Gilman S, Aldridge JW (1993) Primate basal ganglia activity in a precued reaching task: preparation for movement. Exp Brain Res 95:51-64.

Joseph JP, Boussaoud D, Biguer B (1985) Activity of neurons in the cat substantia nigra pars reticulata during drinking. Exp Brain Res 60:375-379.

Kahneman D, Beatty J (1966) Pupil diameter and load on memory. Science 154:1583-1585.

Kalaska JF, Scott SH, Cisek P, Sergio LE (1997) Cortical control of reaching movements. Curr Opin Neurobiol 7:849-859.

Kaufman MT, Churchland MM, Ryu SI, Shenoy KV (2014) Cortical activity in the null space: permitting preparation without movement. Nat Neurosci 17:440-448.

Kaufman MT, Churchland MM, Santhanam G, Yu BM, Afshar A, Ryu SI, Shenoy KV (2010) Roles of monkey premotor neuron classes in movement preparation and execution. J Neurophysiol 104:799-810.

Kaufman MT, Seely JS, Sussillo D, Ryu SI, Shenoy KV, Churchland MM (2016) The Largest Response Component in

the Motor Cortex Reflects Movement Timing but Not Movement Type. eNeuro 3.

Komiyama T, Sato TR, O'Connor DH, Zhang YX, Huber D, Hooks BM, Gabitto M, Svoboda K (2010) Learning-related fine-scale specificity imaged in motor cortex circuits of behaving mice. Nature 464:1182-1186.

Kravitz AV, Freeze BS, Parker PR, Kay K, Thwin MT, Deisseroth K, Kreitzer AC (2010) Regulation of parkinsonian motor behaviours by optogenetic control of basal ganglia circuitry. Nature 466:622-626.

Kravitz AV, Tye LD, Kreitzer AC (2012) Distinct roles for direct and indirect pathway striatal neurons in reinforcement. Nat Neurosci 15:816-818.

Kultas-Ilinsky K, Ilinsky IA, Massopust LC, Young PA, Smith KR (1978) Nigrothalamic pathway in the cat demonstrated by autoradiography and electron microscopy. Exp Brain Res 33:481-492.

Kuramoto E, Fujiyama F, Nakamura KC, Tanaka Y, Hioki H, Kaneko T (2011) Complementary distribution of glutamatergic cerebellar and GABAergic basal ganglia afferents to the rat motor thalamic nuclei. Eur J Neurosci 33:95-109.

Kuramoto E, Furuta T, Nakamura KC, Unzai T, Hioki H, Kaneko T (2009) Two types of thalamocortical projections from the motor thalamic nuclei of the rat: a single neuron-tracing study using viral vectors. Cereb Cortex 19:2065-2077.

Kuramoto E, Ohno S, Furuta T, Unzai T, Tanaka YR, Hioki H, Kaneko T (2015) Ventral medial nucleus neurons send thalamocortical afferents more widely and more preferentially to layer 1 than neurons of the ventral anterior-ventral lateral nuclear complex in the rat. Cereb Cortex 25:221-235.

Kyriakatos A, Sadashivaiah V, Zhang Y, Motta A, Auffret M, Petersen CC (2017) Voltage-sensitive dye imaging of mouse neocortex during a whisker detection task. Neurophotonics 4:031204.

Lara AH, Cunningham JP, Churchland MM (2018a) Different population dynamics in the supplementary motor area and motor cortex during reaching. Nat Commun 9:2754.

Lara AH, Elsayed GF, Zimnik AJ, Cunningham JP, Churchland MM (2018b) Conservation of preparatory neural events in monkey motor cortex regardless of how movement is initiated. Elife 7.

Larkum ME, Zhu JJ (2002) Signaling of layer 1 and whisker-evoked Ca2+ and Na+ action potentials in distal and terminal dendrites of rat neocortical pyramidal neurons in vitro and in vivo. J Neurosci 22:6991-7005.

Larkum ME, Zhu JJ, Sakmann B (1999) A new cellular mechanism for coupling inputs arriving at different cortical layers. Nature 398:338-341.

Larkum ME, Zhu JJ, Sakmann B (2001) Dendritic mechanisms underlying the coupling of the dendritic with the axonal action potential initiation zone of adult rat layer 5 pyramidal neurons. J Physiol 533:447-466.

Ledergerber D, Larkum ME (2010) Properties of Layer 6 Pyramidal Neuron Apical Dendrites. J Neurosci 30:13031-13044.

Lee HJ, Weitz AJ, Bernal-Casas D, Duffy BA, Choy M, Kravitz AV, Kreitzer AC, Lee JH (2016) Activation of Direct and Indirect Pathway Medium Spiny Neurons Drives Distinct Brain-wide Responses. Neuron.

Lee MS, Marsden CD (1994) Movement disorders following lesions of the thalamus or subthalamic region. Mov Disord 9:493-507.

Lewis LD, Voigts J, Flores FJ, Schmitt LI, Wilson MA, Halassa MM, Brown EN (2015) Thalamic reticular nucleus induces fast and local modulation of arousal state. Elife 4:e08760.

Li N, Chen TW, Guo ZV, Gerfen CR, Svoboda K (2015) A motor cortex circuit for motor planning and movement. Nature 519:51-56.

Liu P, Basso MA (2008) Substantia nigra stimulation influences monkey superior colliculus neuronal activity bilaterally. J Neurophysiol 100:1098-1112.

Luo L, Callaway EM, Svoboda K (2018) Genetic Dissection of Neural Circuits: A Decade of Progress. Neuron 98:865.

Ma Y, Shaik MA, Kim SH, Kozberg MG, Thibodeaux DN, Zhao HT, Yu H, Hillman EM (2016a) Wide-field optical mapping of neural activity and brain haemodynamics: considerations and novel approaches. Philos Trans R Soc Lond B Biol Sci 371.

Ma Y, Shaik MA, Kozberg MG, Kim SH, Portes JP, Timerman D, Hillman EM (2016b) Resting-state hemodynamics are spatiotemporally coupled to synchronized and symmetric neural activity in excitatory neurons. Proc Natl Acad Sci U S A 113:E8463-E8471.

Madisen L, Garner AR, Shimaoka D, Chuong AS, Klapoetke NC, Li L, van der Bourg A, Niino Y, Egolf L, Monetti C, Gu H, Mills M, Cheng A, Tasic B, Nguyen TN, Sunkin SM, Benucci A, Nagy A, Miyawaki A, Helmchen F, Empson RM, Knopfel T, Boyden ES, Reid RC, Carandini M, Zeng H (2015) Transgenic mice for intersectional targeting of neural sensors and effectors with high specificity and performance. Neuron 85:942-958.

McGinley MJ, David SV, McCormick DA (2015a) Cortical Membrane Potential Signature of Optimal States for Sensory Signal Detection. Neuron 87:179-192.

McGinley MJ, Vinck M, Reimer J, Batista-Brito R, Zagha E, Cadwell CR, Tolias AS, Cardin JA, McCormick DA (2015b) Waking State: Rapid Variations Modulate Neural and Behavioral Responses. Neuron 87:1143-1161.

McVea DA, Mohajerani MH, Murphy TH (2012) Voltage-sensitive dye imaging reveals dynamic spatiotemporal properties of cortical activity after spontaneous muscle twitches in the newborn rat. J Neurosci 32:10982-10994.

Meyer-Luehmann M, Thompson JF, Berridge KC, Aldridge JW (2002) Substantia nigra pars reticulata neurons code initiation of a serial pattern: implications for natural action sequences and sequential disorders. Eur J Neurosci 16:1599-1608.

Middleton FA, Strick PL (2000) Basal ganglia and cerebellar loops: motor and cognitive circuits. Brain Res Brain Res Rev 31:236-250.

Mink JW (1996) The basal ganglia: focused selection and inhibition of competing motor programs. Prog Neurobiol 50:381-425.

Mitra A, Kraft A, Wright P, Acland B, Snyder AZ, Rosenthal Z, Czerniewski L, Bauer A, Snyder L, Culver J, Lee JM, Raichle ME (2018) Spontaneous Infra-slow Brain Activity Has Unique Spatiotemporal Dynamics and Laminar Structure. Neuron 98:297-305 e296.

Musall S, Kaufman MT, Gluf S, Churchland AK (2018) Movement-related activity dominates cortex during sensory-guided decision making. bioRxiv.

Musall S, von Pfostl V, Rauch A, Logothetis NK, Whittingstall K (2014) Effects of neural synchrony on surface EEG. Cereb Cortex 24:1045-1053.

Mushiake H, Strick PL (1995) Pallidal neuron activity during sequential arm movements. J Neurophysiol 74:2754-2758.

Nambu A, Tokuno H, Takada M (2002) Functional significance of the cortico-subthalamo-pallidal 'hyperdirect' pathway. NeurosciRes 43:111-117.

Nelson AB, Kreitzer AC (2014) Reassessing models of basal ganglia function and dysfunction. Annu Rev Neurosci 37:117-135.

Nicola SM, Surmeier J, Malenka RC (2000) Dopaminergic modulation of neuronal excitability in the striatum and nucleus accumbens. Annu Rev Neurosci 23:185-215.

Niell CM, Stryker MP (2010) Modulation of visual responses by behavioral state in mouse visual cortex. Neuron 65:472-479.

Okun M, Steinmetz NA, Lak A, Dervinis M, Harris KD (2018) Distinct structure of cortical population activity on fast and infraslow timescales. bioRxiv.

Oldenburg IA, Sabatini BL (2015) Antagonistic but Not Symmetric Regulation of Primary Motor Cortex by Basal Ganglia Direct and Indirect Pathways. Neuron 86:1174-1181.

Ozaki M, Sano H, Sato S, Ogura M, Mushiake H, Chiken S, Nakao N, Nambu A (2017) Optogenetic Activation of the Sensorimotor Cortex Reveals "Local Inhibitory and Global Excitatory" Inputs to the Basal Ganglia. Cereb Cortex 27:5716-5726.

Palmer LM, Schulz JM, Larkum ME (2013) Layer-specific regulation of cortical neurons by interhemispheric inhibition. Communicative and Integrative Biology 6.

Palmer LM, Schulz JM, Murphy SC, Ledergerber D, Murayama M, Larkum ME (2012) The cellular basis of GABAB-mediated interhemispheric inhibition. Science 335:989-993.

Palmer LM, Shai AS, Reeve JE, Anderson HL, Paulsen O, Larkum ME (2014) NMDA spikes enhance action potential generation during sensory input. Nature Neuroscience 17:383-390.

Pandarinath C, O'Shea DJ, Collins J, Jozefowicz R, Stavisky SD, Kao JC, Trautmann EM, Kaufman MT, Ryu SI, Hochberg LR, Henderson JM, Shenoy KV, Abbott LF, Sussillo D (2018) Inferring single-trial neural population dynamics using sequential auto-encoders. Nat Methods.

Parent A (1990) Extrinsic connections of the basal ganglia. Trends Neurosci 13:254-258.

Parent A, Hazrati LN (1995) Functional anatomy of the basal ganglia. I. The cortico-basal ganglia-thalamo-cortical loop. Brain Res Brain Res Rev 20:91-127.

Parent M, Parent A (2004) The pallidofugal motor fiber system in primates. Parkinsonism Relat Disord 10:203-211.

Peixoto D, Kiani R, Chandrasekaran C, Ryu SI, Shenoy KV, Newsome WT (2018) Population dynamics of choice representation in dorsal premotor and primary motor cortex. bioRxiv.

Petersen CC, Grinvald A, Sakmann B (2003) Spatiotemporal dynamics of sensory responses in layer 2/3 of rat barrel cortex measured in vivo by voltage-sensitive dye imaging combined with whole-cell voltage recordings and neuron reconstructions. J Neurosci 23:1298-1309.

Pisauro MA, Benucci A, Carandini M (2016) Local and global contributions to hemodynamic activity in mouse cortex. J Neurophysiol 115:2931-2936.

Pivetta C, Esposito MS, Sigrist M, Arber S (2014) Motor-circuit communication matrix from spinal cord to brainstem neurons revealed by developmental origin. Cell 156:537-548.

Polack PO, Friedman J, Golshani P (2013) Cellular mechanisms of brain state-dependent gain modulation in visual cortex. Nat Neurosci 16:1331-1339.

Poulet JF, Petersen CC (2008) Internal brain state regulates membrane potential synchrony in barrel cortex of behaving mice. Nature 454:881-885.

Ratzlaff EH, Grinvald A (1991) A tandem-lens epifluorescence macroscope: hundred-fold brightness advantage for wide-field imaging. J Neurosci Methods 36:127-137.

Redgrave P, Dean P, Donohoe TP, Pope SG (1980) Superior colliculus lesions selectively attenuate apomorphine-induced oral stereotypy: a possible role for the nigrotectal pathway. Brain Res 196:541-546.

Reimer J, Froudarakis E, Cadwell CR, Yatsenko D, Denfield GH, Tolias AS (2014) Pupil fluctuations track fast switching of cortical states during quiet wakefulness. Neuron 84:355-362.

Reimer J, McGinley MJ, Liu Y, Rodenkirch C, Wang Q, McCormick DA, Tolias AS (2016) Pupil fluctuations track rapid changes in adrenergic and cholinergic activity in cortex. Nat Commun 7:13289.

Requin J, Lecas JC, Vitton N (1990) A comparison of preparation-related neuronal activity changes in the prefrontal, premotor, primary motor and posterior parietal areas of the monkey cortex: preliminary results. Neurosci Lett 111:151-156.

Riehle A, Requin J (1989) Monkey primary motor and premotor cortex: single-cell activity related to prior information about direction and extent of an intended movement. J Neurophysiol 61:534-549.

Riehle A, Requin J (1993) The predictive value for performance speed of preparatory changes in neuronal activity of the monkey motor and premotor cortex. Behav Brain Res 53:35-49.

Roseberry TK, Lee AM, Lalive AL, Wilbrecht L, Bonci A, Kreitzer AC (2016) Cell-Type-Specific Control of Brainstem Locomotor Circuits by Basal Ganglia. Cell 164:526-537.

Rossi MA, Li HE, Lu D, Kim IH, Bartholomew RA, Gaidis E, Barter JW, Kim N, Cai MT, Soderling SH, Yin HH (2016) A GABAergic nigrotectal pathway for coordination of drinking behavior. Nat Neurosci 19:742-748.

Russo AA, Bittner SR, Perkins SM, Seely JS, London BM, Lara AH, Miri A, Marshall NJ, Kohn A, Jessell TM, Abbott LF, Cunningham JP, Churchland MM (2018) Motor Cortex Embeds Muscle-like Commands in an Untangled Population Response. Neuron 97:953-966 e958.

Sachidhanandam S, Sreenivasan V, Kyriakatos A, Kremer Y, Petersen CC (2013) Membrane potential correlates of sensory perception in mouse barrel cortex. Nat Neurosci 16:1671-1677.

Sakamoto M, Hikosaka O (1989) Eye movements induced by microinjection of GABA agonist in the rat substantia nigra pars reticulata. Neurosci Res 6:216-233.

Schlag J, Schlag-Rey M (1971) Induction of oculomotor responses from thalamic internal medullary lamina in the cat. Exp Neurol 33:498-508.

Schmidt R, Leventhal DK, Mallet N, Chen F, Berke JD (2013) Canceling actions involves a race between basal ganglia pathways. Nat Neurosci 16:1118-1124.

Schmitt LI, Wimmer RD, Nakajima M, Happ M, Mofakham S, Halassa MM (2017) Thalamic amplification of cortical connectivity sustains attentional control. Nature 545:219-223.

Seeger-Armbruster S, Bosch-Bouju C, Little ST, Smither RA, Hughes SM, Hyland BI, Parr-Brownlie LC (2015) Patterned, but not tonic, optogenetic stimulation in motor thalamus

improves reaching in acute drug-induced Parkinsonian rats. J Neurosci 35:1211-1216.
Seely JS, Kaufman MT, Ryu SI, Shenoy KV, Cunningham JP, Churchland MM (2016) Tensor Analysis Reveals Distinct Population Structure that Parallels the Different Computational Roles of Areas M1 and V1. PLoS Comput Biol 12:e1005164.
Servan-Schreiber D, Printz H, Cohen JD (1990) A network model of catecholamine effects: gain, signal-to-noise ratio, and behavior. Science 249:892-895.
Shen W, Flajolet M, Greengard P, Surmeier DJ (2008) Dichotomous dopaminergic control of striatal synaptic plasticity. Science 321:848-851.
Sherman SM (2007) The thalamus is more than just a relay. Curr Opin Neurobiol 17:417-422.
Shimaoka D, Harris KD, Carandini M (2018) Effects of Arousal on Mouse Sensory Cortex Depend on Modality. Cell Rep 22:3160-3167.
Silasi G, Xiao D, Vanni MP, Chen AC, Murphy TH (2016) Intact skull chronic windows for mesoscopic wide-field imaging in awake mice. J Neurosci Methods 267:141-149.
Sommer MA (2003) The role of the thalamus in motor control. Curr Opin Neurobiol 13:663-670.
Stringer C, Pachitariu M, Steinmetz N, Bai Reddy C, Carandini M, Harris KD (2018) Spontaneous behaviors drive multidimensional, brain-wide population activity. bioRxiv.
Svoboda K (2016) Imaging the Neural Symphony. Cerebrum 2016.
Svoboda K, Li N (2018) Neural mechanisms of movement planning: motor cortex and beyond. Curr Opin Neurobiol 49:33-41.
Taha EB, Dean P, Redgrave P (1982) Oral behaviour induced by intranigral muscimol is unaffected by haloperidol but abolished by large lesions of superior colliculus. Psychopharmacology (Berl) 77:272-278.

Tai LH, Lee AM, Benavidez N, Bonci A, Wilbrecht L (2012) Transient stimulation of distinct subpopulations of striatal neurons mimics changes in action value. Nat Neurosci 15:1281-1289.

Tanji J, Evarts EV (1976) Anticipatory activity of motor cortex neurons in relation to direction of an intended movement. J Neurophysiol 39:1062-1068.

Tecuapetla F, Jin X, Lima SQ, Costa RM (2016) Complementary Contributions of Striatal Projection Pathways to Action Initiation and Execution. Cell 166:703-715.

Tecuapetla F, Matias S, Dugue GP, Mainen ZF, Costa RM (2014) Balanced activity in basal ganglia projection pathways is critical for contraversive movements. Nat Commun 5:4315.

Thura D, Cisek P (2016) On the difference between evidence accumulator models and the urgency gating model. J Neurophysiol 115:622-623.

Toda K, Lusk NA, Watson GDR, Kim N, Lu D, Li HE, Meck WH, Yin HH (2017) Nigrotectal Stimulation Stops Interval Timing in Mice. Curr Biol 27:3763-3770.e3763.

Travers JB, Dinardo LA, Karimnamazi H (1997) Motor and premotor mechanisms of licking. Neurosci Biobehav Rev 21:631-647.

Travers JB, Jackson LM (1992) Hypoglossal neural activity during licking and swallowing in the awake rat. J Neurophysiol 67:1171-1184.

van Donkelaar P, Stein JF, Passingham RE, Miall RC (1999) Neuronal activity in the primate motor thalamus during visually triggered and internally generated limb movements. J Neurophysiol 82:934-945.

van Donkelaar P, Stein JF, Passingham RE, Miall RC (2000) Temporary inactivation in the primate motor thalamus during visually triggered and internally generated limb movements. J Neurophysiol 83:2780-2790.

Vanni MP, Murphy TH (2014) Mesoscale transcranial spontaneous activity mapping in GCaMP3 transgenic mice reveals

extensive reciprocal connections between areas of somatomotor cortex. J Neurosci 34:15931-15946.
Vinck M, Batista-Brito R, Knoblich U, Cardin JA (2015) Arousal and locomotion make distinct contributions to cortical activity patterns and visual encoding. Neuron 86:740-754.
Wallace ML, Saunders A, Huang KW, Philson AC, Goldman M, Macosko EZ, McCarroll SA, Sabatini BL (2017) Genetically Distinct Parallel Pathways in the Entopeduncular Nucleus for Limbic and Sensorimotor Output of the Basal Ganglia. Neuron 94:138-152 e135.
Wei Z, Inagaki H, Li N, Svoboda K, Druckmann S (2018) An orderly single-trial organization of population dynamics in premotor cortex predicts behavioral variability. bioRxiv.
Westby GW, Collinson C, Redgrave P, Dean P (1994) Opposing excitatory and inhibitory influences from the cerebellum and basal ganglia converge on the superior colliculus: an electrophysiological investigation in the rat. Eur J Neurosci 6:1335-1342.
Wichmann T, DeLong MR (1996) Functional and pathophysiological models of the basal ganglia. Curr Opin Neurobiol 6:751-758.
Wise SP, Weinrich M, Mauritz KH (1986) Movement-related activity in the premotor cortex of rhesus macaques. Prog Brain Res 64:117-131.
Yamashita T, Petersen C (2016) Target-specific membrane potential dynamics of neocortical projection neurons during goal-directed behavior. Elife 5.
Yamawaki N, Shepherd GMG (2015) Synaptic circuit organization of motor corticothalamic neurons. Journal of Neuroscience 35:2293-2307.
Yin HH (2014) Action, time and the basal ganglia. Philos Trans R Soc Lond B Biol Sci 369:20120473.
Yttri EA, Dudman JT (2016) Opponent and bidirectional control of movement velocity in the basal ganglia. Nature 533:402-406.

Yu BM, Cunningham JP, Santhanam G, Ryu SI, Shenoy KV, Sahani M (2009) Gaussian-process factor analysis for low-dimensional single-trial analysis of neural population activity. J Neurophysiol 102:614-635.

Yuzgec O, Prsa M, Zimmermann R, Huber D (2018) Pupil Size Coupling to Cortical States Protects the Stability of Deep Sleep via Parasympathetic Modulation. Curr Biol 28:392-400 e393.